Response to Anonymous Referee 1 on "Measurement of ammonia, amines and iodine species using protonated water cluster chemical ionization mass spectrometry"

We thank the referee for the constructive comments that help improving our manuscript. In the following, the comments of the referee are shown in black, shaded font. Our replies are shown in blue font. Text that has been added or revised in the manuscript is shown in red font.

There could be better clarification throughout the manuscript to indicate that the amine and iodine species are detected and that their mixing ratios are estimated semiquantitatively, as formal calibrations have not been performed with a primary standard.

We agree with the referee that the manuscript should clearly indicate that the mixing ratios for amines and iodic acid are estimated and prone to higher uncertainty compared to the ammonia measurement. We have updated the manuscript according to the specific comments from the referee. Our revised text is listed after our replies.

The title should be revised to reflect quantitation of ammonia and detection of DMA and iodine oxide species specifically instead of 'amines and iodine species' which is misleading. The discussion clearly states that the DMA and HIO3 quantities are estimates based off of scaled numbers from H3O+ or NO3- CI-APi-TOF responses to other species (e.g. NH3 or H2SO4). Converting the units from ncps to mixing ratios for those scaled responses leads to values that may be highly inaccurate. The potential for quantification and sensitive detection of these species by H3O+ CI-APi-TOF can be discussed, but the scaled response estimates should not be used to report mixing ratios, such as in Figures 5 and 8. These should be replaced with signal reported as normalized counts per second (ncps). The authors state in several locations in the discussion potential sources of bias from the assumptions made in converting signal to mixing ratios, which are not fully characterized for the CLOUD chamber and could easily represent a factor of 2 or more error. Based on the presented data, mixing ratios for these compounds should be replaced with ncps units throughout the manuscript. The authors make arguments for the validity of some assumptions throughout the manuscript as well, which seem to be undermined by other parts of the discussion. See the technical comments below for instances where this is the case and the discussion should be revisited.

In principle we agree with the referee that it should clearly be stated that the reported mixing ratios for dimethylamine and iodic acid are not based on a direct calibration with these substances. However, in the following we argue that it is nevertheless justified to report mixing ratios in Figures 5 and 8.

A recent publication by Sipilä et al. (2016) reports on measurements of iodic acid with a nitrate CI-APi-TOF (same as the one used in our study for the HIO3 measurements shown in Fig. 5 on the x-axis). No direct calibration for iodic acid was available at that time and it is still not available at present. However, there is good reason to assume that HIO3 is ionized with the same (or at least similar) efficiency as sulfuric acid (for which the nitrate CI-APi-TOFs are directly calibrated). Sulfuric acid is ionized by NO3- at the collision limit because it is a much stronger acid than HNO3. Compared with HNO3 iodic acid has a much stronger acidity. Furthermore, HIO3 is detected at m/z 175, whereas the strongest signal for sulfuric acid is found at m/z 160 (HNO3.HSO4- cluster), therefore both compounds are found at very similar masses in the mass spectrum and mass discrimination effects of the CI-APi-TOF should be very small. Both arguments indicate that HIO3 can be quantified with the nitrate CI-APi-TOF technique. Therefore, we think it is well-justified to use the concentrations from the nitrate CI-APi-TOF as the reference in Figure 5. However, we have added remarks to the abstract, Table 1 and to the caption of the Figures 3 and 5 that indicate that the reported values are not based on measurements with an instrument that was directly calibrated with HIO3. Furthermore, a comment was added to the Figure 3 caption that the estimated systematic uncertainty for the HIO3 values is +100%/-50% (same as reported by Sipilä et al., 2016).

Regarding the measurement of amines, we have also added remarks to the abstract, the main text, Table 1 and Figure 8, which indicate that no direct calibration was performed for DMA. Furthermore, we replaced “amines” with “dimethylamine” throughout the text and only mention in the outlook that other amines (and diamines) can be measured with the protonated water cluster CI-APi-TOF technique. Nevertheless, we think that the reported mixing ratios for DMA should be kept. DMA has a very high proton affinity (929.5 kJ mol-1), i.e., significantly higher than ammonia (853.6 kJ mol-1). Therefore, DMA should efficiently be ionized by protonated water clusters. Hanson et al. (2011) report that for their water cluster mass spectrometer both ammonia and dimethylamine are ionized with a similar efficiency. This was also reported much earlier by Sunner et al. (1988) although they did not report on the sensitivity of DMA but on other amines with a similar proton affinity. The second argument that supports our assumption that DMA can be quantified is based on the data shown in Figure 8 (Figure 9 in our revisited manuscript). The CLOUD chamber offers in principle the possibility to serve as a calibration system itself. With the known flow rates of DMA into the chamber, the chamber volume and the DMA lifetime (known from wall loss decay experiments) the DMA mixing ratio inside the chamber can be calculated (see, e.g., Simon et al., 2016). Figure 8b) (Figure 9a in our revisited manuscipt) indicates good agreement between estimated DMA (using the sensitivity from the ammonia calibration) and the calculated DMA inside the CLOUD chamber. Taking this together, plus the added caveats about the missing direct calibration (that has now been added to the manuscript) we think that the reported DMA mixing ratios should be kept.

Applying these arguments, also the title can be left unchanged. Especially when the lacking direct calibrations for DMA and HIO3 are immediately mentioned in the abstract below the title.

As said above, we have updated our text and Table 1 to clarify our arguments and to make clear that the only direct calibration was performed with ammonia. Specific changes made in the text and in the Table / Figures are listed after the corresponding comments below.

Intercomparison with the Picarro NH3 cavity ring down instrument does not evaluate the measurements correctly and ignores discussion regarding the limitations of the CI-APi-TOF approach (e.g. response times on the order of hours) or the experimental setup of the intercomparison (e.g. the Picarro connected to the exhaust of the CI-APi-TOF).

Our initial text may have been misleading here. The CI-APi-TOF doesn’t have a response time in the order of hours. We just took averages over a time of hours to calculate e.g. the detection limits. The detection limits shown here wouldn’t change dramatically if we splitted this 150minute period into e.g. 7 periods of 20 minutes:

Period	*Calculated detection limit (pptv)*
Period 1	0.42
Period 2	0.81
Period 3	0.39
Period 4	0.51
Period 5	0.74
Period 6	0.39
Period 7	0.42

The reason for taking a 150 minute instead of a 20 minute period was to get more data points and thus a better statistic to calculate the standard deviation. The initial text at table 1 (“The calculated detection limits are based on a 2.5 hour measurement at 278 K and 80% RH (averaging time of single data points: 1 minute).”) may be misleading. Thus, we removed the extra information about the time scale of the measurement. Next to this, we updated our paper by a Figure showing the response time of the CI-APi-TOF between two steady states, which is shown on the following page (Section 3.3 “Response times”).

Figure 7 (Figure 8 in our revised manuscript) shows an ammonia decay over several days at the CLOUD chamber. This may be misleading and interpreted as a response time of the insrument. The CLOUD chamber is a 26.1m^3 vessel of stainless steel. Once, the chamber walls are saturated with ammonia, it takes hours to remove it (as also shown in the PICARRO trace). This time is not due to instrumental response times. We would like to refer to previous publications, eg Kupc et al. (2011) or Duplissy et al. (2016) that describe the CLOUD chamber in a more detailed way. We updated our text accordingly and we also added limitations of the CI-APi-TOF approach (depletion of primary ions at higher concentrations).

We agree with the referee that an intercomparison as shown in Figure 7 (Figure 8 in our revised manuscript) of our paper would be problematic provided the PICARRO would have been connected to the exhaust of the CI-Api-TOF. However, this was not the case during measurements carried out at the CLOUD chamber. Our previous text may have been misleading in this regard and has been updated accordingly (changes are shown at the specific technical comments). The PICARRO was only connected to the exhaust once (24 hour period) for an intercomparison between both instruments. The setup at the CLOUD chamber is shown in the Figure below.

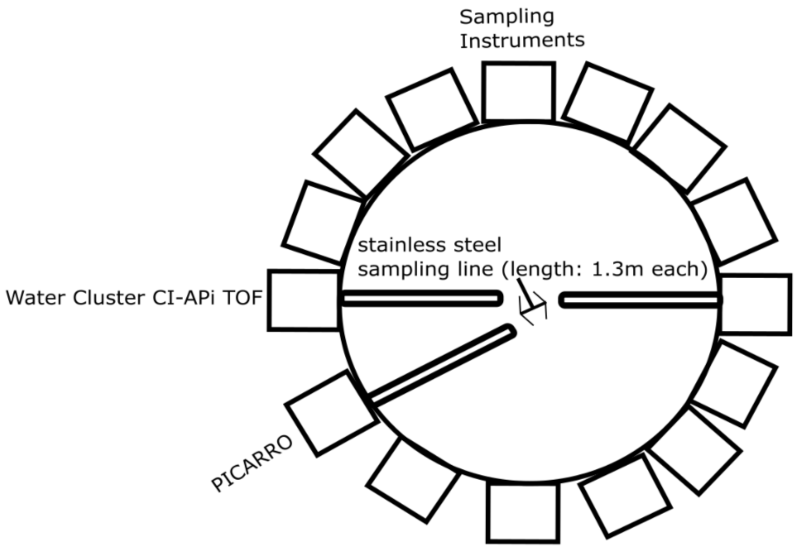

3.3 Response times

The response time of the water cluster CI-APi-TOF is defined as the characteristic time needed for the instrument to react on changes in the ammonia mixing ratio. The response time takes into account two processes. These are the time needed until the instrument reacts on changes in the mixing ratio and the time needed until a steady state is established in the lines. In the following, we define the response time as the time required for the instrument to reach 95% of the new mixing ratio being injected. Figure 4 indicates the typical response times of the water cluster CI-APi-TOF during calibrations (here at 60% relative humidity). It shows a decay between two calibration steps when the injected ammonia is reduced from 9509 pptv to 6911 pptv and a rise in the signal when the ammonia mixing ratio is increased from 500 pptv to 9509 pptv. Panel a) indicates a clear difference between the time needed until the instrument reacts on the changes in the mixing ratio (red line) and the time needed until the lines reach 95% of the new steady state (black line). We expect the same behavior for a decay from 9509 to 500 pptv, however, the mixing ratios were gradually reduced during calibrations. Thus, for the gradual decays, the time needed for the lines to reach a new equilibrium is rather short. While the variation of instrumental response time is small (6 to 10 seconds for decays from 9509 to 6911 pptv and 18 to 25 seconds for a rise from 500 pptv to 9509 pptv, respectively), the time until a steady state is established in the lines varies depending on precursor conditions and relative humidity (see Section 3.8). Thus, an estimation of a response time can vary significantly. In our experiments, the response times (including both processes described above) during a rise in ammonia mixing ratio varied between 535 seconds (20% relative humidity) and 890 seconds (60% relative humidity, shown in Figure 4). For a decay of ammonia mixing ratio from 9509 to 6911 pptv the response times vary between 37 seconds and 54 seconds.

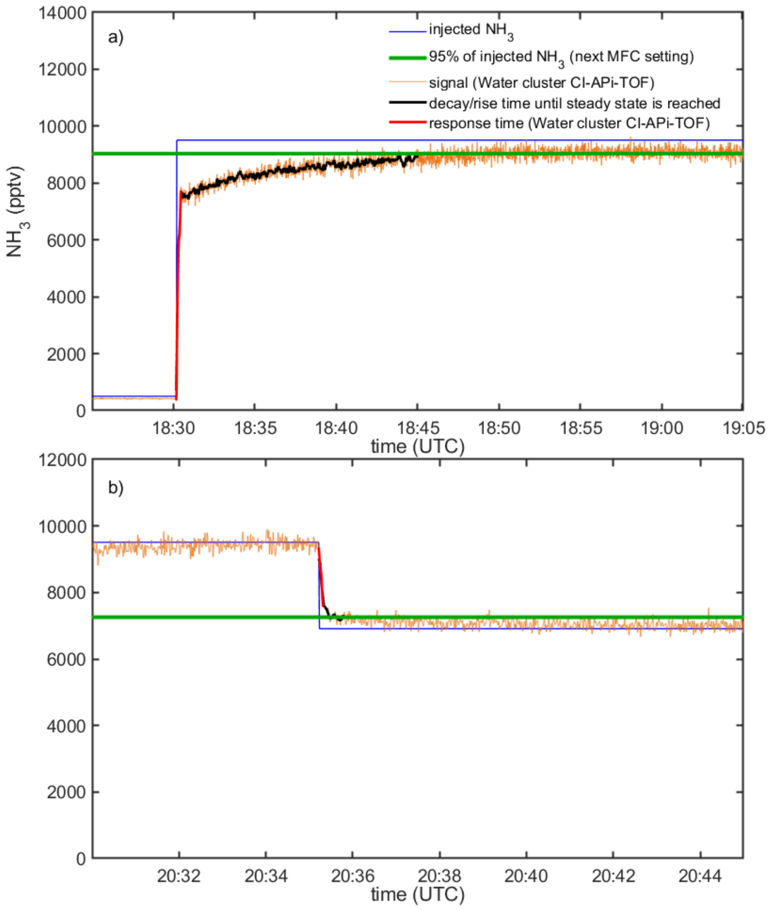

Figure 4: Response time of the water cluster CI-APi-TOF during calibrations at 60% RH. The injected ammonia level is shown by the blue line. The signal of the water cluster CI-APi-TOF is shown by the grey line (here the data are shown with a 1 second time resolution (no averaging applied)). The black line shows the response time until a steady state (panel a)) or 95% of the final measured concentration is reached (panel b)). This response time is defined as the sum of the response time of the water-cluster CI-APi-TOF (red line) and the time required until the lines reach a new steady state. See text for details.

Added in Section 3.7:

The time from 25.10 to 26.10 shows a steep increase in the PICARRO trace, while the ammonia trace derived from the water cluster CI-APi-TOF flattens out at 20 ppbv of ammonia. This indicates that the primary ions of the water cluster CI-APi-TOF are depleted at high vapor concentrations. It is important to mention that not only ammonia concentrations were elevated at this time, but also other vapor concentrations were rather high. During the CLOUD13 campaign, where a revised version of the ion source was used (see Section 3.2), the significant depletion of primary ions has been observed only at ammonia mixing ratios of 40 ppbv.

For example, there is a clear background offset in the Picarro measurements from the chamber that is not accounted for, but for which the CI-APi-TOF dataset is corrected accordingly through its independent calibration. There are other important measurement concepts that are missed in the data analysis here such as the aforementioned background offset correction, inlet and instrument surface sorption/ desorption effects impact on response times, and detection limits. See the technical comments corresponding to these sections of the manuscript below for several specific comments. It is possible that the intercomparison is technically invalid based on the experimental setup and should be removed from the manuscript, but this cannot be assessed without further data provided by the authors regarding the setup of flows to direct the chamber air to the instruments.

We agree with the referee that a correction for background is important when showing analyzed data. However, the data shown for the CI-APi-TOF are not corrected for a background either (this was done by purpose to show the low instrumental background of the CI-Api-TOF). We corrected the background of the PICARRO in a revised Figure shown below (background of water cluster CI-APi-TOF still not corrected). The PICARRO data shown in Figure 7a (Figure 8a in our revised manuscript) were smoothed using a moving average of 5 minutes in our initial Figure. We updated the Figure using the same 1-minute average as for the CI-APi-TOF here to show that the PICARRO trace is below its detection limit. We used the moving average as the PICARRO trace covers half of the Figure when the 1-minute-average is applied. We updated our Figure, where we now use the Figure shown above that includes the background substraction of the PICARRO.

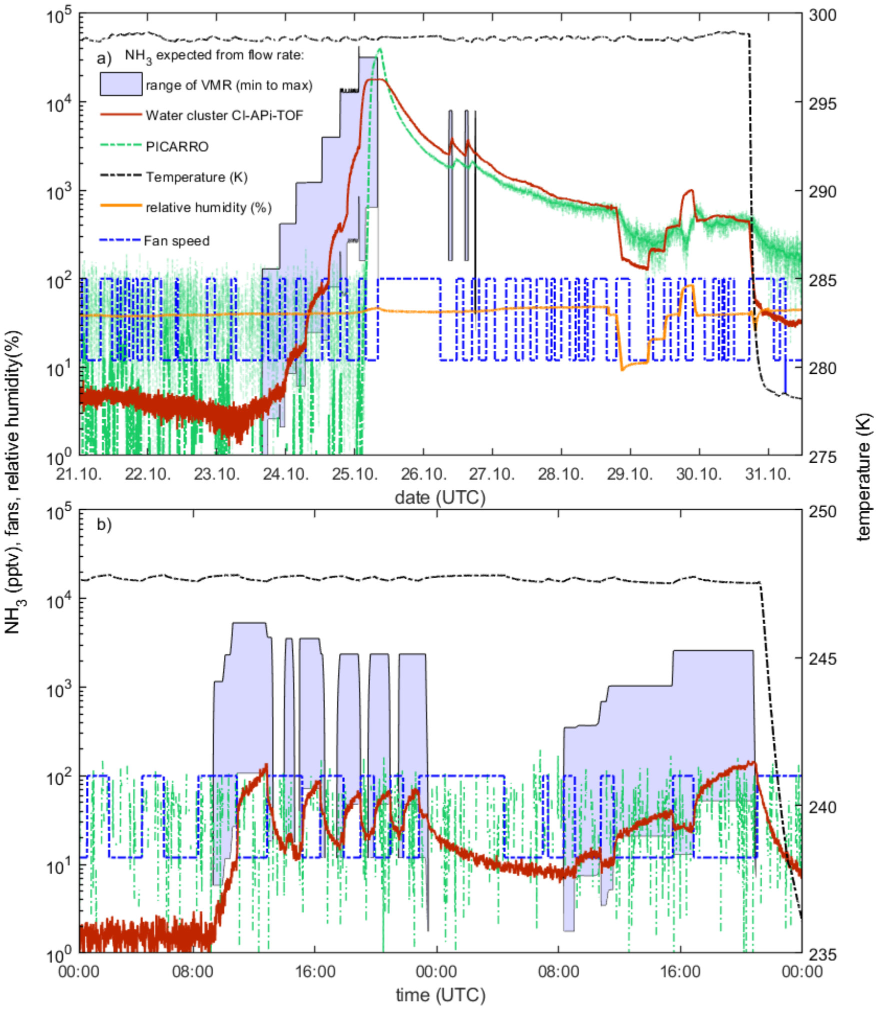

Figure 8: Inter-comparison between calculated (shaded blue area) and measured ammonia mixing ratios (PICARRO: solid green line; water cluster CI-APi-TOF: solid red line) at CLOUD. The PICARRO background (~200 pptv) has been subtracted, while no background was subtracted from the water cluster CI-APi-TOF. The temperature inside the chamber is indicated by the dashed black line. The speed (% of maximum, 397 revolutions per minute) of the two fans that mix the air inside the chamber is shown by the dashed blue line. The calculated ammonia mixing ratios (based on the calculated injection of ammonia into the chamber from the MFC settings) have a wide range due to uncertainties of the ammonia loss rate in the chamber. We display the maximum calculated range assuming, for the lower limit, that the chamber walls act as a perfect sink (wall loss dominated, 25s and 100 s lifetime for fan speeds 100% and 12%, respectively) and, for the upper limit, no net uptake of NH_3 on the walls and a loss rate determined by dilution (6000 s lifetime). For higher fan speeds, the lifetime decreases due to increased turbulence and, in turn, increased wall loss rate. Relative humidity is indicated by the orange line. The water cluster CI-APi-TOF reacts rapidly to changing conditions, such as the ammonia flow into the chamber, relative humidity, temperature or fan speed. At low concentrations, the ammonia lifetime is determined by the wall loss rate (panel b and initial stages of panel a). However, at high ammonia concentrations, the walls of the CLOUD chamber progressively become conditioned and a source of ammonia, with corresponding increases in the ammonia lifetime and the time to reach new equilibria at lower ammonia flow rates (later stages of panel a).

Page 1, Line 17: Diamines are not presented in the manuscript and are mentioned here. Remove. There seem to be several issues of material that was planned for inclusion in this manuscript that have been removed, but not in all locations. The authors should revisit the manuscript with this in mind to improve clarity throughout.

We updated the text according to the comment of the referee:

The instrument selectively measures trace gases with high proton affinity such as ammonia and dimethylamine, which are important for atmospheric new particle formation and growth.

Page 1, Lines 20-21: The detection limit difference for the amines should be stated as 'at least XX times lower' here to be more specific.

We updated the text according to the comment of the referee. :

The limit of detection of the water cluster CI-APi-TOF is estimated to be ~0.5 pptv for ammonia. Although no direct calibration was performed for dimethylamine (DMA), we estimate its detection limit is at least 3 times lower.

Page 2, Line 33: 2.5 is usually a subscript

We updated the text according to the comment of the referee:

Strong reductions in $PM_{2.5}$ mass and the associated adverse health effects could potentially be achieved by decreasing ammonia emissions (Pozzer et al., 2017).

Page 2, Line 36: Use one or the other of 'new particle formation' or 'nucleation' and add 'e.g.' before each example of the ternary and multi-component systems.

We updated the text according to the comment of the referee:

However, ammonia is not only partitioning to existing particles, but is also a key vapour driving new particle formation due to its stabilization of newly-formed clusters in ternary (sulfuric acid-water-ammonia) and multi-component (sulfuric acid-water-ammonia-highly oxygenated organic molecules) systems (Kirkby et al., 2011; Kürten et al., 2016a; Lehtipalo et al., 2018).

Page 2, Lines 40-46: This clarity of this section is not very good because these sentences are discussing too many topics, which should be separate sentences. Delete 'their' and end the sentence after the Dunne et al. reference. In line 42, replace 'show' with 'support this by observing'. On line 44 end the sentence after 'water' and start the next sentence with 'For example' instead of using 'e.g.' in-line.

We updated the text according to the comment of the referee:

In the upper troposphere, model calculations suggest that ammonia can also be important for new particle formation and early growth (Dunne et al., 2016). Recent satellite measurements support this by observing that ammonia can be present at several tens of pptv (parts per trillion by volume) level over Asia (Höpfner et al., 2016).

Page 2, Line 46: It is accurate to state 'enhance nucleation rates'. The 'even stronger' is not necessary and confuses the sentence's evaluation of relative enhancements of amines over ammonia in forming new particles.

We updated the text according to the comment of the referee:

Stronger basic compounds like amines or diamines, have been shown to enhance nucleation rates, despite their much lower atmospheric concentrations (Almeida et al., 2013; Kürten et al., 2014; Jen et al., 2016; Yao et al., 2016).

Page 2, Line 48: Why have the authors stated 'in principle confirmed' here? Perhaps the specific property assessed (e.g. thermodynamically favored formation) would be a more accurate term to place here.

The quantum chemical calculations shown in the studies cited in our article (eg Kurten et al., 2008 in ACP) confirm studies from eg Almeida et al., 2013 in nature (dimethylamine). Thus, stating that the experimental observations are confirmed by quantum chemical calculations is accurate. We deleted the "in principle" in our sentence for clarification:

The experimental measurements are confirmed by quantum chemical calculations that compare the stabilizing effects of ammonia, amines, and diamines (Kurtén et al., 2008; Elm et al., 2017; Yu et al., 2018).

Page 2, Lines 52-53: The list of references for amine mixing ratios is more comprehensively summarized in a review by Ge et al. in Atmos. Environ. (2010) which can replace this list of references[1].

We added Ge et al. to the list of references shown here. However, we disagree that the studies from Ge et al. are able to replace the references listed previously. While Ge et al. is an overall summary of mesurements of amines, studies like, e.g. from You et al (2014) or from Kürten et al (2016b) show more recent measurements using CIMS techniques at low detection limits.

It is important to note that ammonia can easily exceed several ppbv in the boundary layer, whereas amine mixing ratios are typically present at a few pptv only (Ge et al., 2011; Hanson et al., 2011; You et al., 2014; Kürten et al., 2016b; Yao et al., 2016).

Page 2, Lines 54-57: There is an attempted motivation here that CI-APi-TOF is more versatile than other analytical techniques for atmospheric samples of reduced nitrogen species. However, separation techniques are more selective than CI-APi-TOF, particularly when it comes to the detection of structural isomers. Optical absorption techniques by systems such as cavity ringdown and quantum cascade laser systems are easily as sensitive and with as high time resolution as CI-APi-TOF. The limitation of the prior methods that CI-APi-TOF overcomes should be made with greater clarity here in order to motivate the CI-APi-TOF analytical approach. It would be easiest to remove the first sentence of this paragraph and start the second sentence at 'Chemical ionisation atmospheric pressure interface mass spectrometry…'

We agree with the referee that optical absorption techniques and separation techniques like GC-MS can have a clear advantage regarding their selectivity. What we wanted to express, however, that CIMS can often measure many compounds simultaneously with high time resolution and very good sensitivity. To clarify this the sentence was modified as follows:

These measurement techniques are often specialized for the detection of only a few selected compounds, whereas chemical ionization mass spectrometry (CIMS) can often measure a suite of atmospheric trace gases simultaneously at low concentrations and high time resolution.

Page 6, Lines 167-171: This is a big stretch in justification for quantifying amines.
Strong acids detected by CIMS do not have the same response factors per mixing ratio detected and this is well reported in the literature even though their reaction rates would be predicted to be the same for a given ionisation technique (e.g. 2-16 counts per pptv for strong acids by proton exchange in Roberts et al. in Atmos. Meas. Tech. (2010)) [2]. This detail should be clarified here along with the potential outcome of the assumption for amines likely being up to a factor of 10 error in quantitation

as a worstcase outcome. It is likely better to report in this work the measurement of amines only in 'ncps' and to do a ballpark estimation of the mixing ratios in the discussion.

In principle we agree that thermodynamic data alone should not be used to justify the assumption of using the same calibration factor for ammonia and DMA. However, the cited study by Hanson et al. (2011) reports on the calibration with both substances and supports our assumption. Also, the study by Sunner et al. (1988) reports similar data. They studied the sensitivity of ammonia and different amines towards reactions with protonated water and found found collision limited ionization for both substances. To further support our assumption the study by Sunner et al. (1988) was added to the references and cited in Section 2.2:

When mixing ratios for dimethylamine are presented, the same calibration factor is used. This approach can introduce uncertainty as the proton affinity, as well as transmission efficiency differ for dimethylamine compared to ammonia. However, previous studies showed that the ionization efficiency from protonated water clusters is collision-limited for both compounds, ammonia and dimethylamine (Sunner et al., 1988; Hanson et al., 2011). The applicability of this approach is discussed in Section 3.9; it is estimated that the mixing ratios for dimethylamine are correct within a factor of ~3.5.

Page 6, Line 186: A sentence should not begin with an acronym. Rephrase.

We updated the text according to the comment of the referee:

The ammonia was taken from a gas bottle containing an NH_3 mixing ratio, *B*, of 100 ppmv diluted in pure nitrogen (Air Liquide, ±5% uncertainty for the certified NH_3 mixing ratio) that is diluted in two steps, where MFCs (shown as M_n in Figure 1a) are used to obtain different set points for the volume mixing ratio (Figure 1a). During the second dilution step the mixture from the first dilution is injected into the center of the main sample flow (flow rate, Q_{sample}).

Page 7, Lines 207-209: This is quite the string of assumptions and underscores the major issue with claimed quantitation in this work. The detection of HIO3 is, at absolute best, qualitative and units should not be assigned to the measurement in pptv, but 'ncps'.

We agree with the referee that this assumption causes uncertainty. However, we would like to refer to our previous argumentation shown on page 1 (reply to major comment 1). We changed our text in this section accordingly and added the following sentences for clarification (added to line 217-221):

This assumption introduces uncertainty when estimating the detection limit of HIO_3. However, as the reaction of sulfuric acid with nitrate ions is at the kinetic limit, the detection limits shown here based on this assumption can be seen as lower limits. Unfortunately, there is currently no direct calibration technique established for iodic acid in the gas phase. Thus, the applied assumption in the present study was also used in a previous study for deriving gas phase concentrations of iodic acid (Sipilä et al., 2016).

Page 7, Lines 209-212: This intercomparison is shown in Figure 5, but the axis labels do not communicate this. They should both be reported as normalized counts since the NO3- CI-APi-TOF signal is scaled on the H2SO4 response, which does not yield a quantitative calibration factor for HIO3, but only a relative signal.

We thank the referee for this comment. We want to refer to our response to the comments related to the Figures below.

Page 8, Lines 223-226: The authors state that the instrument was independently calibrated. This means that they have data to calculate the detection limit of the Picarro NH3 cavity ringdown system and it should be done here instead of stating the value given from the datasheet.

We thank the referee for this suggestion. However, as the PICARRO is calibrated for higher ammonia mixing ratios by using the permeation tube, a direct comparison of the calibration curves wouldn't make sense. Here we show the calibration curve of the PICARRO from CLOUD 13:

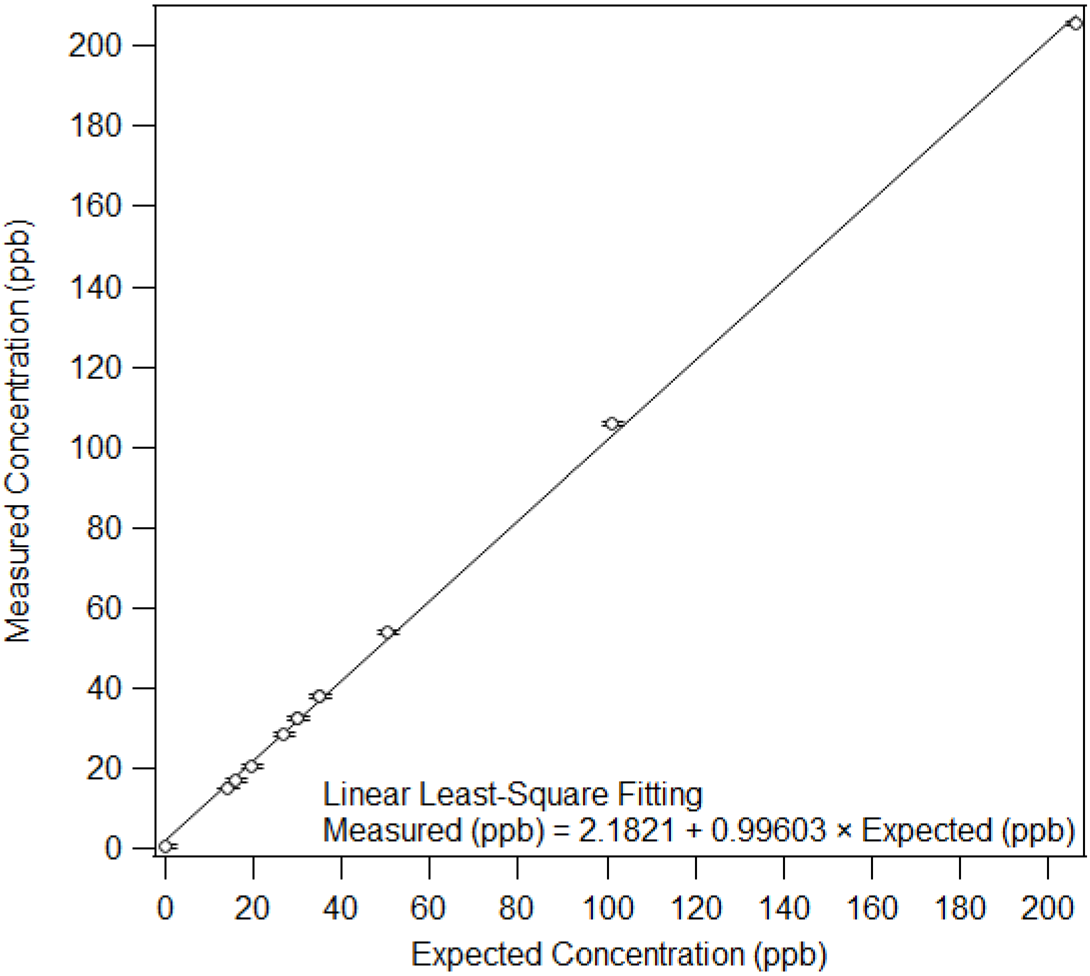

The calculated instrumental background is at 88.9 pptv (during the same 150 minute time as shown for the water cluster CI-APi-TOF). The calculated detection limit during this time is at 366.2 pptv. We added the detection limit to section 2.3 (PICARRO).

The time interval for one measurement of the PICARRO is 5 seconds for which a lower detection limit of 200 pptv is reported (PICARRO Inc., USA; Martin et al., 2016). By using the same method (at the same time period) as shown for the Water Cluster CI-Api-TOF (see section 3.5), we derive a detection limit of 366.2 pptv for the PICARRO unit used in this study.

Page 8, Line 237: The first name of the author should not be given here.

We thank the referee for recognizing this mistake. We corrected this in our new version.

For the analysis of the spectra, the software TOFWARE is used that allows analyzing high resolution spectra (Stark et al., 2015; Cubison and Jimenez, 2015; Timonen et al., 2016).

Page 8, Lines 248-251: This comparison of the stability of reagent ion should be made by calculating the change in the calibration slope (ncps vs NH3 mixing ratio) between high (1-10 ppbv) and low (<1 ppbv) ranges to reach the conclusion that the sensitivity is consistent across the full range of experimental mixing ratios used in CLOUD. The authors also state 'sufficient precision' here without defining what the value they use is. The numeric value should be given. It would also be useful here for the authors to comment on the likelihood that this calibration response will hold up under ambient observations where other atmospheric components will compete for H+ transfer.

As the calibration setup with the MFCs shown in our Figure 1 limits the range of mixing ratios, we can compare the slopes from 500pptv to 2500pptv (low) with the slope from 4200pptv to 9509pptv (high). As shown in our Figure below, the deviation between high and low range is at 4.35%, where the high slope is m~ 6.9e-6 and the low slope is m~6.6e-6.
The second part of the comment (*"The authors also state 'sufficient precision' here without defining what the value they use is. The numeric value should be given"*) refers to potential depletion of the reagent ions at high ambient concentrations of compounds with high proton affinity other than ammonia. Of course this can potentially lead to a change in the sensitivity, which could be accounted for by the addition of an internal calibration standard. A remark regarding this effect is included in Section 3.7 (lines 439 to 444):

The time from 25.10 to 26.10 shows a steep increase in the PICARRO trace, while the ammonia trace derived from the water cluster CI-APi-TOF flattens out at ~20 ppbv of ammonia. This indicates that the primary ions of the water cluster CI-APi-TOF are depleted at high vapor concentrations. It is important to mention that not only ammonia concentrations were elevated at this time, but also other vapor concentrations were rather high. During the CLOUD13 campaign, where a revised version of the ion source was used (see Section 3.2), the significant depletion of primary ions has been observed only at ammonia mixing ratios of ~40 ppbv.

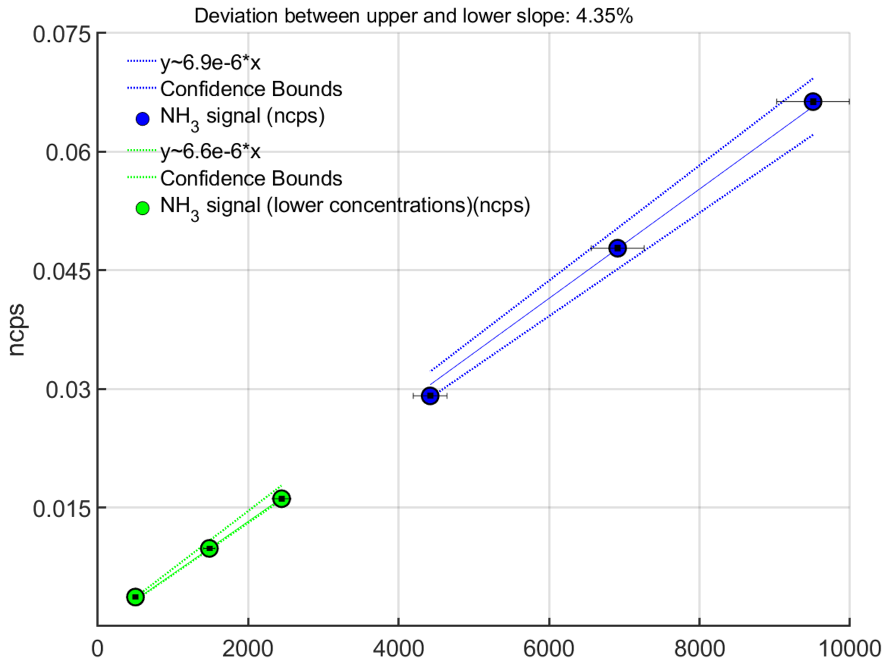

Page 9, Lines 259-261: Here is the HIO3 intercomparison again. The error in the VMR is estimated based on an applied scalar, which is effectively a guess. It is more transparent, and valuable, to report *that the two independent ionisation schemes yields a strong linear response, supporting the sensitive detection of HIO3 using H3O+ chemistry. Extending this further into estimated mixing ratios is not justified.*

We agree with the referee that this assumption causes uncertainty. We would like to refer to our previous argumentation shown on page 1 (reply to major comment 1), as well as to the changes made throughout the manuscript (previous reply to major comment 1). In this section, we also state that the assumption can introduce uncertainties up to a factor of 2. As there is no established technique to calibrate iodic acid in the gas phase, this assumption has also been made in a previous publication, e.g., Sipilä et al. (2016).

Also, for these calibrations, the experiments shown in the remainder of the manuscript are not collecting 20 minute time-resolution data. Averaging at timescales more relevant to the measurement timescale would give a more accurate estimate of calibration response and quantitation accuracy, so long as 20-30 data points are pooled for each calibration mixing ratio.

We agree with the referee that longer timescales would be advantageous. However, when creating these data points, we must adapt to the steady-state periods at the CLOUD experiment, which cannot be longer depending on the experiment (especially during the studies of iodic acid chemistry).

Page 9, Lines 263-264: The resulting difference in the forced and unforced slopes should be reported with the numeric value of the percent difference.

We updated the text according to the comment of the referee:

The fit is forced through the origin; however, even when the fit is not constrained, the resulting slope is essentially the same (the results for the slopes/sensitivities differ by 1.35%).

Page 9, Lines 265-267: 'concentration steps' should be 'calibration mixing ratios' and 'confidence bounds (95 % confidence intervals)' should be '95 % confidence intervals'.

We updated the text according to the comment of the referee. As the calculation of the mixing ratios is shown in this chapter, we use "mixing ratios" instead of "calibration mixing ratios" to stay consistent:

Figure 3 shows that all measured mixing ratios lie in the area of the confidence intervals (95% confidence intervals) and thus the linear model describes the dependency very well.

Page 9, Lines 272-274: The response time of the CI-APi-TOF to a stable signal following the stepped-down changes in NH3 VMR should be provided here explicitly. The discussion following this section states that the instrument and line surfaces contribute to background signals observed. Here, the 'diffusion of ammonia from the capillary into the sampling line' should be clarified to indicate that the background observed also has contributions from all surfaces in the calibration system, the instrument inlet, and the instrument walls.

We added a section 3.3 that discusses response times as already mentioned in a comment previously. Possible wall effects are discussed in this section and in Section 3.8 and are also shown in our new Figure 4 (as shown previously). Regarding the background due the diffusion from the capillary it can be said that this exactly describes the difficulty in determining representative background values. Only after sufficiently long flushing times with clean air, with the calibration capillary removed, representative instrumental background values can be determined. This is discussed in Section 3.5.

Pages 9-10, Lines 282-286: The changes in calibration factor should be explicitly given. Are they a factor of 2 different or a factor of 5? This is a measurement technique manuscript and it is VERY important to highlight how small changes in instrument operation and setup can affect the quality of the measurements. Was the CI-APi-TOF re-calibrated with these slight changes? How was the calibration factor derived for these CLOUD experiments? Did the response time of the inlet change? All of this information has high value here.

As there are too many factors that have been changed in parallel between these two campaigns, a direct comparison is not very meaning in our opinion. The changes between CLOUD12 and CLOUD13 included:

- The sampling flow rate was 5.6 slm during CLOUD12, while it was 19.5 slm during CLOUD13.
- The voltages inside the mass spectrometer were different between the campaigns as shown below. Thus, the transmission efficiency inside the mass spectrometer changed between the campaigns, as well as the response time.
- The distance between injection of primary ions and pinhole of mass spectrometer was different, which affects the ion-molecule reaction time.

This is due to a different ion source (designed for a 0.5'' sampling line in CLOUD12 compared with a 1'' line in CLOUD13), a different sample flow rate and different tuning of the CI-APi-TOF.

Page 10, Line 294: What does 'including all components' mean?

Including all components means in this case the voltages on the ion source, the voltages in the APi section and in the time of flight region. We updated our text for clarification:

In addition, the detection efficiency as function of the ion mass can vary depending on the voltages applied to the ion source and the APi-section, as well as the time of flight region of the mass spectrometer. Thus, the mass spectrometer does not have a constant detection efficiency over the full mass range (Heinritzi et al., 2016).

Page 10, Lines 301-306: This section of discussion is unclear and difficult to follow. Rewrite for clarity since looking at Figure 7, there seems to be disagreement with what is stated here regarding 15 % and 3 % change in signal. Perhaps there is a way to depict this more clearly in a new figure?

The drop in ammonia shown in Figure 7 (between 30.10. and 31.10.) coinciding with the temperature decrease from 298 to 278 K can be attributed to a change in the ammonia wall desorption rate when no ammonia is actively injected into the chamber. During the previous experiments (until 25.20.) very large amounts of ammonia were injected, thus the walls became saturated with ammonia. The temperature decrease led to a sudden decrease of the wall desorption rate and therefore the measured NH_3 dropped significantly. However, this drop is not related to a change in the sensitivity of the water cluster CI-APi-TOF. Due to the change in the ammonia wall loss and desorption rate with the chamber temperature, a potential effect of temperature on the sensitivity cannot easily be tested. We tried this by measuring constant ammonia from the calibration system, while the instrument is connected to the chamber during a temperature transition. No clear trend was observable during this test. We agree with the referee that this section is not very clearly written. Although our test was disturbed by an initial instrumental drift, we concluded that the temperature dependency is much smaller compared with the effect of relative humidity. Therefore we replaced the section mentioned by the referee with the following text:

The effect of temperature on the sensitivity could not be tested during a dedicated calibration experiment as our calibration setup is not temperature-controlled. However, during a transition from high to low temperature in the CLOUD chamber and constant ammonia injection, no significant change in the measured ammonia was observed, which indicates a weak influence of temperature.

Page 10, Lines 308-310: Rewrite this sentence, removing all information in brackets and either placing it explicitly in the sentence or removing it. Also, should the reference to Figure 4 here actually be to Figure 5?

We rewrote the sentence from "While NH_4^+ (without a water molecule) is the dominant signal for ammonia, $H_4IO_4^+$ ($H_2O \cdot HIO_3H^+$ or $HIO_3 \cdot H_3O^+$) yields the highest signal for iodic acid (higher than HIO_3H^+)" to:

While NH_4^+, without a water molecule, is the dominant signal for ammonia, $H_4IO_4^+$, which is $H_2O \cdot HIO_3H^+$ or $HIO_3 \cdot H_3O^+$, yields the highest signal for iodic acid.

The reference towards Figure 4 (now Figure 5) is correct.

Page 11, Section 3.4: Detection limit calculations require a stable background signal when the instrument is known to be sampling a negative control. Quite a bit of this section discusses contamination issues, which should be made into its own section and kept separate from detection limits.

As a drifting background, e.g. due to contamination issues, can have an influence on the standard deviation of the measurement, this discussion can be important when evaluating detection limits. We changed the title of this Section to "Detection limits and instrumental backgrounds".

Page 11, Lines 326-327: These facts should be moved to the calibration section as an addition to the statement about the capillary NH3 contamination since all of these components can be causing the described time lag in the calibrations and the observations.

As the calibration setup is independent from the CLOUD chamber measurements, the capillary from the NH3 calibration setup was not connected to the instrument during this time, which decreases the instrumental background compared to the situation with the calibration setup connected. For this reason, these arguments are well placed in the discussion of Section 3.4 (Section 3.5 in our revised manuscript).

Page 11, Lines 334-335: This is a sentence fragment and does not belong in the part of the discussion. It should be moved to the discussion of the RH-dependent sensitivity along with context driven by the data presented in Figure 4.

We agree that this sentence belongs to the CLOUD chamber discussion as this effect is especially observed on the chamber walls due to the huge volume of the chamber. We moved this sentence to Section 3.7 (CLOUD chamber characterization) and discuss it for clarification:

The influence of relative humidity on the gas phase concentration of ammonia is shown (time from 29.10. to 30.10.). In addition to the change in sensitivity with relative humidity shown for the water cluster CI-APi-TOF (Section 3.4), a change in humidity can lead to an increased ammonia mixing ratio in the gas phase. This is due to the fact that water molecules can displace adsorbed ammonia on surfaces (Vaittinen et al., 2014). This effect can be pronounced when the chamber walls have been conditioned with high ammonia concentrations. It is important to note that the instrument was characterized for humidity dependency during the following CLOUD13 campaign. While changes in sensitivity with relative humidity were taken into account during CLOUD13, this was not the case during CLOUD12. The observed increase in mixing ratios at this time is a combination of a change in sensitivity of the instrument and an increase in the gas phase concentration of ammonia due to re-evaporation from the wall of the CLOUD chamber. Here, the PICARRO trace can provide insight into the magnitude of both effects indicating that the re-evaporation from the chamber walls dominates over the change in sensitivity.

Page 11, Lines 336-340: Giving approximated detection limits, along with the assumptions being made for HIO3 and the amines in the discussion is alright, so long as it is very clear that these are initial guesses. Where these numbers absolutely do not belong is in Table 1, which should be removed from the manuscript. It is highly likely that these numbers will be used out of context and with disregard for the assumptions made here for the estimation (e.g. not everyone will have a NO3- CI-APi-TOF calibrated for H2SO4 to scale their measurement against for HIO3, along with the assumption that the sensitivity is equal on top of that). The authors need to be clear throughout this work that the estimated mixing ratios are consistent with expectations, BUT that a calibration with known quantities of the target analytes should be performed by anyone wanting to make quantitative measurements of these compounds. Again, any figures showing mixing ratios or amines or HIO3 should be converted back to units of ncps since these estimates are based on tenuous assumptions. Keeping some mention of the potential detection limits in the discussion is alright as it motivates further work in using this instrumental platform for quantitative analysis. For this reason, the title of the manuscript needs to be revised to reflect what species can be quantified and which can only be detected. Without calibration from a primary standard, HIO3 and amines are only detected in this work, while NH3 is quantified and this should be kept clear.

We agree that it should be made very clear that the numbers provided in the table and in the figures are subject to some uncertainty because no direct calibration was applied. However, as outlined in our reply the first major comment, we still would like to keep the numbers as there are good arguments, in our opinion, to keep them. In the revised manuscript we have, however, made very clear that uncertainties exist and that the direct calibrations are lacking. One specific change, relevant for this comment, is the addition of remarks to the numbers provided for DMA and iodic acid in Table 1. An updated version of Table 1, including its caption, is provided in the following:

Table 1. Estimated limits of detection (LOD) for some compounds with high proton affinity, and for iodic acid, measured with the water cluster CI-APi-TOF. The LOD is derived by background measurements at the CLOUD chamber, where LOD = 3•σ (You et al., 2014). σ is defined as the standard deviation of the background signal. The detection limits are based on a measurement at 278 K and 80% RH (1 minute averaging time). The measured instrumental background mixing ratios (mean values) during this time period are also indicated.

Detected compound	**LOD (pptv)**	**Instrumental background (pptv)**	**Measured *m/z* values (Th)**
NH_3 (ammonia)	0.5 ± 0.05	3.73 ± 0.35	18.0338 (NH_4^+); 36.0444 ($(H_2O)NH_4^+$)
$(CH_3)_2NH$ (dimethylamine)*	0.047*	0.058*	46.0651 ($(CH_3)_2NH_2^+$)

HIO_3 (iodic acid)**	0.007**	< LOD**	176.9043 ($(HIO_3)H^+$); 194.9149 ($(HIO_3)H_3O^+$)

*Amine mixing ratios are estimated using the same calibration factor derived for ammonia. This can cause uncertainties. The applicability of this assumption is discussed in Section 3.9.

**Iodic acid mixing ratios are derived from an inter-comparison with a nitrate CI-APi-TOF, which evaluates HIO_3 based on a calibration factor derived for sulfuric acid. This assumption can lead to uncertainties but is necessary because no direct calibration method exists for such low gas phase HIO_3 concentrations.

Page 11, Lines 341-347: This part of the discussion is quite unclear. 'E.g.' should be 'For example,'. What is the peak with the highest count rate for the amines and why does this avoid interference for the mentioned fragments? This is not adequately explained.

As shown in Table 1, the peak with the highest count rate is $(CH_3)_2NH_2^+$ for dimethylamine. Interference with other masses strongly depends on the resolution of the mass spectrometer. As the water cluster CI-APi-TOF was mainly used during experiments on the CLOUD chamber, where either biogenic or urban regions were simulated, there were more compounds injected than just ammonia and/or DMA. Thus, compounds interfering can also be reaction products, e.g., from reaction of alpha pinene or o-cresol with ozone. On the integer mass of $(CH_3)_2NH_3O^+$ (m/z 63) we observe, e.g., interference with at least 5 other species (e.g., a compound tentatively assigned to $C_5H_4^+$).

In the final two sentences, the authors undermine their assumptions regarding the detection of amines identically as they detect ammonia, stating that they omit the use of larger product ions, which will skew the sensitivity of detection. Then, this bias is dismissed as negligible because the water cluster signals are smaller for the bases than ammonia. Clearly, this indicates different reagent ion chemistry and product distribution for the amines relative to ammonia, which is inconsistent with assumption that they are the same and that the NH3 calibration factor can be applied to the calculation of amine mixing ratios and detection limits. This is strong evidence against reporting mixing ratios and detection limits for C2-amines in this work. The strength of this paper lies in the quantitative detection of NH3 and show focus on that data, with discussion of these additional species kept to a minimum.

We want to refer to our manuscript, where we state that $(CH_3)_2NH_2^+ > (CH_3)_2NH_3O^+$ which is also the case for the NH3 chemistry. The studies from Sunner (1988) and Hanson et al. (2011) indicate that the ionisation mechanism is comparable to the NH_3 case. However, we agree that there is an uncertainty in our assumption of scaling the calibration factor from ammonia to dimethylamine. We discussed the applicability of our assumption in a more detailed way in Section 3.9 and refer here to this discussion. Additionally, the following was added to Line 368:

The applicability of the assumption (using the calibration constant derived for ammonia for dimethylamine) is discussed in Section 3.9.

Page 12, Line 361: 'Thus, the sensitivity…' this sentence is redundant with the preceding discussion and can be removed. This paragraph and the one preceding are nice guides to some of the technical considerations for measuring these target analytes and the controls on signal/noise for each of the *ions. The discussion of LOD in these two paragraphs for amines and iodic acid should be changed to discuss signal-to-noise of the instrument.*

According to our replies shown above, we changed the discussion in chapter 3.5 by adding "calculated detection limits" in front of the values discussed for ammonia, while adding "estimated" in front of the values discussed for amines and iodic acid. Together with the note placed below the table (shown above), the reader should be aware that the use of the estimated detection limits creates a degree of uncertainty. As suggested by the referee, we removed the sentence in Line 361.

We updated a sentence in line 362 (line 360 in our revised manuscript):

Besides the **calculated** values for ammonia, Table 1 lists the **estimated** backgrounds and LODs for dimethylamine and iodic acid.

We added "estimated" to a sentence in Line 370:

The instrumental background for $\mathrm{NH_3}$ is higher than the estimated backgrounds for the other compounds shown in Table 1.

Page 12, Line 372: 'up to the tetramer (…' could easily be replaced with 'molecules containing 1-4 iodine atoms' and be much more accurate. This should be changed throughout the manuscript, including Figure 6. Calling these species monomers, dimers, etc suggests that the rest of the atoms are part of a fundamental subunit one would typically find in describing a polymer, which does not seem to be the case here?
If there are fundamental subunits for these I-containing species and the terminology of monomers, dimers, etc holds, then this should be more clearly written to specify the atoms found in remainder of the subunit.

We agree with the referee that 'molecules containing 1-4 iodine atoms' is more accurate than 'monomers, …tetramers'. We adapted our manuscript accordingly, as well as Figure 6 (as shown below in the discussion related to the figures).

During this time period, we observed compounds containing up to 4 iodine atoms.

Page 13, Line 395: The accuracy of the chamber concentrations being much less certain than those from the measurements of NH3 by the CI-APi-TOF should be used earlier on to motivate the need for this instrument being characterized fully.

The instrument shows the correct mixing ratios based on an independent calibration. The chamber concentrations can spread over a huge range and are shown here to give an overview on the response time of the instrument. In addition, it can be estimated how quickly the instrument reacts, e. g., on injections of ammonia or on changes in fan speed. The chamber is suitable for the determination of instrumental backgrounds and detection limits due to the ultra-clean conditions, provided no ammonia was added to the chamber. Measurements in ambient air can also result in large potential mixing ratios, depending on source and transport terms.

Page 13, Lines 400-401: Could this difference in response time during NH3 mixing ratio increases be due to inlet location differences between the instruments inside the chamber? Are the different responses due to concentration gradients as NH3 mixes throughout the chamber? Or are there very different inlet line lengths? The intercomparison description on Page 7, Lines 219-223 are insufficient to determine if these strumental measurements are even capable of being properly compared. The authors suggest that in 'some intercomparison measurements' that the Picarro was hooked up to the *exhaust of the CI-APi-TOF instead of sharing the same sampling line. Surely there are huge losses of NH3 inside the CI-APi-TOF such that it is unreasonable to expect quantitative transfer of NH3 out of the instrument exhaust? This type of setup would dramatically bias an intercomparison and may invalidate its applicability altogether in this work. The authors should re-evaluate whether the experimental setup was sufficiently robust to expect NH3 to be transmitted to both instruments in a manner that does not compromise the sample composition. If the conclusion is that this is not possible, then this section of the manuscript needs to be removed as it is likely invalid.*

As shown in our reply to major comment 2 above, both instruments were connected to the chamber directly with their individual sampling lines. The PICARRO was connected to the exhaust of the water cluster CI-APi-TOF only during a calibration measurement that was carried out during a ~24 hour period. As stated in our text, the change in response time is also due to higher sampling line losses that are, e. g., caused by different sampling flow rates: The water cluster CI-APi-TOF samples air with flow rates of ~20 slm (no core sampling applied), while the PICARRO samples with <1 slm. This is also mentioned in section 2.4 (PICARRO). During all measurements, the flow towards the PICARRO was increased using core sampling (5slm). The connection to the exhaust of the water cluster CI-APi-TOF was arranged directly behind the ion source, where the aim was to increase the flow rate towards the PICARRO to 20 slm to reduce the response time. As we didn't see a sufficient change, this setup was not used during measurements carried out on the CLOUD chamber. During the time period shown at Figure 7 (Figure 8 in our revised manuscript), both instruments were connected to the CLOUD chamber independently, where both instruments were sampling using the flow rates mentioned above. We realized that it leads to confusion when we report these tests without further discussion. As this test is not relevant for our manuscript and for the data shown in this study, we removed the sentence from our manuscript. Next to this, we replaced the sentence in line 401 (previous draft; line 419 in the updated manuscript):

This is due to the much higher LOD of the PICARRO and its much higher sampling line losses that require a considerably longer time for equilibration.

By the following sentence:

This increased response time can be explained by a combination of the longer sampling line (~1.8 m compared to 1.3 m for the water cluster CI-APi-TOF), the lower flow rate (~ 1 slm with a core sampling of 5 slm compared to ~ 20 slm for the water cluster CI-APi-TOF) and the higher detection limit of the PICARRO.

Also, why was a background correction not applied to the Picarro data based on having it sample zero air? The Picarro gas analyzers typically arrive from the factory with a calibration factor and offset applied and can be much more sensitive than the operators' specifications sheets. Given that an independent calibration was done using a permeation device and, presumably an overflow with zero air, the instrument detection limits should have been possible to independently calculate, along with any systematic offset in the instrument response, which could be corrected where this is identified as a factory offset. The calibration of this instrument with external NH3 would have allowed the LOD for the instrument to be determined the same was as it was for the CI-APi-TOF (i.e. using S/N=3 from the blank observations and comparing that to the background measurement). Making the intercomparison with more consistent treatment of the calibrations performed on both instruments would strengthen the discussion throughout this portion of the manuscript.

We evaluated the PICARRO detection limit by using the same background measurements from the CLOUD chamber used for the water cluster CI-APi-TOF, based on the PICARRO calibrations (as shown in a previous comment above). As shown on our reply to major comment 2, there was no instrumental background subtracted for both instruments to show the low instrumental backgrounds of the water cluster CI-APi-TOF. In our revised manuscript, the background of the PICARRO has been subtracted in Figure 8.

Page 14, Line 417: The material used for the sampling line is not discussed. Part of the discussion from literature line losses (Line 426) talks about stainless steel, but this would be atypical for an NH3 sampling inlet. The authors need to clarify this material so the context can be properly evaluated. Given the incredibly long decay time constants from the chamber (on the order of days according to Figure 7?), which are also not presented for the instrument from the calibrations, it is hard to determine the relative order of the effects here. See comments on the calibration figures for some improvements to the manuscript with additional figures that could be made.

We would like to refer to Section 2.2 of our manuscript (“water cluster CI APi-TOF”): “The inlet of the water cluster CI-APi-TOF consists of a stainless steel tube with 1 inch outer diameter that is housed by a stainless steel body that also holds the ion source and the counter electrode; additional parts made of PEEK insulate the electrodes.” The reason for using stainless steel instead of e.g. glass is that the CLOUD chamber is- next to low contamination studies- also designed for studying effects of ions on atmospheric physics and chemistry. Thus, stainless steel is needed when voltages are applied to the chamber (see Duplissy et al., 2016). As mentioned in our comments above, we added a new Section (3.3) discussing response times during calibrations (together with a Figure (4)). The decays shown for the chamber measurements (that are in the order of days) are discussed in Section 3.7 (CLOUD chamber characterization). These long decays are also due to the huge surface of the CLOUD chamber (26.1 m^3 volume), where ammonia desorbs from the walls over a long time.We updated a sentence in Line 452 (updated manuscript):

At CLOUD, the sampling line is made of stainless steel and is kept as short as possible. The total length is still 1.3 m because the sampling line protrudes into the chamber over a distance of 0.5 m in order to sample air from the well-mixed center region of the chamber.

Page 14, Lines 426-434: The water effects on line losses seem to be ignoring an established effect from the literature. Water on inlet surfaces can allow weak acids and bases to dissociate into their conjugate compounds on the surface, increasing the partitioning to the surface. Adsorption on surface sites alone is too simple of an interpretation. Further to this, data is not presented that decouples the effect of the inlet lines from the desorption of NH3 from the CLOUD chamber walls. The value for inlet desorption is only described as ‘it can take a long time’. It would be nice to see some form of time constant determined for the inlet to return to initial conditions and a reflection on whether this waiting period is reasonable compared to replacing the lines between experiments.

We thank the referee for pointing out the additional effect of wall uptake followed by dissociation. We will include a remark regarding this effect in the revised manuscript. Added to line 460:

Water on surfaces can affect the uptake or release of ammonia. Vaittinen et al. (2014) showed that increased humidity can displace ammonia from surfaces. Additionally, water on surfaces can allow weak acids and bases to dissociate into their conjugate compounds on the surface, thereby affecting the partitioning to the surface (Coluccia et al., 1987).

Furthermore, we agree that a remark should be added that it is currently not possible to distinguish sampling line effects from chamber wall effects. Added to line 470:

At CLOUD, the sampling lines are attached to the chamber and cannot easiliy be removed during the experiments. Thus, it is not possible to quantitatively distinguish between interactions with the surface of the sampling line and the surface of the CLOUD chamber.

This effect should clearly be further investigated in the future as it can have an important effect on the measurements. Replacing the sampling lines is, however, not an option during the CLOUD chamber runs as the sampling lines cannot easily be removed from the chamber. With the inlet line being attached to the chamber during the runs, desorption of ammonia from the inlet lines cannot easily be decoupled from desorption from the chamber walls. Thus, a time constant for inlet line desorption would be associated with huge uncertainties and variations depending on the chamber conditions.

Page 14, Line 441: All of Section 3.8 needs to be rewritten in terms of signal instead of mixing ratios, except where estimates are discussed. Figures referred to in this section should all report signal using units of ncps since a direct calibration has not been performed.
The comments on how the estimated calibration factor and the observations in the chamber are consistent within the factor of 10-100 uncertainty for DMA put in the chamber can be retained to demonstrate that the assumptions for the CI-APi-TOF calibration factor are also likely within this same factor of 10-100. In particular, the line of reasoning on Page 15 from Lines 461-464 is based on biased expectations where an arbitrary correction estimated at a value of 2 would bring the observations 'into even better agreement' with the expected mixing ratios, but this does not have much factual basis since the concentrations shown in Figure 8 span an order of magnitude depending on wall losses and chamber dilution. Perhaps stating that the observations fall within the expected range of values is sufficient for this section and the speculation on correction factors can be removed since a direct calibration of DMA was not actually performed.

In our replies to previous comments we have argued that dimethylamine mixing ratios should be reported instead of ncps.

However, we agree with the referee that the discussion regarding Figure 9 and the approach of deriving an uncertainty for the dimethylamine measurements should be revised.

We have implemented the following modifications to the data shown in Figure 9:

(1) We know from a previous study regarding dimethylamine measurements inside the CLOUD chamber (Simon et al., 2016) that the life time of dimethylamine is dominated by wall loss for the low mixing ratios relevant for this study. The wall loss life time is 432 s for a fan speed of 12%. From previous chamber measurements, we know that the wall loss life time decreases by a factor of 4 when the fan speed is increased from 12% to 100%. Thus, we used 108 s for a fan speed of 100%. Therefore, the shaded area (which previously included the dilution life time) has been replaced with a line that takes only the wall loss life time into account (gray line).

(2) Since we know from Simon et al. (2016) and from the CLOUD measurements of the current study that dimethylamine sticks to the chamber walls, a wall loss correction is required for the mixing ratios measured with the water cluster CI-APi-TOF, a wall loss correction factor of 1.96 was therefore applied to the data, which is based on a flow rate of 18.5 slm, a diffusivity of 0.1 $cm^2 s^{-1}$ and a sampling line length of 1.3 m.

After implementing the described modifications, the mean ratio between measured and calculated/expected DMA is 3.48. We take this value as the uncertainty of the dimethylamine measurments.

We changed this Section (Section 3.9 in our revised manuscript), where the focus is now on the discussion regarding the uncertainty of our approach (scaling of the calibration factor from ammonia to dimethylamine). As the chamber background shown in this chapter is based on the estimated mixing ratios, we now show the comparison between the wall loss lifetime and the estimated mixing ratios in panel a). This Figure compares our approach directly with calculated mixing ratios, thus, it is important to keep the unit mixing ratio, where we show a range (factor +3.48/-3.48) now in our time series in panel b).

As mentioned in Section 3.5 and shown in Table 1, the same calibration factor derived for ammonia was used to estimate the mixing ratio of dimethylamine. We caution, that this assumption can lead to uncertainties as the sensitivity of the measurement is expected to depend on the proton affinity of the measured substance (Hanson et al., 2011). To estimate the validity of this assumption, we compared the mixing ratios measured with the water cluster CI-APi-TOF with the calculated mixing ratios for a period when dimethylamine was actively injected into the CLOUD chamber. A chamber characterization for dimethylamine was already conducted by Simon et al. (2016), where the wall loss lifetime was determined as 432s for condtions where the chamber walls acted as a perfect sink (12% fan speed). Additionally, as discussed in Section 3.7, we use a lifetime of 108s at 100% fan speed (change in a factor of 4 when the fan speed is changed from 12% to 100%). The dilution life time during CLOUD13 is 6000 s and represents the maximum possible life time when wall loss would be negligible. Thus, the wall loss lifetime used in this study gives a lower limit for dimethylamine mixing ratios in the CLOUD chamber. Figure 9a shows the time period when dimethylamine was added. Since it takes a certain time until the stainless steel pipes of the gas dilution system are saturated with dimethylamine there is a short time delay between the switching of a valve that allows dimethylamine to enter the chamber and the rise in the measured dimethylamine mixing ratio. Once the lines are conditioned and the dimethylamine is homogenously mixed into the chamber, the measured and estimated mixing ratios are generally in good agreement with each other when the wall loss life time is used to estimate the mixing ratios. Fluctuations in the measured mixing ratio can be explained by changes in the fan speed. To estimate the consistency of the approach of scaling the calibration factor derived for ammonia to estimate dimethylamine mixing ratios, we use the ratio between the mixing ratio calculated for the Water Cluster CI-APi-TOF and the calculated mixing ratios based on the wall loss lifetime for the CLOUD chamber. For these measurements, we estimated a wall loss rate in the sampling lines of ~1.96 for dimethylamine, where a diffusivity of 0.1 cm^2s^{-1} was used (Freshour et al., 2014; Simon et al., 2016). The mean deviation between the estimated dimethylamine mixing ratio and the calculated mixing ratio is 3.48 indicating that the approach of scaling the calibration factor derived for ammonia introduces uncertainties within a factor of ~3.5. The deviations at the end of the time series shown in Figure 9a are caused by nucleation experiments in which high concentrations of other vapors are used. During these stages a significant uptake of dimethylamine on particles can explain the discrepancy between measured and expected dimethylamine. Figure 9b shows a measurement of the chamber background for dimethylamine carried out during CLOUD13 over a time period of 5 days. The mean instrumental background for the time period shown in Figure 9b is ~0.14 pptv (for a temperature of 278 to 290 K and a relative humidity between ~50 and 60 %). The background values shown here are close to the background values obtained for 80% RH and 278 K (see Table 1). The observed variations are in a range of ~0.1 to 0.3 pptv provided that the measurement is not interrupted, e.g., due to the replenishment of the water source that humidifies the flow for generating the reagent ions (which explains the first drop of the background measurement in Figure 9b). The estimated detection limits shown here are below or at similar detection limits reported in previous publications (You et al., 2014; Simon et al., 2016).

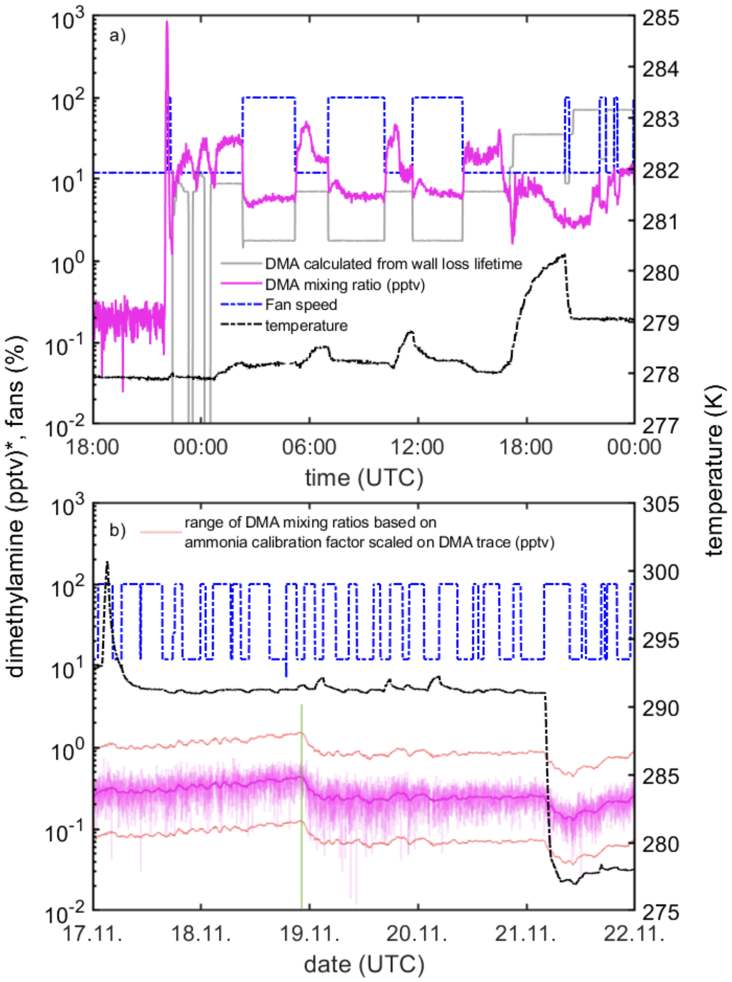

Figure 9: Dimethylamine mixing ratios (magenta line) during the CLOUD13 experiment. The dashed black line shows the temperature inside the CLOUD chamber. The dashed blue line shows the fan speed. Panel a) shows the dimethylamine signal during active injection into the chamber. The grey line indicates the dimethylamine mixing ratio in the chamber calculated from the MFC settings and the wall loss lifetime. The upper limit for the uncertainty in the dimethylamine mixing ratio is a factor of ~3.5 (see text for details). Panel b) shows a measurement of background dimethylamine in the chamber over a period of 5 days, when there was zero dimethylamine flow. We consider this to be due to instrumental background and not to an actual dimethylamine background in the chamber. The thin red lines show the possible range of dimethylamine based on the scaled calibration factor (factor 3.48, 95% CL). The thick magenta line indicates a moving average of the dimethylamine background measurement. The water source has been replenished during the period shown (green line). The mean instrumental background of dimethylamine over this period is ~0.14 pptv.

*Note that the dimethylamine mixing ratio is determined with the calibration factor for ammonia.

Page 15, Line 473: The specific analytes discussed are ammonia, dimethylamine, and iodic acid and this should be specified here. Depending on the actual chemical species comprising the remaining iodine oxides (or up to tetramers of iodic acid if this is the case), the iodine species detected can be made more chemically specific in the conclusion. Based on Table 2, iodine oxides seems to me to be the best term, and it could be used effectively throughout the manuscript.

We adjusted this section according to the comment from the referee:

The present study demonstrates the successful application of a water cluster CI-APi-TOF during controlled chamber experiments for ammonia, dimethylamine and iodic acid measurements. During the experiments involving iodide, neutral clusters containing up to 4 iodine atoms are detected.

Page 15, Line 474: Neither fast time response or time resolution values are given in the manuscript. Indeed, they could yield wonderful proof of the developed technique and should be included. See comments on Figures with some suggestions.

We thank the referee for this suggestion. As shown in our previous comments, we added a Figure as well as a section discussing the time response of the water cluster CI-APi-TOF.

Page 16, Lines 488-491: In addition to having high proton affinity, this perfluorinated amine is also a strong surfactant which promotes its ionisation further.

We thank the referee for this interesting information but have suggested not to implement any changes to the manuscript regarding this comment.

Page 16, Conclusions: Revise in light of all other changes to the manuscript.

We added a sentence concerning the estimated iodic acid detection limits for clarification:

As there is no established calibration method for iodic acid, detection limits have been derived under the assumption that HIO_3 is measured with the same efficiency as sulfuric acid, for which the nitrate CI-APi-TOF is calibrated for. The estimated LOD for the water cluster CI-APi-TOF regarding iodic acid was as low as 0.007 pptv.

Page 27, Table 1: Remove. The only true detection limit measured is for NH3 and the rest are estimated based on assumptions that may have significant error. Further to this, the LODs were acquired over 2.5 hours of signal acquisition, while the measurements are reported at 1 minute intervals. A more accurate assessment of detection limits would have been determined at similar timescales, using about 20-30 background measurements.

We want to refer to our replies above, where we discussed the changes made to Table 1 and where we also discussed the reason for using 2.5 hour time scales.

Page 29, Figure 1: Numeric or alphabetic labeling of the instrument parts with corresponding descriptions in the caption would make this diagram easier to follow as a lot of the text is obscured by color or very small. The 'argon+oxygen+water vapour' could be replaced with 'Ar + O2 + H2O'.

We thank the referee for this suggestion. We changed the Figure accordingly. We also added a panel b) showing the technical details of the ion source in a more detailed way. This additional information was requested by the other referee.

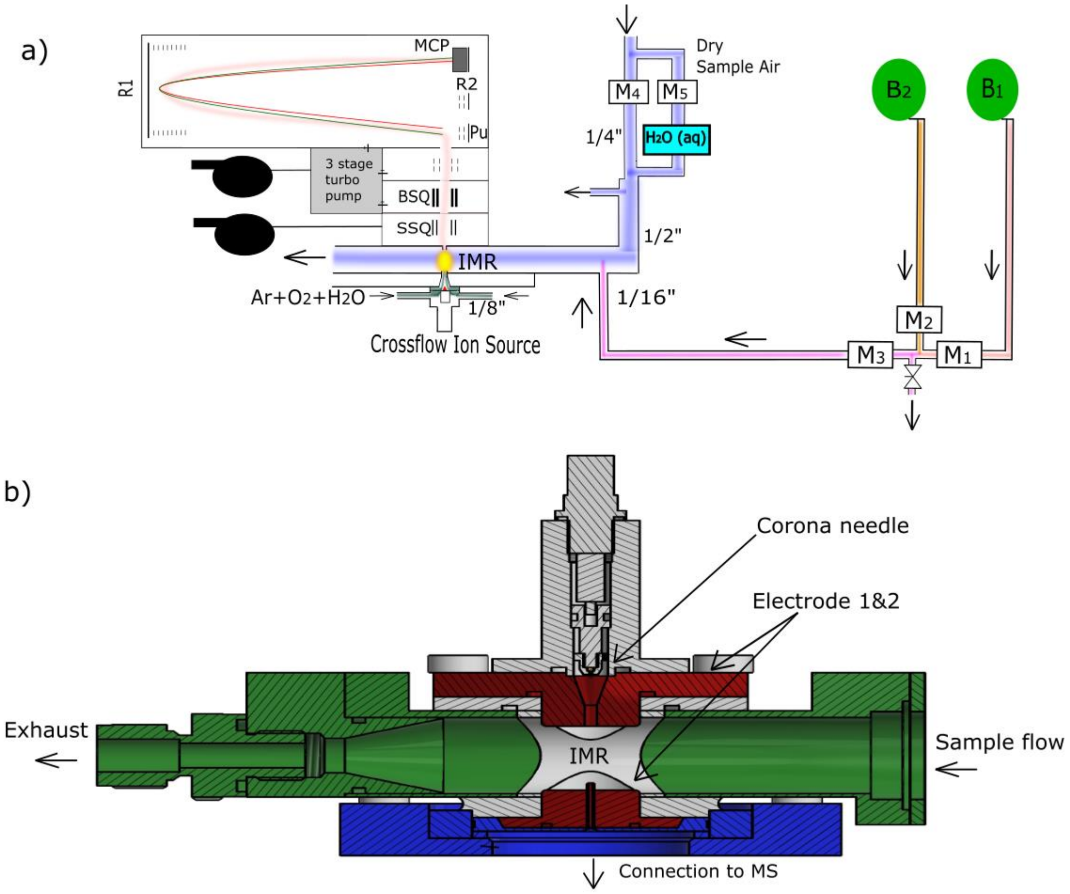

Figure 1: The experimental setup of the water cluster CI-APi-TOF during ammonia calibration is shown in panel a) The blue color indicates the sample flow. It consists of a mixture of 80% nitrogen and 20% oxygen. A portion of the sample flow can be humidified with a water bubbler (H_2O aq) to achieve different relative humidities. B_1 represents the ammonia gas bottle, while B_2 represents a gas bottle containing pure nitrogen. There are five mass flow controllers (MFCs; labeled as M_{1-5}) allowing two dilution steps. Three MFCs (M_1, M_2, M_3) control the amount of ammonia that is added through a 1/16’’ capillary into the center of the sample flow, where the second dilution stage occurs. The reagent ions (i.e., protonated water clusters) are produced when the ion source gas (argon, oxygen, water vapor) passes a corona needle at a positive high voltage (detailed in panel b). The calibration setup is disconnected during the measurements at the CLOUD chamber to reduce backgrounds (leakage from the 1/16’’ capillary). Details of the ion source used during CLOUD13 are shown in panel b. The primary ions are guided towards the sample flow using a counter electrode (Electrode 1). Additionally, a funnel is used to accelerate the primary ions towards the sample flow. A second electrode (Electrode 2) is installed directly in front of the pinhole of the mass spectrometer. The ions enter the mass spectrometer through a capillary on the top of Electrode 2.

Page 31, Figure 3: If a fit is forced through the origin, then a measure of instrument signal while ultra pure zero air should be included as a blank to determine if there is an offset in detection, particularly for NH3. For the HIO3 measurement, the x-axis is a scaled value based off of H2SO4 detection and not a true measure of HIO3 and a comparison of ncps would be more useful to describe the sensitivity of the H3O+ CIAPi- TOF versus the NO3-. For this second plot, was any background value subtracted?

As shown in our comments above, the deviation between forced and unforced slope is small (9.48e-8 or 1.35%). We changed the label of the x-axis to clarify that our mixing ratios for iodic acid are scaled from the calibration factor for sulfuric acid determined for the Nitrate CI-Api-TOF and added a sentence under the Figure. For the comparison between the mass spectrometers, the background of the NO3- Api-TOF was subtracted.

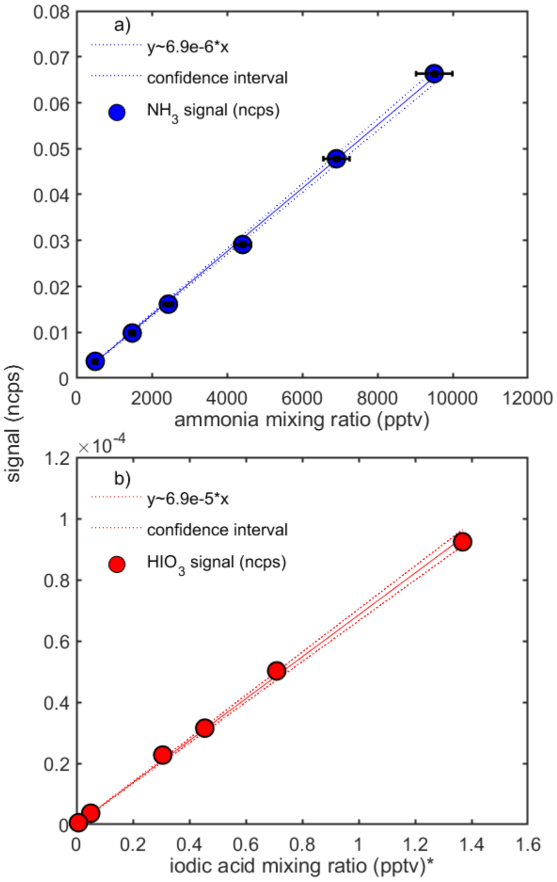

Figure 3: Calibration curves for ammonia (a) and iodic acid (b) at 40% relative humidity. The *y*-axes show the normalized counts per second (ncps) measured with the water cluster CI-APi-TOF. The ammonia mixing ratios are determined from the calibration set-up and the iodic acid mixing ratios are taken from simultaneous measurements with a nitrate CI-APi-TOF at the CLOUD chamber. The systematic uncertainty of the iodic acid mixing ratios is estimated as +100%/-50% (Sipilä et al., 2016). The inverse slopes from the linear fits yield the calibration factors (see equation (1) and (2)).
*Note that the iodic acid mixing ratio is derived by applying a calibration factor for sulfuric acid to the nitrate CI-APi-TOF data.

An important component of instrument performance that can be evaluated while doing calibrations such as these is instrument response times (both with increasing and decreasing analyte concentration) from 0-95 % of max signal and 100-5 %. The authors claim that the instrument has a rapid time response with high time resolution, yet no such data is presented in figures and no numeric values reported. This is critical to report as it also helps provide clear context in the interpretation of the chamber observations.

We thank the referee for raising this important point. As shown in our replies above (reply to major comment 2) we have added a section (3.3) indicating response times during calibrations.

Page 32, Figure 4: Was this sensitivity dependence on RH used to correct the dataset shown from the chamber? With the changes in temperature, if there is water in the chamber, then there will be a change in sensitivity that should be applied and may change the interpretation of the datasets.

During CLOUD13, the change in sensitivity due to RH was taken into account and thus, all data (including detection limits and instrumental backgrounds shown here) are corrected for these changes. However, during CLOUD12, this change in sensitivity was not taken into account when another version of the ion source was used. This is also mentioned in our manuscript in Section 3.7. We added a sentence to Table 1 for clarification (see reply to a comment on page 17-18 above).

Page 33, Figure 5: The x-axis should also be signal-based units. The caption states that there is no RH dependence, yet there is a clear difference within the regressed data that shows this and suggests that it is also statistically significant between 40 to 80 % RH (color suggests that T is constant for these), and consistent with the findings for detection of NH3 increasing in sensitivity with increasing RH.

We want to draw attention that Figure 5 is now Figure 6. We changed the x-axis label of Figure 6 to clarify that our mixing ratios are scaled values and added a sentence under the Figure. The intention here was to show that the dependency on the relative humidity is small compared with the temperature dependency. We changed our caption for clarification.

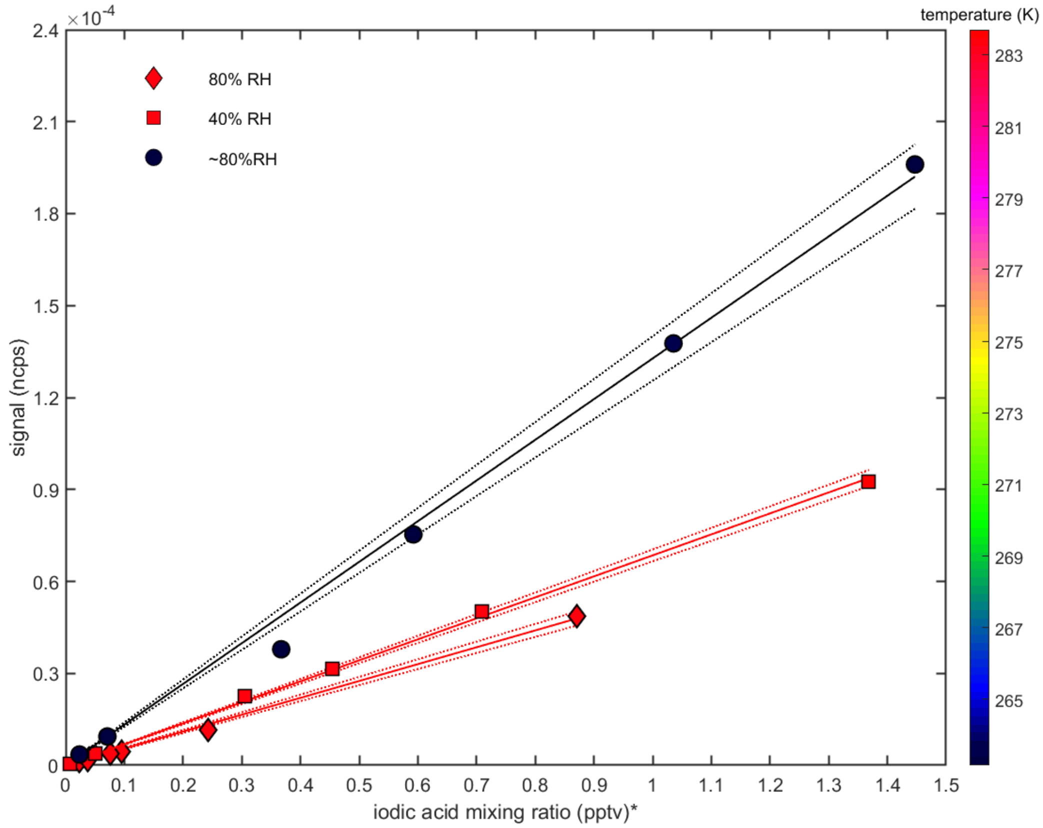

Figure 6: Calibration curves for iodic acid at different relative humidities and temperatures in the CLOUD chamber. The normalized counts per second (*y*-axis) are shown against the iodic acid mixing ratio measured with a nitrate CI-APi-TOF (*x*-axis). The sensitivity increases at lower temperatures, while no strong dependency on relative humidity is found at 283 K.
* Note that the iodic acid mixing ratio is derived by applying a calibration factor for sulfuric acid to the nitrate CI-APi-TOF data.

Page 34, Figure 6: The logarithmic scale for the marker size should be provided here.
The nomenclature replacing 'monomers', etc. should be revised as necessary.

We want to draw attention that Figure 6 is now Figure 7. We changed our Figure 7 according to the referees comment. We added a sentence in the caption giving the marker size of the logarithmic scale.

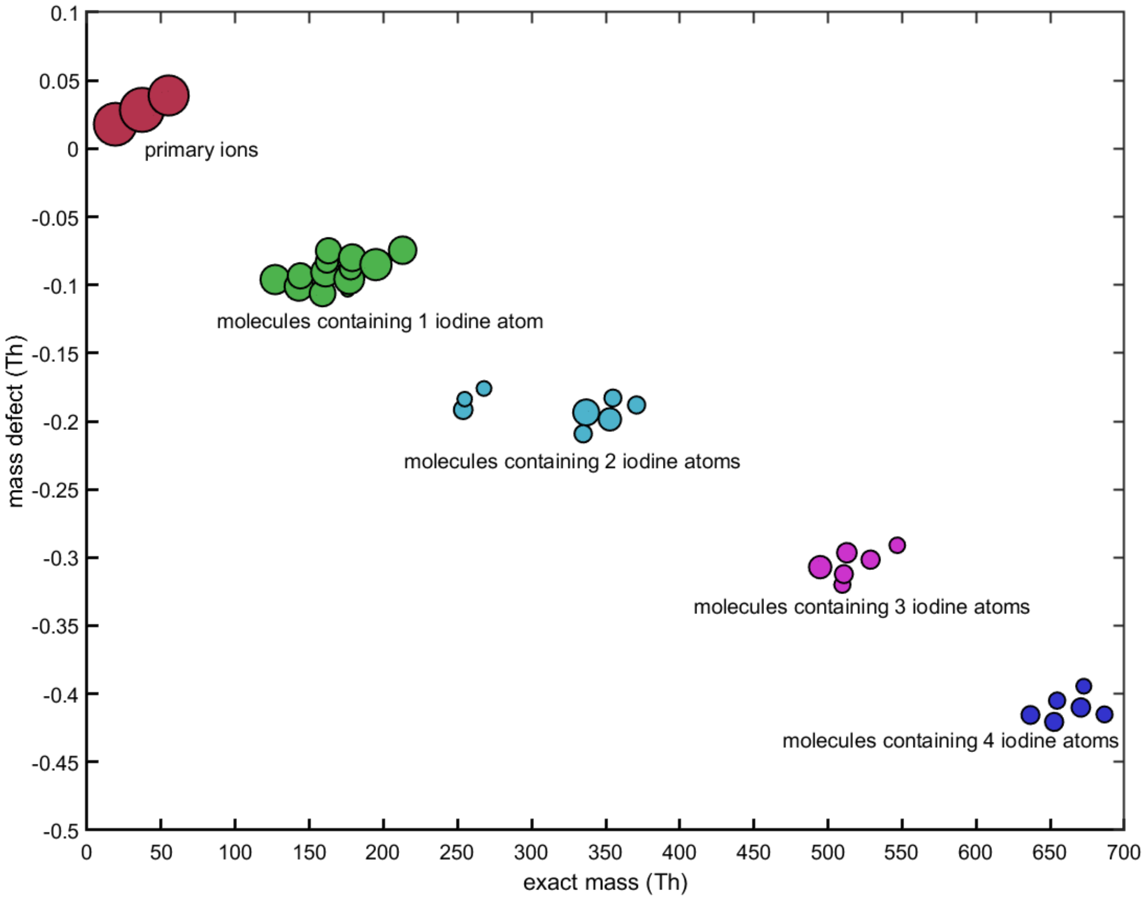

Figure 7: Mass defect plot for the iodine compunds, as well as the most prominent reagent ions, during a CLOUD experiment on new particle formation from iodine. The estimated iodic acid mixing ratio is ~0.98 pptv. The *y*-axis shows the mass defects of the compounds (see Table 2 and text for details), while the *x*-axis shows the absolute masses. The size of the symbols is proportional to the measured signal intensities on a logarithmic scale (from $1.24\cdot10^{-6}$ to 14.04 ions/s).

Page 35, Figure 7: The two data components on the y-axis should be separated with a ',' and not with a '/' which implies division. The font size of everything in this figure needs to be made larger. Depending on the outcome of the details of the intercomparison assessment, the Picarro data may need to be removed from this figure, especially if it was connected to the exhaust line of the CI-APi-TOF here. Panels a) and b) are not described in the caption and should be. An additional panel that may be of use in the intercomparison is a regression of the CI-APi-TOF measurement against that of the Picarro when both detection limits are properly accounted for (i.e. properly background corrected based on calibrations that were performed). In the case where one instrument has a higher detection limit than the other (which seem likely to be the case given the sensitivity of the CI-APi-TOF), then the higher LOD should be used as the cut-off for the intercomparison.

We want to draw attention that Figure 7 is now Figure 8. We changed our Figure according to the comments from the referee. We showed in our comments above that the PICARRO was measuring while being connected to the chamber directly (i.e. not through the exhaust line). We also showed that the background of the water cluster CI-APi-TOF is not subtracted in this plot. In our updated version, the PICARRO background is subtracted. The PICARRO calibrations were shown in our comments above, where we think that the addition of a third panel to this plot wouldn't add more information as the range of mixing ratios is different compared to the water cluster CI-APi-TOF.

We added a relative humidity trace to Figure 8 as this Figure shows CLOUD12 data, where the change in sensitivity with RH was not taken into account for the water cluster CI-APi-TOF.

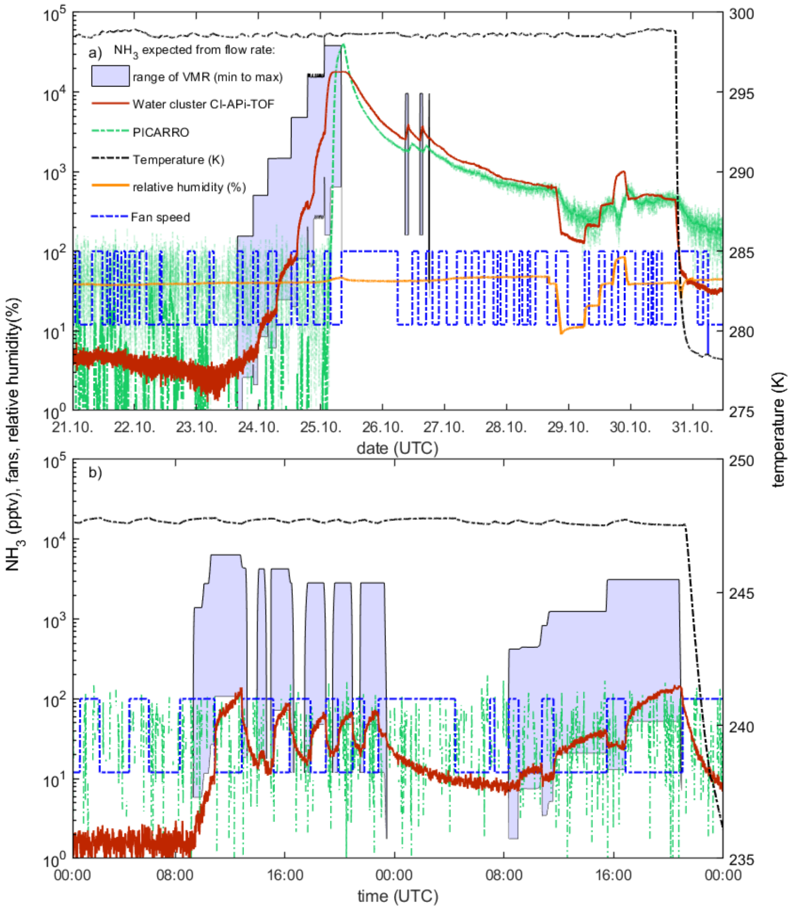

Figure 8: Inter-comparison between calculated (shaded blue area) and measured ammonia mixing ratios (PICARRO: solid green line; water cluster CI-APi-TOF: solid red line) at CLOUD. The PICARRO background (~200 pptv) has been subtracted, while no background was subtracted from the water cluster CI-APi-TOF. The temperature inside the chamber is indicated by the dashed black line. The speed (% of maximum, 397 revolutions per minute) of the two fans that mix the air inside the chamber is shown by the dashed blue line. The calculated ammonia mixing ratios (based on the calculated injection of ammonia into the chamber from the MFC settings) have a wide range due to uncertainties of the ammonia loss rate in the chamber. We display the maximum calculated range assuming, for the lower limit, that the chamber walls act as a perfect sink (wall loss dominated, 25s and 100 s lifetime for fan speeds 100% and 12%, respectively) and, for the upper limit, no net uptake of NH_3 on the walls and a loss rate determined by dilution (6000 s lifetime). For higher fan speeds, the lifetime decreases due to increased turbulence and, in turn, increased wall loss rate. Relative humidity is indicated by the orange line. The water cluster CI-APi-TOF reacts rapidly to changing conditions, such as the ammonia flow into the chamber, relative humidity, temperature or fan speed. At low concentrations, the ammonia lifetime is determined by the wall loss rate (panel b and initial stages of panel a). However, at high ammonia concentrations, the walls of the CLOUD chamber progressively become conditioned

and a source of ammonia, with corresponding increases in the ammonia lifetime and the time to reach new equilibria at lower ammonia flow rates (later stages of panel a).

Page 36, Figure 8: Add a marker where the H3O+ source water was changed on panel a) and make a note of it in the caption. Convert the mixing ratio to ncps and comment on the expected range of values with an assumed calibration constant in the caption.It is surprising that a direct calibration of DMA was not performed since permeation devices for this compound are commercially available, as they are for NH3.

We want to draw attention that Figure 8 is now Figure 9. As shown in our comments above, we changed this Figure according to the changes made to chapter 3.9:

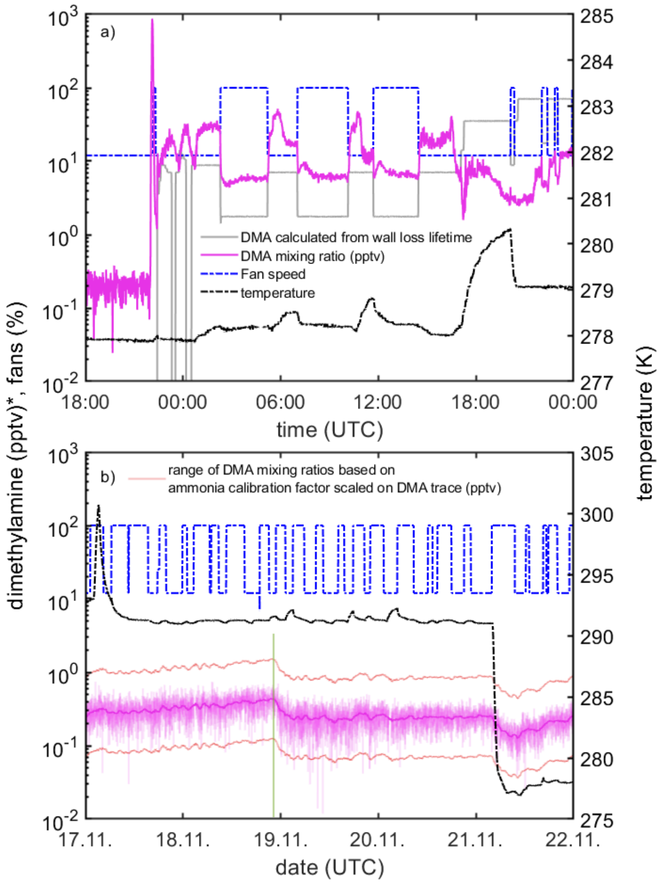

Figure 9: Dimethylamine mixing ratios (magenta line) during the CLOUD13 experiment. The dashed black line shows the temperature inside the CLOUD chamber. The dashed blue line shows the fan speed. Panel a) shows the dimethylamine signal during active injection into the chamber. The grey line indicates the dimethylamine mixing ratio in the chamber calculated from the MFC settings and the wall loss lifetime. The upper limit for the uncertainty in the dimethylamine mixing ratio is a factor of ~3.5 (see text for details). Panel b) shows a measurement of background dimethylamine in the chamber over a period of 5 days, when there was zero dimethylamine flow. We consider this to be due to instrumental background and not to an actual dimethylamine background in the chamber. The thin red lines show the possible range of dimethylamine based on the scaled calibration factor (factor 3.48, 95% CL). The thick magenta line indicates a moving average of the dimethylamine background measurement. The water source has been replenished during the period shown (green line). The mean instrumental background of dimethylamine over this period is ~0.14 pptv.

*Note that the dimethylamine mixing ratio is determined with the calibration factor for ammonia.

Response to Anonymous Referee 2 on “Measurement of ammonia, amines and iodine species using protonated water cluster chemical ionization mass spectrometry”

We thank the referee for the constructive comments that help improving our manuscript. In the following, the comments of the referee are shown in black, shaded font. Our replies are shown in blue font. Text that has been added or revised in the manuscript is shown in red font.

Though powerful, CIMS is not an absolute measurement technique. A good, defensible calibration is necessary. The manuscript should do a better and clearer job indicating that only the ammonia detection is calibrated with a primary standard and that the mixing ratios for the other species are estimated qualitatively. It is too easy for the reader to lose sight of this fact, since no differentiation between calibrated and estimated mixing ratio results is made in the table or the figures.

We agree with the referee that the manuscript should clearly indicate that the mixing ratios for amines and iodine species are not determined by a direct calibration. We updated the relevant text passages accordingly throughout the manuscript. Major changes are listed below:

- Estimated mixing ratios shown in this manuscript are now marked in tables and figures with an asterisk and a comment that indicates that these mixing ratios are estimated.

- We added a discussion related to our approach of deriving mixing ratios for dimethylamine from the ammonia calibration factor in Section 3.9. We refer to this discussion when mixing ratios of dimethylamine are mentioned.

- We added a comment to Figure 3 stating that the estimated uncertainty for the HIO3 values is +100%/-50% (same as reported by Sipilä et al., 2016).

Updated changes in the manuscript are detailed in the replies to the technical comments below.

The main product of this work is the development of the ion source. However, details of the ion source are lacking in the text and figures. Figure 1 is more of a cartoon than a schematic. The details that are given in the text (page 5, lines 143 – page 6, 162) are difficult to translate to Figure 1. For example, a counter electrode and capillary are described in the text but not identified in the figure. Dimensions are given in the text that are not shown in the figure. This makes it unnecessarily difficult for the reader to follow how the ion source truly works and evaluate its performance. Also, details such as tubing length and flow rates for the calibration dilution components should also be given.

We thank the referee for this helpful comment. We added a panel b) to our Figure 1 showing a more detailed drawing of the ion source. This drawing is now also described in our text. The added text is shown in red font below.

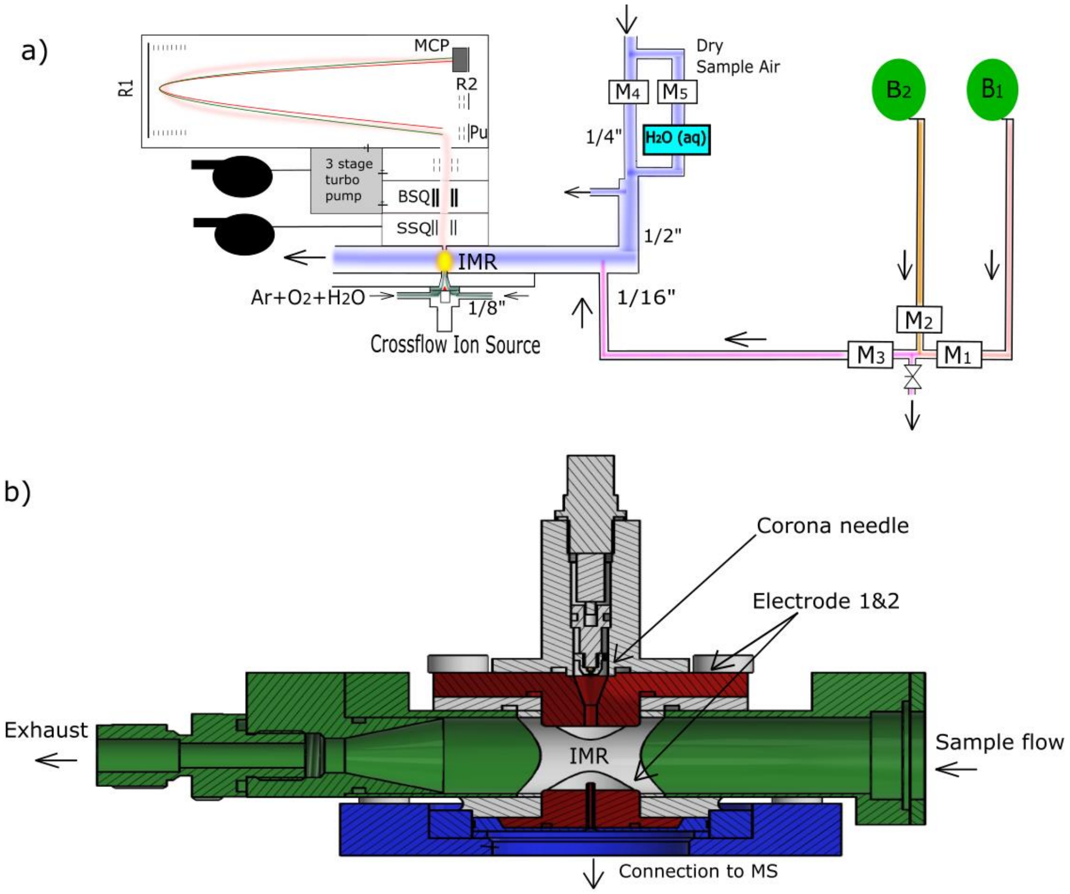

Figure 1: The experimental setup of the water cluster CI-APi-TOF during ammonia calibration is shown in panel a) The blue color indicates the sample flow. It consists of a mixture of 80% nitrogen and 20% oxygen. A portion of the sample flow can be humidified with a water bubbler (H_2O aq) to achieve different relative humidities. B_1 represents the ammonia gas bottle, while B_2 represents a gas bottle containing pure nitrogen. There are five mass flow controllers (MFCs; labeled as $M_{1\text{-}5}$) allowing two dilution steps. Three MFCs (M_1, M_2, M_3) control the amount of ammonia that is added through a 1/16'' capillary into the center of the sample flow, where the second dilution stage occurs. The reagent ions (i.e., protonated water clusters) are produced when the ion source gas (argon, oxygen, water vapor) passes a corona needle at a positive high voltage (detailed in panel b). The calibration setup is disconnected during the measurements at the CLOUD chamber to reduce backgrounds (leakage from the 1/16'' capillary). Details of the ion source used during CLOUD13 are shown in panel b. The primary ions are guided towards the sample flow using a counter electrode (Electrode 1). Additionally, a funnel is used to accelerate the primary ions towards the sample flow. A second electrode (Electrode 2) is installed directly in front of the pinhole of the mass spectrometer. The ions enter the mass spectrometer through a capillary on the top of Electrode 2.

Modified in Section 2.2 (Line 143):

A schematic drawing of the calibration setup and the ion source is shown in Figure 1. The gas mixture for the ion source is composed of argon, oxygen and water vapor. It is introduced from two lines placed in the opposite direction to each other at an overall flow rate of ~2.6 slm (Figure 1a). The Electrodes of the ion source are displayed in red colors in Figure 1b. The connection to the mass spectrometer is shown using blue color. The 1" sampling line and the inlet (22 mm inner diameter) consist of stainless steel and are shown in green color. Components used for insulation are shown in white colors. A total sample flow rate of ~ 19.5 slm is maintained by a vacuum pump and a mass flow controller. The overall length of the sampling line connecting the CLOUD chamber and the ion molecule reaction zone is 1.3 m. A voltage of 3600 V is applied to the corona needle while 500 V are applied to the conically-shaped counter electrode (Electrode 1 in Figure 1b) made of stainless steel. The housing of the ion source is made of polyether ether ketone (PEEK). The ion source gas and the generated reagent ions flow through a funnel (smallest inner diameter 2.5 mm) before they mix with the sample flow. A small capillary (inner diameter of 0.8 mm) is located opposite of the funnel (Electrode 2 in Figure 1b). The electric field between the counter electrode and the capillary (at ground potential) accelerates the ions towards the entrance of the mass spectrometer. The pinhole plate (pinhole inner diameter of 350 µm) and the capillary are in electric contact and ~0.8 slm flow through the capillary and the pinhole into the mass spectrometer. The measured product ions are generated in the ion-molecule reaction zone (IMR, yellow area in Figure 1a) at atmospheric pressure. The dimension of the IMR is defined by the distance between the counter Electrode and the capillary (~ 16.4 mm). After passing the pinhole, the ions are transported through two quadrupoles (Small Segmented Quadrupole, SSQ and Big Segmented Quadrupole, BSQ) towards the detection region of the mass spectrometer (Micro-Channel Plate, MCP; pressure is approx. 1×10^{-6} hPa). The estimated reaction time is <1 ms. This short reaction time allows the measurement ofhigh ammonia mixing ratios (up to ~10 ppbv) without significant depletion of the reagent ions, which would be the case when using an ion source design for the measurement of sulfuric acid (Eisele and Tanner, 1993; Kürten et al., 2011), which is typically present at much lower concentrations than ammonia. The principle of a cross-flow ion source was introduced by Eisele and Hanson (2000) who used this technique to detect molecular sulfuric acid clusters. In more recent studies, this technique was used for the measurement of ammonia (Nowak et al., 2002; Nowak et al., 2006; Hanson et al., 2011).

The comparison of the LOD and low background for this water cluster CI-APi-TOF instrument to others is not as straight forward as presented here. Here the calculated detection limits are based on a 2.5 hour measurement of synthetic air generated from liquid nitrogen and oxygen with a 1 minute average for a single data point (See 2.1 and Table 1). This leads to the question are the values given in Table 1 those after sampling the synthetic air for 2.5 hrs or the values for the full 2.5 hr time period? If is the latter, what was the time required, if any, for the signal to drop to the 3 pptv level after removal of a 5-10 ppbv ammonia calibration addition?

The values shown in Table 1 are values shown for the entire 2.5 hour time period (i.e. we didn't wait for 2.5 hours before measuring these values). If we splitted this period into 20-minute-periods, our LOD wouldn't change significantly:

Period	*Calculated detection limit (pptv)*
Period 1	0.42
Period 2	0.81
Period 3	0.39
Period 4	0.51
Period 5	0.74
Period 6	0.39
Period 7	0.42

The mean value of these periods would yield a mean LOD of 0.525 pptv. A time series of this period is shown below:

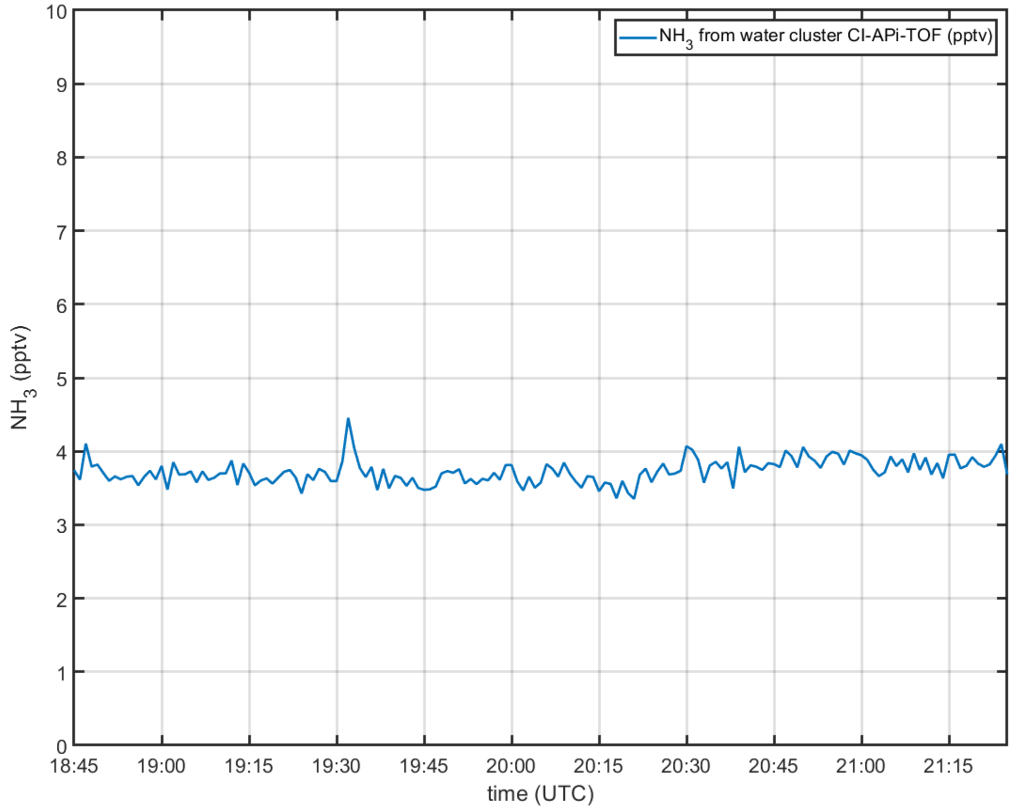

The initial text at table 1 ("The calculated detection limits are based on a 2.5 hour measurement at 278 K and 80% RH (averaging time of single data points: 1 minute).") may be misleading. Thus, we removed the extra information about the time scale of the measurement (these changes on table 1 are shown in another reply below). The calibrations shown in our study are carried out by stepping the mixing ratios from high to low values using the technique shown in our new section 3.3 (which is described at another comment below). Thus, we can show response times for small steps (e.g. from 10ppbv to 7ppbv), where we don't have data for a decay from e.g. 10 ppbv to 3 pptv.

Unfortunately, no data is presented to support the low background and LOD claim. The time series in Figure 7 is not applicable because the effects of the CLOUD chamber cannot be separated from those of the instrument. Here a time series showing the addition of ammonia and the instrument response to its removal in the set-up shown in Figure 1 would be extremely useful. This would also better mimic field measurements, for example, measurements at a ground site when wind shifts from a region with ammonia sources to one without. Then a better comparison could be made to other instruments and their field measurements. Other factors, affecting signal stability, i.e., LOD, include vibrations, for instruments on mobile platforms such as vehicles or aircraft, and heat, for instruments in trailers, on towers, in vehicles, and in aircraft. In many ways the controlled laboratory conditions associated with the CLOUD chamber provide an ideal environment. While the work presented here is impressive, care should be taking comparing the performance there to that reported in a field campaign. This also highlights the necessity of evaluating instrument performance in-situ for every campaign and not relying on spec sheets or one laboratory test.

We agree with the referee that vibrations, e.g. when measuring on an aircraft or mobile vehicles can affect the LOD. However, despite its ultra clean air, the CLOUD chamber in particular is not an ideal place. Although it is possible to purge the lines at CLOUD for long time periods, the surface of the

CLOUD chamber is huge (26.1 m^3). Thus, precursors from previous experiments can desorb for a long time. Next to this, the instruments are limited by the length of the sampling lines (1.3m) and by the flow rate (in order to maintain the overpressure of the chamber, there is an upper limit at ~20 slm). Furthermore, the CLOUD chamber is not an ideal place compared to e.g. field stations in regard to boundary conditions like vibrations. The CLOUD chamber is located in the east hall at CERN, with the instrument presented here installed alongside <20 other instruments (including their pumps and other installations) on a steel platform. There are sufficient sources for possible vibrations along the CLOUD chamber. Figure 7 (Figure 8 in our revised manuscript) shows a measurement of the water cluster CI-APi-TOF on the chamber with no instrumental background deducted. Thus, the low background shown in Figure 7 (close to 1pptv) should give sufficient evidence on the detection limits shown in this paper.

No data is shown to support that this is a fast time resolution measurement either. Similar to my previous comment, a time series showing the signal decay after removal of ammonia would be helpful in evaluating the time response of the instrument. Also, if this is a fast time resolution measurement why does it take at least 20 minutes (Page9, line 254) for the signal to reach the mean value of a steady state measurement used in the calibration curve shown in Figure 3a?

We thank the referee for this comment. We added a section (3.3, response times) to describe the time resolution of the water cluster CI-APi-TOF. Changes made to the manuscript are shown below.

3.3 Response times

The response time of the water cluster CI-APi-TOF is defined as the characteristic time needed for the instrument to react on changes in the ammonia mixing ratio. The response time takes into account two processes. These are the time needed until the instrument reacts on changes in the mixing ratio and the time needed until a steady state is established in the lines. In the following, we define the response time as the time required for the instrument to reach 95% of the new mixing ratio being injected. Figure 4 indicates the typical response times of the water cluster CI-APi-TOF during calibrations (here at 60% relative humidity). It shows a decay between two calibration steps when the injected ammonia is reduced from 9509 pptv to 6911 pptv and a rise in the signal when the ammonia mixing ratio is increased from 500 pptv to 9509 pptv. Panel a) indicates a clear difference between the time needed until the instrument reacts on the changes in the mixing ratio (red line) and the time needed until the lines reach 95% of the new steady state (black line). We expect the same behavior for a decay from 9509 to 500 pptv, however, the mixing ratios were gradually reduced during calibrations. Thus, for the gradual decays, the time needed for the lines to reach a new equilibrium is rather short. While the variation of instrumental response time is small (6 to 10 seconds for decays from 9509 to 6911 pptv and 18 to 25 seconds for a rise from 500 pptv to 9509 pptv, respectively), the time until a steady state is established in the lines varies depending on precursor conditions and relative humidity (see Section 3.8). Thus, an estimation of a response time can vary significantly. In our experiments, the response times (including both processes described above) during a rise in ammonia mixing ratio varied between 535 seconds (20% relative humidity) and 890 seconds (60% relative humidity, shown in Figure 4). For a decay of ammonia mixing ratio from 9509 to 6911 pptv the response times vary between 37 seconds and 54 seconds.

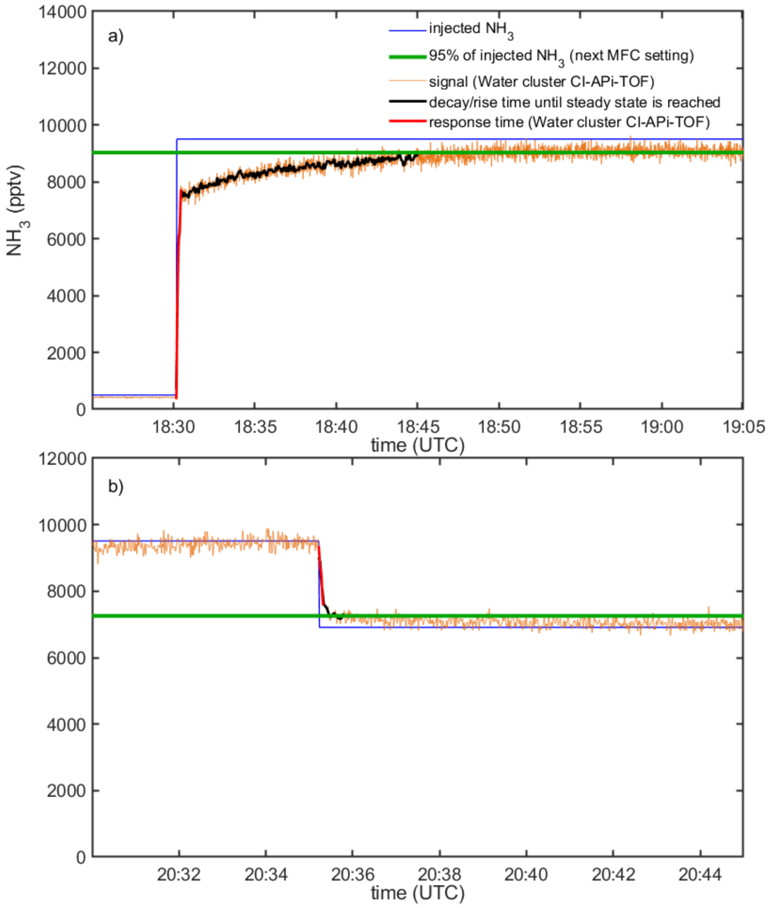

Figure 4: Response time of the water cluster CI-APi-TOF during calibrations at 60% RH. The injected ammonia level is shown by the blue line. The signal of the water cluster CI-APi-TOF is shown by the grey line (here the data are shown with a 1 second time resolution (no averaging applied)). The black line shows the response time until a steady state (panel a)) or 95% of the final measured concentration is reached (panel b)). This response time is defined as the sum of the response time of the water-cluster CI-APi-TOF (red line) and the time required until the lines reach a new steady state. See text for details.

Page 1 line 17, If the authors did not explicitly demonstrate the quantitative measurement of diamines (see page 16 line 504) then they should not be mentioned in the abstract. Similarly, amines should be changed to dimethylamine since that is the only amine for which data is shown. Speculative future application should be saved for the discussion in the manuscript not the abstract.

We agree with the referee and updated the text accordingly:

Here we describe the design and performance of a new water cluster Chemical Ionization-Atmospheric Pressure interface-Time Of Flight mass spectrometer (CI-APi-TOF). The instrument selectively measures trace gases with high proton affinity such as ammonia and dimethylamine, which are important for atmospheric new particle formation and growth.

Page 1 line 22, Classifying 10 ppbv ammonia as high is very subjective. What is high for the CLOUD experiment may be typical or even low for many areas as seen in many of the publications cited in this manuscript.

While You et al (2014) reported ammonia mixing ratios of ~200 to 2000 pptv in remote areas (forests), ~ 50 to 100 ppbv of ammonia have been measured next to sources (after fertilization in an agricultural area; v. Bobrutzki et al., 2010). Thus, we consider 10 ppbv as a rather high mixing ratio. Nevertheless, we replaced the word “high” with the word “elevated” in the abstract.

Page 5 line 151, Please show how the reaction time is estimated here.

The reaction time can be determined by using the calibration (VMR_{NH3} = (1/6.9*10-6 pptv) * ncps) and the equation [NH3] = 1/(t*k)*ncps. Making use of the fact that 1 pptv corresponds to 2.5e+07 molecule cm-3, the relationship

$$\frac{1}{t*k} = (1/(6.9 \times 10^{-6} pptv)) \cdot 2.5 \times 10^{7} molecule\ cm^{-3}\ pptv^{-1}$$

yields a reaction time of 0.14 s for a collision-limited reaction rate of 2e-09 cm^3 $molecule^{-1}$ s^{-1} (Sunner et al., 1988). This reaction time is consistent with an estimate that takes into account the geometry and the applied electric field across the ion-molecule reaction region. However, due to electric field and flow inhomogeneities no exact reaction time can be derived using only the geometry and the flows.

Page 5, line 158, Are all tubing diameters given in the manuscript representing the outer diameter? The inner diameter should also be given as that affects the flow characteristics.

We agree and added information about the inner diameter of the stainless steel sampling line. For the remaining tubing we do not consider the inner diameter important and report only the outer diameters.

The Electrodes of the ion source are displayed in red colors in Figure 1b. The connection to the mass spectrometer is shown using blue color. The 1” sampling line and the inlet (22 mm inner diameter) consist of stainless steel and are shown in green color. Components used for insulation are shown in white colors.

Page 6, line 180, What is the uncertainty in the mixing ratio of the ammonia bottle and who is the manufacturer? It should be given here with the calibration set-up details not later in the manuscript discussing the calibration results.

We updated the text according to the comment of the referee:

The ammonia was taken from a gas bottle containing an NH_3 mixing ratio, *B*, of 100 ppmv diluted in pure nitrogen (Air Liquide, ±5% uncertainty for the certified NH_3 mixing ratio) that is diluted in two steps, where MFCs (shown as M_n in Figure 1a) are used to obtain different set points for the volume mixing ratio (Figure 1a).

Page 7 line 199, What is meant by ‘a fairly short equilibration time’? Minutes, hours, seconds? Please show the time series of the ammonia signal as a function of the step changes in ammonia added in addition to the calibration curve shown in Figure 3.

We added a new section (3.3) indicating the response time of the water cluster CI-APi-TOF. In the discussion of this section estimated equilibration times are reported.

Page 7, line 209-210, How is the assumption given here that both sulfuric and iodic acid are detected with the same efficiency by the nitrate CI-APi-TOF justified? Wouldn’t this make the estimated iodic mixing ratio a limit in some regard?

We agree with the referee that the estimation of the iodic acid mixing ratios rely on the assumption that sulfuric acid and iodic acid are detected with the same efficiency by nitrate ionization.

Unfortunately, there is no established method for a direct calibration with iodic acid (neither for the nitrate nor the water cluster CI-APi-TOF). Thus, for the nitrate CI-APi-TOF the same calibration factor as for sulfuric acid has been used. This method can at the moment be regarded as the best that can be done and has been adopted elsewhere (see Sipilä et al., 2016). However, we agree with the referee that this results in a lower limit for the iodic acid concentration since sulfuric acid reacts at the kinetic limit with the reagent ions. We added marks on mixing ratios shown throughout this manuscript related to iodic acid to show more clearly that the mixing ratios are estimated.

Page 7, line 219, The text mentions the PICARRO being connected to the exhaust line of the water cluster CI-APi-TOF for comparison. Is this comparison discussed or shown in the manuscript? If not, why? Or am I incorrect that Figure 7 is showing PICARRO measurements being made from its own sampling line on the CLOUD chamber and the comparison is shown in Figure 7? The text also mentions tests when the flow is increased to the PICARRO. When is this used? If used when the PICARRO is sampling the exhaust of the water cluster CI-APi-TOF is the flow to the water cluster CI-APi-TOF increased also? Again, another instance lacking enough detail to evaluate the experiment and experimental results.

As the PICARRO was only connected to the exhaust from the water cluster CI-APi-TOF for a ~24 hour-period (which was not during the campaign but during tests after the CLOUD campaign), this intercomparison is not shown in our manuscript. One reason why we didn't show the direct comparison was that the time until the PICARRO reached a steady state was too long and thus, no clear steady state for the PICARRO was reached during these calibrations. We updated the section comparing water cluster CI-APi-TOF and PICARRO for clarification. We realized that it leads to confusion when we report these tests without further discussion. Thus, we removed the sentence from our previous manuscript.

Added to Section 2.4, PICARRO:

The G1103-t was installed at the CLOUD chamber with its own sampling line coated with Sulfinert (Restek GmbH, Germany), where the coating reduced the losses of ammonia to the sampling line walls considerably.

Added to Section 3.7:

The time from 25.10 to 26.10 shows a steep increase in the PICARRO trace, while the ammonia trace derived from the water cluster CI-APi-TOF flattens out at 20 ppbv of ammonia. This indicates that the primary ions of the water cluster CI-APi-TOF are depleted at high vapor concentrations. It is important to mention that not only ammonia concentrations were elevated at this time, but also other vapor concentrations were rather high. During the CLOUD13 campaign, where a revised version of the ion source was used (see Section 3.2), the significant depletion of primary ions has been observed only at ammonia mixing ratios of 40 ppbv.

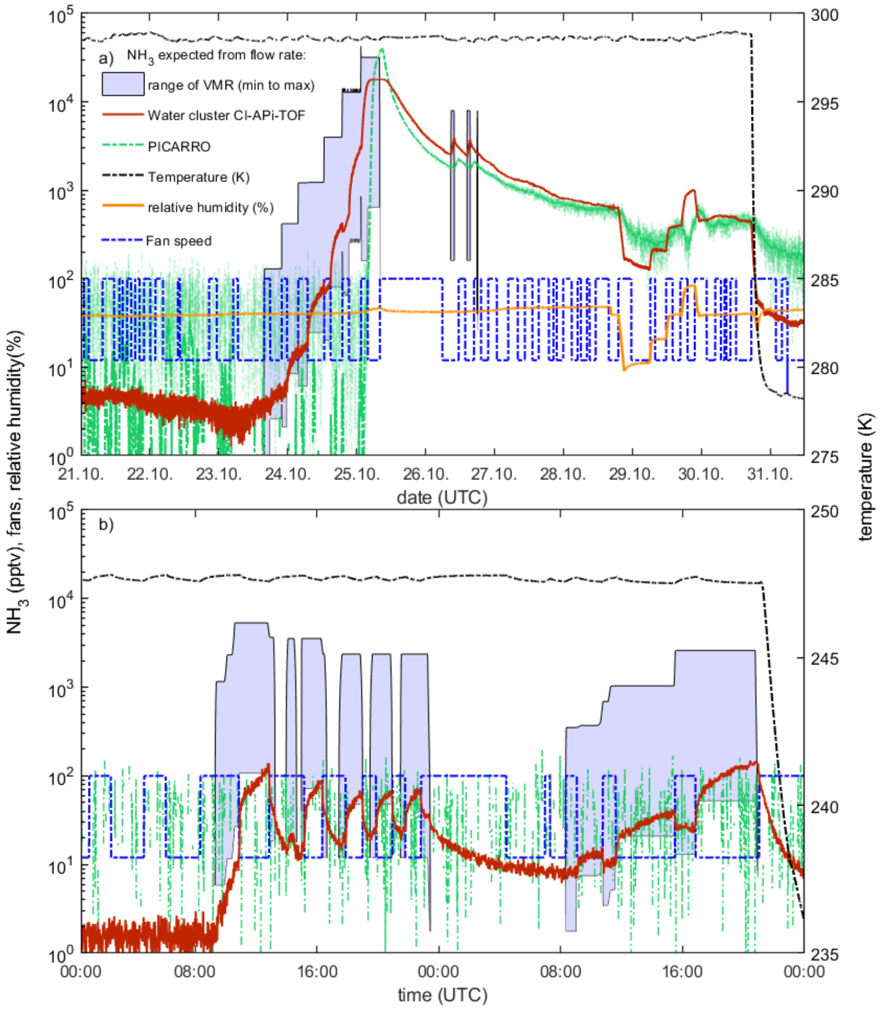

Figure 8: Inter-comparison between calculated (shaded blue area) and measured ammonia mixing ratios (PICARRO: solid green line; water cluster CI-APi-TOF: solid red line) at CLOUD. The PICARRO background (~200 pptv) has been subtracted, while no background was subtracted from the water cluster CI-APi-TOF. The temperature inside the chamber is indicated by the dashed black line. The speed (% of maximum, 397 revolutions per minute) of the two fans that mix the air inside the chamber is shown by the dashed blue line. The calculated ammonia mixing ratios (based on the calculated injection of ammonia into the chamber from the MFC settings) have a wide range due to uncertainties of the ammonia loss rate in the chamber. We display the maximum calculated range assuming, for the lower limit, that the chamber walls act as a perfect sink (wall loss dominated, 25s and 100 s lifetime for fan speeds 100% and 12%, respectively) and, for the upper limit, no net uptake of NH$_3$ on the walls and a loss rate determined by dilution (6000 s lifetime). For higher fan speeds, the lifetime decreases due to increased turbulence and, in turn, increased wall loss rate. Relative humidity is indicated by the orange line. The water cluster CI-APi-TOF reacts rapidly to changing conditions, such as the ammonia flow into the chamber, relative humidity, temperature or fan speed. At low concentrations, the ammonia lifetime is determined by the wall loss rate (panel b and initial stages of panel a). However, at high ammonia concentrations, the walls of the CLOUD chamber progressively become conditioned and a source of ammonia, with corresponding increases in the ammonia lifetime and the time to reach new equilibria at lower ammonia flow rates (later stages of panel a).

Page 9, line 264, I am confused by the use of ppm in this context. Please clarify.

We updated the text according to the comment of the referee:

The fit is forced through the origin; however, even when the fit is not constrained, the resulting slope is essentially the same (the results for the slopes/sensitivities differ by 1.35%).

Page 9, lines 282- page10, line 286, This supports my earlier comment that every instrument needs to be evaluated in the in-situ setup employed.

We agree with the referee that instrument calibration can differ depending on the setup. It is important to mention here that between the setups applied during CLOUD12 and CLOUD13, several parameters changed in parallel:

- The ion source was different (other dimensions of inner diameter of inlet).
- The voltages applied to the ion source were different.
- The voltages applied to SSQ and BSQ area of the mass spectrometer were different.
- The flow rate through the ion source (primary ions and sample flow) was different.

Thus, a change in the calibration factor is expectable.

Page 11, line 337-338, This is fairly deep into the manuscript before stating that the calibration factor for ammonia is used for dimethylamine and pyridine. It should be made clear to the reader earlier.

We marked tables and figures with an asterisk and a comment that indicates that these mixing ratios are estimated. We also added a subsection in Section 2.2 (water cluster CI APi-TOF, line 180-184):

When mixing ratios for dimethylamine are presented, the same calibration factor is used. This approach can introduce uncertainty as the proton affinity, as well as transmission efficiency differ for dimethylamine compared to ammonia. However, previous studies showed that the ionization efficiency from protonated water clusters is collision-limited for both compounds, ammonia and dimethylamine (Sunner et al., 1988; Hanson et al., 2011). The applicability of this approach is discussed in Section 3.9; it is estimated that the mixing ratios for dimethylamine are correct within a factor of ~3.5.

Page 27, Table 1, It should be noted here that only ammonia was directly calibrated and the other calibration factors were assumed or parameterized from other measurements.

We agree and updated Table 1 to indicate more clearly that the mixing ratios are estimated:

Table 1. Estimated limits of detection (LOD) for some compounds with high proton affinity, and for iodic acid, measured with the water cluster CI-APi-TOF. The LOD is derived by background measurements at the CLOUD chamber, where LOD = 3•σ (You et al., 2014). σ is defined as the standard deviation of the background signal. The detection limits are based on a measurement at 278 K and 80% RH (1 minute averaging time). The measured instrumental background mixing ratios (mean values) during this time period are also indicated.

Detected compound	**LOD (pptv)**	**Instrumental background (pptv)**	**Measured values (Th)**	***m/z***

NH_3 (ammonia)	0.5 ± 0.05	3.73 ± 0.35	18.0338 (NH_4^+); 36.0444 ($(H_2O)NH_4^+$)
$(CH_3)_2NH$ (dimethylamine)*	0.047*	0.058*	46.0651 ($(CH_3)_2NH_2^+$)
HIO_3 (iodic acid)**	0.007**	< LOD**	176.9043 ($(HIO_3)H^+$); 194.9149 ($(HIO_3)H_3O^+$)

*Amine mixing ratios are estimated using the same calibration factor derived for ammonia. This can cause uncertainties. The applicability of this assumption is discussed in Section 3.9.

**Iodic acid mixing ratios are derived from an inter-comparison with a nitrate CI-APi-TOF, which evaluates HIO_3 based on a calibration factor derived for sulfuric acid. This assumption can lead to uncertainties but is necessary because no direct calibration method exists for such low gas phase HIO_3 concentrations.

Page 29, Figure 1, This figure needs better labeling of the parts, consistent with the description in the text. Include the lengths of tubing. Consider a blow-up insert of the ion source with more detail.

We thank the referee for this helpful comment. We have updated Figure 1 accordingly (see reply to major comment 2 above).

Page 31, Figure 3, Why no x-axis error bars in panel b? Page 9, line 259 seems to suggest that there is a factor of 2 uncertainty in the iodic acid mixing ratio determined by the nitrate CI-APi-TOF.

We added a sentence stating the overall uncertainty accorind to Sipilä et al. (2016) to the Figure. As the data will most likely shift systematically, adding error bars to panel b of Figure 3 would only show the region where the data could shift, but not the error of the measurement.

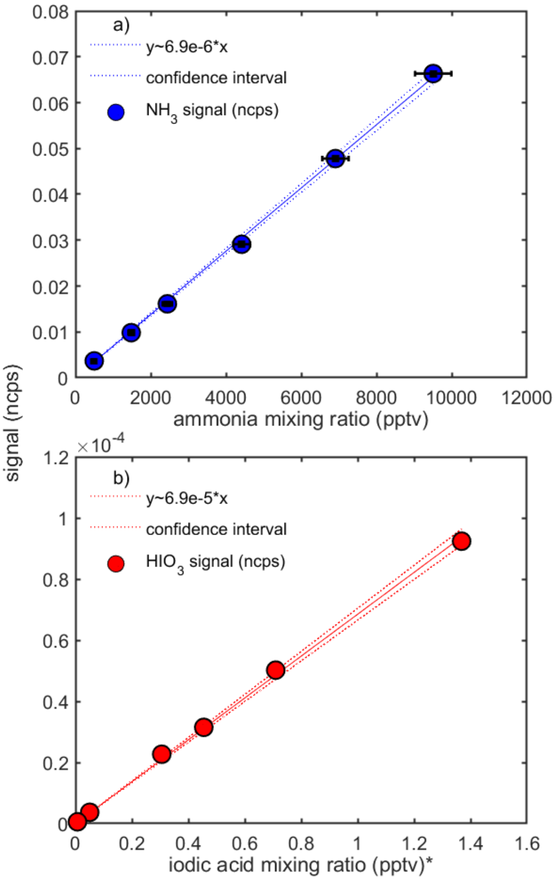

Figure 3: Calibration curves for ammonia (a) and iodic acid (b) at 40% relative humidity. The *y*-axes show the normalized counts per second (ncps) measured with the water cluster CI-APi-TOF. The ammonia mixing ratios are determined from the calibration set-up and the iodic acid mixing ratios are taken from simultaneous measurements with a nitrate CI-APi-TOF at the CLOUD chamber. The systematic uncertainty of the iodic acid mixing ratios is estimated as +100%/-50% (Sipilä et al., 2016). The inverse slopes from the linear fits yield the calibration factors (see equation (1) and (2)).
*Note that the iodic acid mixing ratio is derived by applying a calibration factor for sulfuric acid to the nitrate CI-APi-TOF data.

Page 35, Figure 7. Figure 7 is very busy. The agreement between the water cluster CI-APi-TOF and the PICARRO is mediocre, especially when noting that the ammonia mixing ratio access is logarithmic, though for the most part they are trending in the same direction. However, what is causing the deviation observed 29.10 – 30.10 where the water cluster CI-APi-TOF shows a significant ammonia drop and then increase that does not correlate with fan cycling or temperature changes?

We want to draw attention that Figure 7 is now Figure 8. There are several reasons for deviations between the PICARRO and the water cluster CI-APi-TOF (high detection limits (PICARRO) and depletion of primary ions (water cluster CI-APi-TOF)). Those are stated in our updated text. The mentioned deviations observed between 29.10. and 30.10. are explained in the updated text and shown in the following:

The influence of relative humidity on the gas phase concentration of ammonia is shown (time from 29.10. to 30.10.). In addition to the change in sensitivity with relative humidity shown for the water cluster CI-APi-TOF (Section 3.4), a change in humidity can lead to an increased ammonia mixing ratio in the gas phase. This is due to the fact that water molecules can displace adsorbed ammonia on surfaces (Vaittinen et al., 2014). This effect can be pronounced when the chamber walls have been conditioned with high ammonia concentrations. It is important to note that the instrument was characterized for humidity dependency during the following CLOUD13 campaign. While changes in sensitivity with relative humidity were taken into account during CLOUD13, this was not the case during CLOUD12. The observed increase in mixing ratios at this time is a combination of a change in sensitivity of the instrument and an increase in the gas phase concentration of ammonia due to re-evaporation from the wall of the CLOUD chamber. Here, the PICARRO trace can provide insight into the magnitude of both effects indicating that the re-evaporation from the chamber walls dominates over the change in sensitivity. The time from 25.10 to 26.10 shows a steep increase in the PICARRO trace, while the ammonia trace derived from the water cluster CI-APi-TOF flattens out at ~20 ppbv of ammonia. This indicates that the primary ions of the water cluster CI-APi-TOF are depleted at high vapor concentrations. It is important to mention that not only ammonia concentrations were elevated at this time, but also other vapor concentrations were rather high. During the CLOUD13 campaign, where a revised version of the ion source was used (see Section 3.2), the significant depletion of primary ions has been observed only at ammonia mixing ratios of ~40 ppbv.

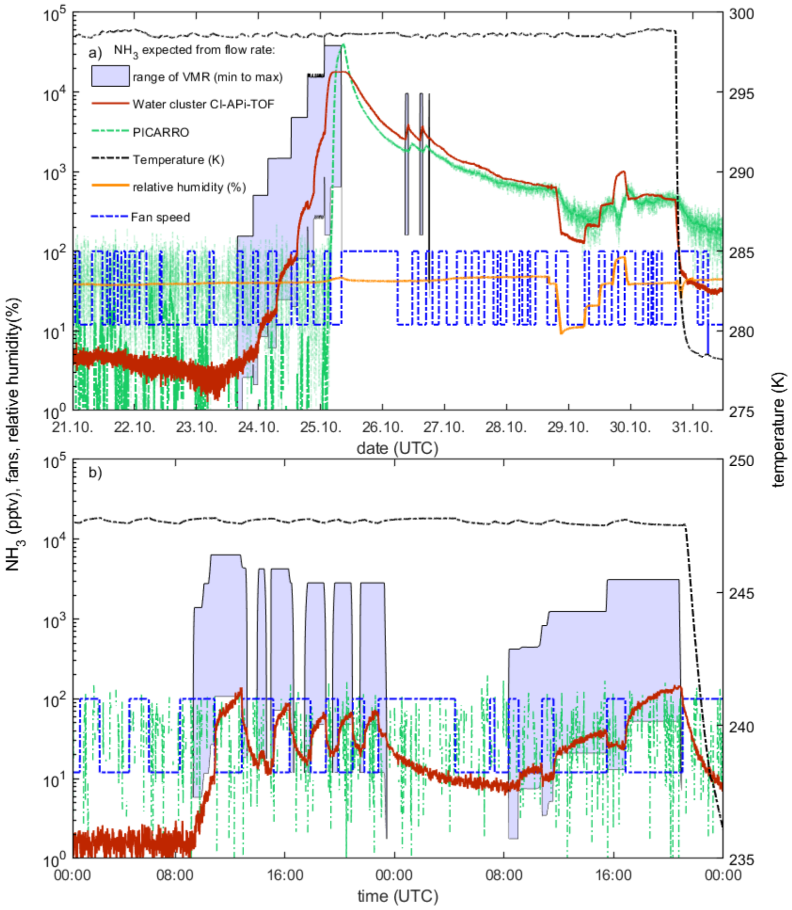

Figure 8: Inter-comparison between calculated (shaded blue area) and measured ammonia mixing ratios (PICARRO: solid green line; water cluster CI-APi-TOF: solid red line) at CLOUD. The PICARRO background (~200 pptv) has been subtracted, while no background was subtracted from the water cluster CI-APi-TOF. The temperature inside the chamber is indicated by the dashed black line. The speed (% of maximum, 397 revolutions per minute) of the two fans that mix the air inside the chamber is shown by the dashed blue line. The calculated ammonia mixing ratios (based on the calculated injection of ammonia into the chamber from the MFC settings) have a wide range due to uncertainties of the ammonia loss rate in the chamber. We display the maximum calculated range assuming, for the lower limit, that the chamber walls act as a perfect sink (wall loss dominated, 25s and 100 s lifetime

for fan speeds 100% and 12%, respectively) and, for the upper limit, no net uptake of NH_3 on the walls and a loss rate determined by dilution (6000 s lifetime). For higher fan speeds, the lifetime decreases due to increased turbulence and, in turn, increased wall loss rate. Relative humidity is indicated by the orange line. The water cluster CI-APi-TOF reacts rapidly to changing conditions, such as the ammonia flow into the chamber, relative humidity, temperature or fan speed. At low concentrations, the ammonia lifetime is determined by the wall loss rate (panel b and initial stages of panel a). However, at high ammonia concentrations, the walls of the CLOUD chamber progressively become conditioned and a source of ammonia, with corresponding increases in the ammonia lifetime and the time to reach new equilibria at lower ammonia flow rates (later stages of panel a).

List of relevant changes made in the manuscript

- We highlighted throughout the manuscript, where our mixing ratios are based on direct calibrations and where we derived the mixing ratios based on calibrations for different substances. All fiugres and tables have been updated accordingly, where we now show an asterix whenever a mixing ratio is estimated. Under each figure or table, we added a hint with an asterix telling how the mixing ratios are estimated.
- We replaced “C2-amines” and “amines” with “dimethylamine” throughout the manuscript for clarification about the substances that have been measured in this study.
- A discussion about the uncertainty of the estimation of dimethylamine mixing ratios has been added to Section 3.9.
- We added a Section 3.3 (“response times”) to clarify the response times of the water cluster CI-APi-TOF. In this Section, we also added a new figure showing how the instrument reacts on changes in ammonia mixing ratios.
- We changed the figures showing the comparison with the PICARRO measurements, where we now added a relative humidity time series. In addition, the instrumental background of the PICARRO has been substracted.
- We edited our Figure 1 showing the calibration setup of the instrument, where we now added a Panel b) which shows a detailed drawing of the ion source that has been used during our studies.

Measurement of ammonia, amines and iodine species using protonated water cluster chemical ionization mass spectrometry

Joschka Pfeifer[1,2], Mario Simon[2], Martin Heinritzi[2], Felix Piel[2,a], Lena Weitz[2,b], Dongyu Wang[3], Manuel Granzin[2], Tatjana Müller[2], Steffen Bräkling[4], Jasper Kirkby[1,2], Joachim Curtius[2], and Andreas Kürten[2]

[1]CERN, Geneva, 1211, Switzerland
[2]Institute for Atmospheric and Environmental Sciences, Frankfurt Am Main, 60438, Germany
[3]Paul Scherrer Institute, Villigen, 5232, Switzerland
[4]TOFWERK AG, Thun, 3600, Switzerland

[a]now at: Ionicon Analytik GmbH, 6020 Innsbruck, Austria
[b]now at: GSI Helmholtzzentrum für Schwerionenforschung GmbH, Darmstadt, 64291, Germany

Correspondence to: Joschka Pfeifer (joschka.pfeifer@cern.ch)

Abstract. Here we describe the design and performance of a new water cluster Chemical Ionization-Atmospheric Pressure interface-Time Of Flight mass spectrometer (CI-APi-TOF). The instrument selectively measures trace gases with high proton affinity such as ammonia and dimethylamine, which are important for atmospheric new particle formation and growth. Following the instrument description and characterization, we demonstrate successful measurements at the CLOUD (Cosmics Leaving OUtdoor Droplets) chamber where very low ammonia background levels of ~4 pptv were achieved (at 278 K and 80% RH). The limit of detection of the water cluster CI-APi-TOF is estimated to be ~0.5 pptv for ammonia. Although no direct calibration was performed for dimethylamine (DMA), we estimate its detection limit is at least 3 times lower. Due to a short ion-molecule reaction time (< 1ms) and high reagent ion concentrations ammonia mixing ratios of at least up to 10 ppbv can be measured without significant reagent ion depletion. Besides the possibility to measure compounds like ammonia and amines (dimethylamine), we demonstrate that the ionization scheme is also suitable for the measurement of trace gases containing iodine. During CLOUD experiments to investigate the formation of new particles from I_2, many different iodine-containing species were identified with the water cluster CI-APi-TOF. The compounds include iodic acid as well as neutral molecular clusters containing up to four iodine atoms. However, the exact molecular composition of the iodine-containing clusters are ambiguous, due to the presence of an unknown number of water molecules. The quantification of iodic acid (HIO_3) mixing ratios is performed from an inter-comparison with a nitrate CI-APi-TOF. Using this method the detection limit for HIO_3 can be estimated as 0.007 pptv. In addition to presenting our measurements obtained at the CLOUD chamber, we discuss the applicability of the water cluster CI-APi-TOF for atmospheric measurements.

1 Introduction

Ammonia (NH_3) is an important atmospheric trace gas that is mainly emitted by agricultural activity due to animal husbandry and the use of fertilizers, and by vehicles in urban environments. It can partition to the aerosol phase and is one of the most important compounds contributing to secondary aerosol formation (Jimenez et al., 2009). Strong reductions in $PM_{2.5}$ and the associated adverse health effects could potentially be achieved by decreasing ammonia emissions (Pozzer et al., 2017). However, ammonia is not only partitioning to existing particles, but is also a key vapor driving new particle formation due to its stabilization of newly-formed clusters in ternary (sulfuric acid-water-ammonia) and multi-component (sulfuric acid-water-ammonia-highly oxygenated organic molecules) systems (Kirkby et al., 2011; Kürten et al., 2016a; Lehtipalo et al., 2018). On a global scale, a large fraction of newly formed particles and cloud condensation nuclei involves ammonia (Dunne et al., 2016). The involvement of ammonia in nucleation has recently been measured in the free troposphere, in Antarctica, and in the boreal forest (Bianchi et al., 2016; Jokinen et al., 2018; Yan et al., 2018). In the upper troposphere, model calculations suggest that ammonia is important for new particle formation and early growth (Dunne et al., 2016). Recent satellite measurements support this finding by the observation of up to several tens of pptv (parts per trillion by volume) of ammonia over Asia (Höpfner et al., 2016). Ammonia has a very strong effect on nucleation involving sulfuric acid and water, e. g., recent studies have shown that very low amounts of NH_3 in the pptv-range, or even below, can enhance nucleation rates by orders of magnitude compared with the pure binary system of sulfuric acid and water (Kirkby et al., 2011; Kürten et al., 2016a; Kürten, 2019). Stronger basic compounds like amines or diamines, have been shown to enhance nucleation rates even stronger compared to NH_3, despite their much lower atmospheric concentrations (Almeida et al., 2013; Kürten et al., 2014; Jen et al., 2016; Yao et al., 2016). The experimental measurements are confirmed by quantum chemical calculations that compare the stabilizing effects of ammonia, amines, and diamines (Kurtén et al., 2008; Elm et al., 2017; Yu et al., 2018). For these reasons the measurement of these compounds is required in order to understand new particle formation and the partitioning between the gas and aerosol phase. It is important to note that ammonia can easily exceed several ppbv in the boundary layer, whereas amine mixing ratios are typically present at a few pptv only (Ge et al., 2011; Hanson et al., 2011; You et al., 2014; Kürten et al., 2016b; Yao et al., 2016).

In some previous studies, ammonia has been measured using optical absorption or chromatographic methods (Norman et al., 2009; Bobrutzki et al., 2010; Verriele et al., 2012; Bianchi et al., 2012; Pollack et al., 2019). These measurement techniques are often specialized for the detection of only a few selected compounds, whereas chemical ionization mass spectrometry (CIMS) can often measure a suite of atmospheric trace gases simultaneously at low concentrations and high time resolution. The use of different reagent ions has been described in the literature for ammonia and amine measurements, e. g., protonated acetone, protonated ethanol, O_2^+, and protonated water clusters have been successfully applied (Nowak et al., 2007; Norman et al., 2007; Benson et al., 2010; Hanson et al., 2011; You et al., 2014; Yao et al., 2016). Nowak et al. (2010) deployed their instrument on an aircraft for measurements at up to ~5 km altitude. The limit of detection (LOD) varies between 35 pptv (You et al., 2014) and 270 pptv (Norman et al., 2009) for ammonia, whereas dimethylamine (and other amines) can be detected in the sub-pptv range (You et al., 2014; Sipilä et al., 2015; Simon et al., 2016). In this study we introduce a newly developed chemical ionization mass spectrometer that uses protonated water clusters for selective ionization of ammonia and dimethylamine. The instrument is based on a high resolution Chemical Ionization-Atmospheric Pressure interface-Time Of Flight mass spectrometer (CI-APi-TOF, Aerodyne Inc. and TOFWERK AG) combined with a home-built ion source. The instrument is termed water cluster CI-APi-TOF, in accordance with other established techniques using the same mass spectrometer but different reagent ions, e. g., the nitrate CI-APi-TOF for sulfuric acid, highly-oxygenated organic molecule, and cluster measurements (Jokinen et al., 2012; Ehn et al., 2014; Kürten et al., 2014). Here we describe and characterize the instrument during experiments performed at the CLOUD (Cosmics Leaving OUtdoor Droplets) chamber at CERN (European Organization for Nuclear Research). We show that the detection limit for ammonia is below 1 pptv, which is unprecedented to our knowledge. Besides the measurement of basic compounds with high proton affinity, it was observed that the protonated water clusters are also well-suited to measure iodine-containing species such as iodic acid (HIO_3) and neutral molecular clusters containing up to four iodine atoms. The corresponding signals in the mass spectra were identified during CLOUD experiments on new particle formation from the oxidation of molecular iodine. The relevance of such compounds for nucleation in the atmosphere has recently been reported (Sipilä et al., 2016). Our findings indicate that the water cluster CI-APi-TOF can provide sensitive real-time measurements of several trace gases that are important for atmospheric new particle formation and growth: ammonia, amines (dimethylamine) and iodine species.

2. Methods

2.1 CLOUD chamber

The measurements presented here were carried out at the CLOUD (Cosmics Leaving OUtdoor Droplets) chamber at CERN (European Organization for Nuclear Research) during fall 2017 (CLOUD12 campaign) and fall 2018 (CLOUD13 campaign). The CLOUD chamber is used to investigate new particle formation from different trace gas mixtures under controlled atmospheric conditions regarding temperature, relative humidity, UV light intensity and ionization level (Kirkby et al., 2011; Kupc et al., 2011, Duplissy et al., 2016). The cylindrical stainless steel chamber has a volume of 26.1 m^3. It is designed to ensure that trace gas contaminants are low enough to allow precisely controlled nucleation experiments (Kirkby et al., 2016). The chamber is continuously flushed with synthetic air generated from liquid nitrogen and oxygen. The temperature and relative humidity of the air inside the chamber can be precisely controlled. For the present study, ammonia and dimethylamine from gas bottles were injected using a two-step dilution system (Simon et al., 2016; Kürten et al., 2016a). The calibration of the water cluster CI-APi-TOF with ammonia (Figure 1) was carried out while the instrument was disconnected from the chamber. For the calibration measurements, the two-step dilution system from the CLOUD chamber was replicated (Figure 1 and Section 2.2).

Iodine is introduced into the chamber by nitrogen flowing over solid, molecular iodine (I_2, Sigma-Aldrich, 99.999% purity) placed in a stainless steel evaporator immersed in a water bath at 303 K, with a temperature stability near 0.01 K. The generation of iodine-containing species for new particle formation is initiated by photolysis of I_2 in the presence of ozone and water. Measurements presented here were carried out at chamber temperatures between 223 and 298 K, with relative humidity (RH) ranging between 10 and 90%. A Pt100 sensor string measured the air temperature in the CLOUD chamber (Dias et al., 2017).

A chilled dew point mirror (Edgetech Instruments) measured the dew point inside the CLOUD chamber. The relative humidity is derived from water vapor pressure formulations published by Murphy and Koop (2005). Additionally, the RH was measured by a Tunable Diode Laser system (TDL) developed by Karlsruhe Institute for Technology (KIT), which was installed in the mid plane of the chamber (Skrotzki, 2012). The relative humidity was derived using the mean value of both instruments, with a combined measurement uncertainty of 5%.

2.2 Water cluster CI-APi-TOF

The selective detection of ammonia and amines by atmospheric pressure chemical ionization using positively-charged water clusters has been demonstrated recently (Hanson et al., 2011). The same ionization technique is used in the present study. The reagent and product ions are measured with an Atmospheric Pressure interface-Time Of Flight mass spectrometer (APi-TOF), which is coupled with a newly-designed crossflow chemical ionization (CI) source operated at ambient pressure (Figure 1). The reagent ions, i.e., protonated water clusters ($(H_2O)_nH_3O^+$) are generated by positive corona discharge in the presence of argon (95 %), oxygen (5 %), and water vapor. The water vapor is added by bubbling the argon through a stainless steel humidifier (containing about 1 liter of Millipore purified water) held at ambient temperature of ~20 °C. As suggested by Hanson et al. (2011), a few droplets of sulfuric acid were added to the water in order to minimize potential contamination with ammonia from the water supply. Flow rates of 2.5 standard liters per minute (slm) for argon and 0.1 slm for oxygen were used, respectively. All flow rates were controlled by calibrated mass flow controllers (MFC). A conversion factor for the measured argon flow (provided by the MFC manufacturer) was applied. First attempts have been made using nitrogen instead of argon for the flow that passes the corona needle, but this resulted in much higher ammonia backgrounds. These backgrounds are most likely explained by NH_3 production involving N_2 in the corona plasma. Furthermore, the addition of oxygen is necessary for the generation of a stable corona discharge in positive mode when using argon as the main ion source gas (Weissler, 1943).

Protonated water is also used in proton-transfer-reaction mass spectrometry (PTR-MS) that has been described in numerous publications (Good et al., 1970; Kebarle, 1972; Zhao and Zhang, 2004; Hansel et al., 2018). A simplified reaction scheme leading to the formation of protonated water clusters is shown below (Sunner et al., 1988):

$$e^- + O_2 \rightarrow O_2^+ + 2\,e^-, \tag{R1}$$

$$O_2^+ + (H_2O)_2 \rightarrow O_2^+(H_2O)_2 \rightarrow H_3O^+(OH) + O_2, \tag{R2}$$

$$H_3O^+(OH) + (H_2O)_n \rightarrow H_3O^+(H_2O)_n + OH. \qquad \text{(R3)}$$

The PTR-MS operates its ion-molecule reaction zone (IMR) typically at low pressure (~ 10 hPa) and uses an electric field (~ 100 V mm^{-1}) to break up water clusters such that mainly H_3O^+ ions react. The use of charged water clusters ($(H_2O)_{n\geq1}H_3O^+$ instead of H_3O^+) can increase the selectivity as water clusters have a much higher proton affinity compared with the water monomer (Aljawhary et al., 2013). However, due to their high proton affinity, ammonia and amines can still be detected according to the following reaction scheme:

$$H_3O^+(H_2O)_n + \mathrm{X} \rightarrow \mathrm{X}H^+(H_2O)_b + (n+1-b)\cdot(H_2O), \qquad \text{(R4)}$$

where X represents the substance that is ionized in the ion-molecule reaction zone (see below) and detected in the mass spectrometer. As water molecules can evaporate in the atmospheric pressure interface of the mass spectrometer, some of the product ions can be detected without water, e. g., ammonia is mainly detected as NH_4^+ (see Figure 2).

A schematic drawing of the calibration setup and the ion source is shown in Figure 1. The gas mixture for the ion source is composed of argon, oxygen and water vapor. It is introduced from two lines placed in the opposite direction to each other at an overall flow rate of ~2.6 slm (Figure 1a). The Electrodes of the ion source are displayed in red colors in Figure 1b. The connection to the mass spectrometer is shown using blue color. The 1” sampling line and the inlet (22 mm inner diameter) consist of stainless steel and are shown in green color. Components used for insulation are shown in white colors. A total sample flow rate of ~ 19.5 slm is maintained by a vacuum pump and a mass flow controller. The overall length of the sampling line connecting the CLOUD chamber and the ion molecule reaction zone is 1.3 m. A voltage of 3600 V is applied to the corona needle while 500 V are applied to the conically-shaped counter electrode (Electrode 1 in Figure 1b) made of stainless steel. The housing of the ion source is made of polyether ether ketone (PEEK). The ion source gas and the generated reagent ions flow through a funnel (smallest inner diameter 2.5 mm) before they mix with the sample flow. A small capillary (inner diameter of 0.8 mm) is located opposite of the funnel (Electrode 2 in Figure 1b). The electric field between the counter electrode and the capillary (at ground potential) accelerates the ions towards the entrance of the mass spectrometer. The pinhole plate (pinhole inner diameter of 350 µm) and the capillary are in electric contact and ~0.8 slm flow through the capillary and the pinhole into the mass spectrometer. The measured product ions are generated in the ion-molecule reaction zone (IMR, yellow area in Figure 1a) at atmospheric pressure. The dimension of the IMR is defined by the distance between the counter electrode and the capillary (~ 16.4 mm). After passing the pinhole, the ions are transported through two quadrupoles (Small Segmented Quadrupole, SSQ and Big Segmented Quadrupole, BSQ) towards the detection region of the mass spectrometer (Micro-Channel Plate, MCP; pressure is approx. 1×10^{-6} hPa). The estimated reaction time is <1 ms. This short reaction time allows the measurement of high ammonia mixing ratios (up to ~10 ppbv) without significant depletion of the reagent ions, which would be the case when using an ion source design for the measurement of sulfuric acid (Eisele and Tanner, 1993; Kürten et al., 2011), which is typically present at much lower concentrations than ammonia. The principle of a cross-flow ion source was introduced by Eisele and Hanson (2000) who used this technique to detect molecular sulfuric acid clusters. In more recent studies, this technique was used for the measurement of ammonia (Nowak et al., 2002; Nowak et al., 2006; Hanson et al., 2011).

The measured volume mixing ratio (VMR, in pptv) of detected compounds is derived from a calibration factor (*C*) and the sum of the product ion counts per second (pcs) normalized against the sum of the reagent ion counts per second (rcs) (Kürten et al., 2016b; Simon et al., 2016):

$$VMR = C \cdot \ln\left(1 + \frac{\sum pcs}{\sum rcs}\right) = C \cdot ncps. \tag{1}$$

Equation (1) yields the VMR measured by the water cluster CI-APi-TOF as a function of the normalized counts per second (*ncps*). A calibration factor, *C*, which includes factors like the reaction rate and the effective reaction time, is required to convert the *ncps* to a mixing ratio. This factor can be derived from the inverse slope of a calibration curve (see Section 3.2). While Hanson et al. (2011) report a maximum for the water cluster distribution at the pentamer, evaporation of water seems to be stronger in our instrument. The maximum signal in clean spectra is usually found for the water dimer ($(H_2O)H_3O^+$, see Figure 2) and a strong drop in the reagent ion signals is found beyond the tetramer ($(H_2O)_3H_3O^+$). Therefore, the sample quantification includes, using ammonia as an example, the product ions $(H_2O)_nNH_4^+$ with n = 0,1 and the reagent ions $(H_2O)_mH_3O^+$ with m = 0-3. Possible losses in the sampling line are not taken into account by the calibration factor (see Section 3.8 for discussion of sampling line losses). The only compound for which a direct calibration is performed in the present study is ammonia (Section 2.3). When mixing ratios for dimethylamine are presented, the same calibration factor is used. This approach can introduce uncertainty as the proton affinity, as well as the transmission efficiency differ for dimethylamine compared to ammonia. However, previous studies showed that the ionization efficiency from protonated water clusters is collision-limited for both ammonia and dimethylamine (Sunner et al., 1988; Hanson et al., 2011). The applicability of this approach is discussed in Section 3.9; it is estimated that the mixing ratios for dimethylamine are correct within a factor of ~3.5.

2.3 Calibrations

2.3.1 Ammonia

Figure 1a shows a schematic drawing of the experimental setup during the calibrations with ammonia. The ammonia was taken from a gas bottle containing an NH_3 mixing ratio, *B*, of 100 ppmv diluted in pure nitrogen (Air Liquide, ±5% uncertainty for the certified NH_3 mixing ratio) that is diluted in two steps, where MFCs (indicated as M_n in Figure 1a) are used to obtain different set points for the volume mixing ratio (Figure 1a). During the second dilution step the mixture from the first dilution is injected into the center of the main sample flow (flow rate, Q_{sample}). The theoretical VMR_{theor} is given by (Simon et al., 2016):

$$\mathrm{VMR_{theor}} = \frac{\mathrm{M_1}}{\mathrm{M_1}+\mathrm{M_2}} \cdot \frac{\mathrm{M_3}}{\mathrm{M_3}+Q_{sample}} \cdot B. \tag{2}$$

The flow of ammonia from the gas bottle is adjusted by M_1 (0.01 slm max.), whereas M_2 (2 slm range) controls the flow of nitrogen for the first dilution step. The flow of diluted ammonia that is introduced into the sample flow is controlled by M_3 (0.1 slm range). The calibration flow consists of the same synthetic air that is used for the CLOUD chamber. The flow is provided by two MFCs that control a dry portion (M_4) and a wet portion of the flow that has passed a stainless steel water bubbler (M_5, see Figure 1). By adjusting M_4 and M_5 (both 50 slm range) the RH of the sample flow can be controlled in order to test whether a humidity dependence exists for reaction (R4). Care is taken that the sum of M_4 and M_5 is always somewhat larger than Q_{sample}. To avoid overpressure in the sampling line, the excess flow is vented through an exhaust before the sampling line.

Accordingly, the measured sample air consists of synthetic air (80% nitrogen, 20% oxygen) with adjustable RH and ammonia mixing ratio. To obtain calibration curves, the highest targeted ammonia mixing ratio is adjusted first. The calibration points are then recorded by stepping down the flow of M_3. In this way, equilibration times are fairly short as the NH_3 mixing ratio before and directly after M_3 remains constant (see also Section 3.2).

2.3.2 Iodine Oxides

Besides the detection of ammonia and dimethylamine by the described ionization scheme, product ions from iodine-containing species were detected during new particle formation experiments initiated from I_2 photolysis during the CLOUD13 run. Prominent signals ($HIO_3 \cdot H^+$ and $HIO_3 \cdot H_3O^+$) corresponding to the neutral species of HIO_3 were observed among others (discussed in Section 3.6 and Table 2). These species can be unambiguously identified due to the large negative mass defect of the iodine atom and the high mass resolution (> 3000 Th/Th). No direct calibration for HIO_3 was performed; however, another chemical ionization mass spectrometer using nitrate reagent ions (nitrate CI-APi-TOF) was also measuring HIO_3 at CLOUD. Therefore, a calibration factor for HIO_3 is derived by scaling concentrations measured by the nitrate CI-APi-TOF that is calibrated for sulfuric acid (Kürten et al., 2012). We further assume that both sulfuric and iodic acid are detected with the same efficiency by the nitrate CI-APi-TOF. This assumption introduces uncertainty when estimating the detection limit of HIO_3. However, as the reaction of sulfuric acid with nitrate ions is at the kinetic limit, the detection limits shown here based on this assumption can be seen as lower limits. Unfortunately, there is currently no direct calibration technique established for iodic acid in the gas phase. Thus, the same assumption as in a previous study for deriving gas phase concentrations of iodic acid are used in the present study (Sipilä et al., 2016).

For the instrument inter-comparison (and the indirect calibration of the water cluster CI-APi-TOF), 18 different CLOUD experimental runs were chosen and mean values were calculated for different steady-state concentrations. We took 6 steady-state concentrations each at temperatures of 263 K (80% RH) and 283 K (40% RH and 80% RH).

2.4 PICARRO

A PICARRO G1103-t NH_3 Analyzer (PICARRO Inc., USA) measured ammonia mixing ratios based on cavity-ring down spectroscopy during CLOUD12 and CLOUD13. The instrument is suitable for real-time monitoring of ammonia in ambient air and has been presented in previous studies (Bell et al., 2009). The G1103-t was installed at the CLOUD chamber with its own sampling line coated with Sulfinert (Restek GmbH, Germany), where the coating reduced the losses of ammonia to the sampling line walls considerably. Since the PICARRO has a rather small sample flow rate (< 1 slm), an additional pump was used to enhance the flow rate to 5 slm just before the instrument inlet. This was done in order to minimize line losses and to decrease the response times. It was, however, not quantitatively tested in how far these measures (Sulfinert and increased flow rate) helped with the measurements. The PICARRO was also independently calibrated with a NH_3 permeation tube (Fine Metrology, Italy) using a multigas calibrator (SONIMIX 6000 C1, LNI Swissgas, Switzerland). The time interval for one measurement of the PICARRO is 5 seconds for which a lower detection limit of 200 pptv is reported (PICARRO Inc., USA; Martin et al., 2016). By using the same method (at the same time period) as shown for the water cluster CI-APi-TOF (see Section 3.5), we derive a detection limit of 366.2 pptv for the PICARRO unit used in this study.

3. Results and Discussion

3.1 Main peaks in spectrum

Figure 2 shows a typical spectrum during calibrations, where 10 ppbv of ammonia are injected (40% RH, ~293 K). The most prominent primary ions are $H_3O^+, (H_2O)H_3O^+$ and $(H_2O)_2H_3O^+$. $(H_2O)H_3O^+$ is the dominant primary ion in the mass spectrum. The water tetramer ($(H_2O)_3H_3O^+$) is usually the largest water cluster that can be detected. The addition of ammonia generates NH_4^+ and $(H_2O)NH_4^+$; a small signal from NH_3^+ is also visible. At low ammonia concentrations the signal from NH_4^+ can have a similar magnitude compared with the signal from H_2O^+ (possibly from reactions of O_2^+ and H_2O). Since these ions have the same integer mass, a high mass resolving power is essential in terms of reaching low detection limits as otherwise the differentiation between the two signals is not possible. At the low masses the APi-TOF used in the present study reaches a resolving power of ~2000 Th/Th, which is sufficient to separate the two peaks. For the analysis of the spectra, the software TOFWARE is used that allows analyzing high resolution spectra (Stark et al., 2015; Cubison and Jimenez, 2015; Timonen et al., 2016). Prominent peaks from N_2H^+, NO^+ and O_2^+ can also be found in the spectrum shown in Figure 2. It is not clear how these ions are formed and why they survive the relatively long reaction time of ~1 ms since Good et al. (1970) report that O_2^+ reacts rapidly away in moist air. For the analysis the presence of these background peaks is currently ignored and they are not counted as reagent ions (in equation (1)) as no evidence exists that they interact with the target species relevant for the present study. An exception could be NH_3^+ (possibly from reaction of O_2^+ and NH_3); but NH_3^+ is not considered and is only a small fraction of NH_4^+.

In contrast to the spectrum shown in Figure 2 with relatively small water clusters, Hanson et al. (2011) observe the highest signal in the water cluster distribution for the pentamer. We explain this difference in more pronounced fragmentation and evaporation of ion clusters in the atmospheric pressure interface of our mass spectrometer.

For estimating an ammonia mixing ratio according to equation (1), the product ion count rates are normalized against the dominating reagent ion count rates. Figure 2 shows that even at 10 ppbv of injected ammonia the reagent ion signals are significantly higher than the product ion count rates. This indicates that no significant reagent ion depletion occurs and thus the normalized counts per second respond linearly with the ammonia VMR at least up to 10 ppbv (see Section 3.2).

3.2 Ammonia and iodic acid calibration

Figure 3 shows the calibration curves obtained for NH_3 and HIO_3 (for the CLOUD13 campaign). Each dot represents the mean value of a steady state measurement of at least 20 minutes. The normalized counts per second are based on the two highest signals assigned to the analyzed compound (ammonia: NH_4^+ and $(H_2O)NH_4^+$; iodic acid: HIO_3H^+ and $HIO_3H_3O^+$). The total error of the VMR (on the *x*-axis) is calculated by Gaussian error propagation taking into account the standard deviation of the flow rates from the mass flow controllers and the uncertainty of the VMR inside the ammonia gas bottle. Since we obtained the VMR shown in Figure 3b by scaling the concentrations measured by a nitrate CI-APi-TOF calibrated for sulfuric acid, the error on the *x*-axis equals the uncertainty of these measurements (estimated as a factor of two for the iodic acid concentration). The error on the *y*-axis is given by the standard deviation of the normalized counts per second. We derive a calibration curve from a linear regression model using the Wilkinson-Rogers Notation (Wilkinson and Rogers, 1973). The fit is forced through the origin; however, even when the fit is not constrained, the resulting slope is essentially the same (the results for the slopes/sensitivities differ by 1.35%). The derived slopes represent the inverse of the calibration factor, *C* (~ 1.46×10^5 pptv at 40% RH), in equation (2). Figure 3 shows that all measured mixing ratios lie in the area of the confidence intervals (95% confidence intervals) and thus the linear model describes the dependency very well. The calibration was performed before the CLOUD13 experiment (Sept. 2018), during and after the experiment (Dec. 2018) at different levels of humidity (calculated relative humidity levels between ~3% and 82%) and ambient temperatures. The calibrations for ammonia were performed by introducing the highest mixing ratio first. However, it took almost a day to reach stable signals as the tubing and the two MFCs through which the ammonia was flown (M_1 and M_3) needed to equilibrate. The further calibration points were then recorded by reducing the flow rate of M_3. In this way, no change in the ammonia mixing ratio inside the capillary before the main sampling line and in the MFCs was necessary. This allowed for a relatively fast stepping through the calibration set points. However, even when the ammonia flow was shut-off there was still significant diffusion of ammonia from the capillary into the sampling line, which resulted in relatively high background values (with nominally zero NH_3). For this reason, we derived the limit of detection by measuring the background of the CLOUD chamber with the calibration lines removed (Section 3.5). During the calibrations, the relative humidity was calculated by assuming that the sample flow passing the water reservoir is saturated with water (Figure 1a). For the calibrations carried out after the campaign, the temperature of the total sample flow was measured to derive the absolute humidity. The calibration points in Figure 3 were taken at measured gas flow temperatures of 288 to 290 K. The relative humidity was set to 40% RH by adjusting the dry and the wet flow rates for the sample flow; these conditions correspond to an absolute humidity of ~ 0.0057 kg m^{-3}. The calibration factor derived for CLOUD12 (for ammonia) differs from the calibration factor shown here. This is due to a different ion source (designed for a 0.5'' sampling line in CLOUD12 compared with a 1'' line in CLOUD13), a different sample flow rate and different tuning of the CI-APi-TOF.

3.3 Response times

The response time of the water cluster CI-APi-TOF is defined as the characteristic time needed for the instrument to react on changes in the ammonia mixing ratio. The response time takes into account two processes. These are the time needed until the instrument reacts on changes in the mixing ratio and the time needed until a steady state is established in the lines. In the following, we define the response time as the time required for the instrument to reach 95% of the new mixing ratio being injected. Figure 4 indicates the typical response times of the water cluster CI-APi-TOF during calibrations (here at 60% relative humidity). It shows a decay between two calibration steps when the injected ammonia is reduced from 9509 pptv to 6911 pptv and a rise in the signal when the ammonia mixing ratio is increased from 500 pptv to 9509 pptv. Panel a) indicates a clear difference between the time needed until the instrument reacts on the changes in the mixing ratio (red line) and the time needed until the lines reach 95% of the new steady state (black line). We expect the same behavior for a decay from 9509 to 500 pptv, however, the mixing ratios were gradually reduced during calibrations. Thus, for the gradual decays, the time needed for the lines to reach a new equilibrium is rather short. While the variation of instrumental response time is small (6 to 10 seconds for decays from 9509 to 6911 pptv and 18 to 25 seconds for a rise from 500 pptv to 9509 pptv, respectively), the time until a steady state is established in the lines varies depending on precursor conditions and relative humidity (see Section 3.8). Thus, an estimation of a response time can vary significantly. In our experiments, the response times (including both processes described above) during a rise in ammonia mixing ratio varied between 535 seconds (20% relative humidity) and 890 seconds (60% relative humidity, shown in Figure 4). For a decay of ammonia mixing ratio from 9509 to 6911 pptv the response times vary between 37 seconds and 54 seconds.

3.4 Influence of the humidity on the sensitivity

Figure 5 shows the sensitivity dependence for the ammonia measurements with varying relative humidity. These data points are derived from calibration curves similar to the one shown in Figure 3a. However, during the calibrations the humidity was changed by adjusting the dry and wet sample flow rates. For all conditions NH_4^+ has the highest product ion count rate. However, the ratio of the signals for $(H_2O)NH_4^+$ and NH_4^+ increases with humidity as well as the sensitivity. A possible explanation for the observed sensitivity dependence could be increased collision rates at high humidity where larger water clusters are present. In addition, the detection efficiency as function of the ion mass can vary depending on the voltages applied to the ion source and the APi-section, as well as the time of flight region of the mass spectrometer. Thus, the mass spectrometer does not have a constant detection efficiency over the full mass range (Heinritzi et al., 2016). A higher detection efficiency at *m*/*z* 36 ($(H_2O)NH_4^+$) compared with *m*/*z* 18 (NH_4^+) together with the higher fraction of $(H_2O)NH_4^+$ compared with NH_4^+ at high humidity could explain some of the observed effect. However, the observed increase in sensitivity is not dramatic (increase by a factor of ~2.5 when the humidity increases by a factor of 10). Nevertheless, the effect is taken into account by using the measured relative humidity inside the CLOUD chamber (see Section 2.1) to correct the derived ammonia mixing ratio. The effect of temperature on the sensitivity could not be tested during a dedicated calibration experiment as our calibration setup is not temperature-controlled. However, during a transition from high to low temperature in the CLOUD chamber and constant ammonia injection, no significant change in the measured ammonia was observed, which indicates a weak influence of temperature.

The dependency of the sensitivity with relative humidity and temperature is different for the measurement of iodic acid as shown in Figure 6. While NH_4^+, without a water molecule, is the dominant signal for ammonia, $H_4IO_4^+$, which is $H_2O \cdot HIO_3H^+$ or $HIO_3 \cdot H_3O^+$, yields the highest signal for iodic acid. We observed an increasing sensitivity at lower temperatures, while the humidity dependency appears to be smaller compared to the ammonia measurements (Figure 5). The higher count rate of $H_4IO_4^+$ compared to $H_2IO_3^+$ could indicate that iodic acid requires additional water in order to be associated with a positively charged ion. However, during the transition from ambient pressure into the vacuum of the mass spectrometer, water molecules can evaporate and leave $H_2IO_3^+$ in a non-equilibrium process. Besides the observation of iodic acid, additional signals from iodine-containing species can be found in the spectra. These species are listed in Table 2. Elucidating the exact formation pathways of these ions and the corresponding neutral species is subject for future work.

3.5 Detection limits and instrumental backgrounds

Determining the limit of detection (LOD) for ammonia is not trivial as the background signal is not constant. During the calibrations a relatively high background was observed, which was usually decreasing slowly after the ammonia flow through the capillary was shut off. A typical value reached a couple of minutes after the ammonia flow was turned off is ~30-60 pptv. When the water cluster CI-APi-TOF was connected to the CLOUD chamber the NH_3 signals usually dropped significantly when no ammonia was actively added. However, even under these conditions the ammonia was not zero and the measured signal changed when the RH or temperature of the chamber was adjusted. There is evidence that the contaminant level of the CLOUD chamber with respect to ammonia is on the order of several pptv at 278 K and 38% RH (Kürten et al., 2016a). During CLOUD13 the measured background (at 278 K and 80% RH) was 3.7 pptv, which in principle confirms the previous estimates. The fact that the sampling line of the instrument can also be a source of contamination could explain the somewhat higher value. Another source of background ammonia could be the ion source. During the early stages of our development we used nitrogen instead of argon as the main ion source gas. This led to ammonia backgrounds of several 100 pptv since ammonia can be generated by the nitrogen plasma from the corona tip when it mixes with the humid sample flow (Haruyama et al., 2016). However, replacing nitrogen with argon quite drastically decreased the background ammonia signals. Still, traces of nitrogen containing gases in the ion source could contribute to the ammonia background. For the present study we report a background ammonia mixing ratio of 3.7 pptv (Table 1) for 278 K and 80% RH but note that the background is significantly lower for lower chamber temperatures, which argues against the ion source being a significant source of ammonia since it is always at ambient temperature.

The LOD is defined as the additional ammonia mixing ratio that is necessary to exceed three times the standard deviation at background conditions (You et al., 2014). This value corresponds to 0.5 pptv for an averaging time of 1 minute. Assuming the same sensitivity as for ammonia and taking into account the background signals for the exact masses, LODs for other compounds can be estimated. Besides the calculated values for ammonia, Table 1 lists the estimated backgrounds and LODs for dimethylamine and iodic acid. The evaluation of high resolution data is necessary for deriving the values shown in Table 1 as for some compounds several species occur at the same integer mass. For example, for dimethylamine (exact mass of protonated compounds at 46.0651 Th) other species like NO_2^+ (45.9924 Th) or CH_4NO^+ (46.0287 Th) can interfere. For dimethylamine only the peak with the highest count rate is taken into account, since $(C_2H_7N)H_3O^+$ interferes with other compounds measured during the experiments even when using high resolution data. In principle, the omission of the larger product ions (with one additional water molecule) should lead to a different calibration constant. However, the effect is small as the ion signals with the associated water are smaller than the products without the water molecule for the measured bases. The applicability of the assumption (using the calibration constant derived for ammonia for dimethylamine) is discussed in Section 3.9.

The instrumental background for NH_3 is higher than the estimated backgrounds for the other compounds shown in Table 1. This might be the case, since low levels of NH_3 are more difficult to achieve due to the ubiquitous presence of ammonia. In any case, the detection limit derived for ammonia is well below the LOD reported for other measurement techniques and instruments (Bobrutzki et al., 2010; You et al., 2014; Lin; Wang et al., 2015). However, the performance of the water cluster CI-APi-TOF during atmospheric measurements remains to be tested. The signal of dimethylamine is most of the time below the estimated limit of detection.

The estimated detection limit of iodic acid is well below the LOD calculated for ammonia and dimethylamine (Table 1). We might explain this when looking at signals that could possibly interfere with the measured compounds. All compounds shown in Table 1 have an integer mass, where other signals are also detected, e.g., H_2O^+ at the nominal mass of ammonia, or NO_2^+ at the nominal mass of dimethylamine. For the high masses of the iodine containing species with their strong negative mass defects these isobaric compounds are much less crucial. Additionally, iodic acid has a much lower vapor pressure compared with ammonia and is not emitted efficiently from surfaces at temperatures relevant for the present study. Therefore, much lower backgrounds can be expected even if the sampling line and the instrument were exposed to high concentrations before.

3.6 Identified iodine species during CLOUD13

The signals for HIO_3 measured by the water cluster CI-APi-TOF show an excellent correlation with the iodic acid concentration from the nitrate CI-APi-TOF measuring in negative ion mode (see Figure 3b). Additionally, we were able to detect iodine-containing species at higher mass to charge ratios (e.g., iodine pentoxides) during several experimental runs. Figure 7 shows the detected iodine species during an experimental run, when a high iodine concentration was injected into the chamber (mean values over a duration of 120 minutes). The derived mean iodic acid mixing ratio is ~0.98 pptv according to the measurements of the water cluster CI-APi-TOF. During this time period, we observed compounds containing up to 4 iodine atoms. The size of the circles shown in Figure 7 corresponds to the mean count rate of the signals on a logarithmic scale. For comparison, the intensities of the reagent ions are also shown. To provide more details on the observed signals, Table 2 lists the sum formulas of some identified iodine species.

During some runs, an electric field was applied to the chamber to get rid of ions and cluster ions for the study of purely neutral (i.e., uncharged) nucleation. Even during these experiments the signals as displayed in Figure 7 were present. This indicates that the water cluster CI-APi-TOF measures neutral compounds after ionizing them in the ion-molecule reaction zone. The present study only gives a short overview of the iodine signals observed so far with the water cluster CI-APi-TOF. Further CLOUD publications will focus on the chemistry of the iodine-containing species and on their role in new particle formation processes.

3.7 CLOUD chamber characterization

The performance of the water cluster CI-APi-TOF during measurements at CLOUD12 is shown in Figure 8. We compare the derived mixing ratios with the measurements of the PICARRO. In addition, both measurements are compared with an estimated range of ammonia mixing ratios based on the injected amount of NH_3 into the CLOUD chamber, the chamber volume and the ammonia life time (see, e.g., Simon et al. (2016) and Kürten et al. (2016a) for the equations linking these quantities to the estimated CLOUD mixing ratios). While the injected ammonia can easily be determined from the MFC settings, the ammonia life time in the chamber can span a wide range. For a very clean chamber or at very low temperatures the chamber walls can essentially represent a perfect sink and the ammonia has a short life time. A wall loss life time of 100 s at 12% fan speed was previously reported by Kürten et al. (2016a). Measurements of sulfuric acid at different fan speeds suggest a change of a factor of 4 in the mixing ratios when the fan speed is changed from 12% to 100%. Scaling these measurements to the ammonia measurements yields a wall loss lifetime of 25 s at 100% fan speed. On the other hand, once the walls have been exposed for a long time with ammonia they reach eventually an equilibrium where condensation and evaporation rates become balanced. Under these conditions, the ammonia life time is determined by the chamber dilution life time alone (6000 s), and so the NH_3 increases to higher equilibrium concentrations. Furthermore the walls can act as a source of ammonia due to re-evaporation of ammonia molecules attached to the surface. This effect can be significant when the concentrations previously injected into the chamber were higher than the current concentrations. Thus, the estimated range can vary by a factor of ~200 based on the chamber conditions. This wide range is indicated by the shaded areas in Figure 8 (light blue color).

Figure 8a shows the measurements of the water cluster CI-APi-TOF, the PICARRO, and the calculated value for ammonia. The signal measured by the water cluster CI-APi-TOF follows the injected ammonia almost instantaneously (first injection is on Oct. 23), whereas the PICARRO only shows elevated concentrations above its background of ~200 pptv much later. This increased response time can be explained by a combination of the longer sampling line (~1.8 m compared to 1.3 m for the water cluster CI-APi-TOF), the lower flow rate (~ 1 slm with a core sampling of 5 slm compared to ~ 20 slm for the water cluster CI-APi-TOF) and the higher detection limit of the PICARRO. After the flow of ammonia is shut-off, both the mass spectrometer and the PICARRO show almost identical values when the chamber is being cleaned. Before the first ammonia injection it can also be seen that the water cluster CI-APi-TOF shows progressively lower background ammonia values. Whether this is due to the chamber, the instrument or the sampling line becoming cleaner is unclear. Figure 8a also indicates the influence of temperature on the background ammonia level. When the chamber temperature drops from 298 K to 278 K (shortly before Oct. 31) the residual NH_3 decreases by around a factor of 5, which is caused by a reduction in the re-evaporating ammonia from the chamber walls. Due to the higher LOD, the PICARRO, however, can hardly detect this decrease in the VMR.

The influence of relative humidity on the gas phase concentration of ammonia is shown (time from 29.10. to 30.10.). In addition to the change in sensitivity with relative humidity shown for the water cluster CI-APi-TOF (Section 3.4), a change in humidity can lead to an increased ammonia mixing ratio in the gas phase. This is due to the fact that water molecules can displace adsorbed ammonia on surfaces (Vaittinen et al., 2014). This effect can be pronounced when the chamber walls have been conditioned with high ammonia concentrations. It is important to note that the instrument was characterized for humidity dependency during the following CLOUD13 campaign. While changes in sensitivity with relative humidity were taken into account during CLOUD13, this was not the case during CLOUD12. The observed increase in mixing ratios at this time is a combination of a change in sensitivity of the instrument and an increase in the gas phase concentration of ammonia due to re-evaporation from the wall of the CLOUD chamber. Here, the PICARRO trace can provide insight into the magnitude of both effects indicating that the re-evaporation from the chamber walls dominates over the change in sensitivity. The time from 25.10 to 26.10 shows a steep increase in the PICARRO trace, while the ammonia trace derived from the water cluster CI-APi-TOF flattens out at 20 ppbv of ammonia. This indicates that the primary ions of the water cluster CI-APi-TOF are depleted at high vapor concentrations. It is important to mention that not only ammonia concentrations were elevated at this time, but also other vapor concentrations were rather high. During the CLOUD13 campaign, where a revised version of the ion source was used (see Section 3.2), the significant depletion of primary ions has been observed only at ammonia mixing ratios of 40 ppbv. Figure 8b shows how the ammonia mixing ratios inside the CLOUD chamber react on changes of the fan speed. The fan speed was varied between 12% (default value) and 100% to realize different wall loss rates of condensable species. As the temperature in this example is low (248 K) and the chamber is rather clean the walls act as a perfect sink for ammonia. Therefore, the measured mixing ratios almost instantaneously react to the changing fan speed indicating a change of a factor 4 in the mixing ratios. Thus, the measurements coincide with the calculated values using the wall loss life times reported above. The PICARRO is insensitive at these low mixing ratios and cannot respond to conditions that change quickly.

3.8 Ammonia wall loss rates in the sampling line

The largest uncertainty in the ammonia measurement is related to the sampling line losses. At CLOUD, the sampling line is made of stainless steel and is kept as short as possible. The total length is still 1.3 m because the sampling line protrudes into the chamber over a distance of 0.5 m in order to sample air from the well-mixed center region of the chamber. Additionally, the sampling line has to bridge the thermal housing around the chamber walls. Using an ammonia diffusivity of 0.1978 cm^2 s^{-1} (Massman, 1998) and a sample flow rate of 20 slm, the sample line penetration efficiency can be estimated as 33.7% for a laminar flow (Dunlop and Bignell, 1997; Baron and Willeke, 2001; Yokelson, 2003). This means, that if the walls of the sampling line act as a perfect sink, then the measured NH_3 mixing ratios would need to be corrected with a factor of ~3. However, it is quite likely that the sampling line not always acts as a perfect sink for ammonia due to desorption and re-evaporation. Furthermore, the interactions of ammonia with the surface of the sampling line depend on the humidity. Water on surfaces can affect the uptake or release of ammonia. Vaittinen et al. (2014) showed that increased humidity can displace ammonia from surfaces. Additionally, water on surfaces can allow weak acids and bases to dissociate into their conjugate compounds on the surface, thereby affecting the partitioning to the surface (Coluccia et al., 1987). Vaittinen et al. (2014) studied the adsorption of ammonia on various surfaces and found a value of 1.38×10^{14} molecule cm^{-2} for the surface coverage on stainless steel. For humid conditions this value is, however, significantly smaller and drops to ~5×10^{12} cm^{-2} for a water vapor mixing ratio of 3500 ppmv at 278 K, which can be explained by the displacement of ammonia by water molecules (Vaittinen et al., 2014). This indicates that, depending on the ammonia mixing ratio and the gas conditions (temperature and RH), eventually an equilibrium can be reached between the gas and the surface. In such a case, no wall loss correction would be necessary. Furthermore, ammonia may re-evaporate from the inlet line walls if saturation happened at higher concentrations previously. At CLOUD, the sampling lines are attached to the chamber and cannot easily be removed during the experiments. Thus, it is not possible to quantitatively distinguish between interactions with the surface of the sampling line and the surface of the CLOUD chamber. This complicates the evaluation of the influence of the sampling line regarding the measured ammonia as a function. One practical solution would be to report average of the values considering the wall loss correction factor and neglecting the factor. When going from high values to low values, the sampling line walls can also become a source of ammonia. This can potentially lead to a strong over-estimation of the measured value and the time until a new equilibrium is reached depends on the history of the measurements.

We are aware that the sampling line losses introduce some uncertainty on the ammonia measurement. However, this is an effect other in-situ techniques also have to struggle with (see, e.g., Leifer et al. (2017)). We also want to note that the effect is much smaller for larger molecules, e.g., the penetration for triethylamine (diffusivity of 0.067 cm^2 s^{-1}, Tang et al. (2015)) reaches 61%. For atmospheric measurements, we suggest to use an inlet system where a short piece of the 1’’ sampling line only takes the core sample flow from a large diameter inlet. A blower can generate a fast flow in the large inlet to essentially reduce the losses for the core flow to zero before it enters the actual sampling line (Berresheim et al., 2000).

3.9 Measurement of dimethylamine

As mentioned in Section 3.5 and shown in Table 1, the same calibration factor derived for ammonia was used to estimate the mixing ratio of dimethylamine. We caution, that this assumption can lead to uncertainties as the sensitivity of the measurement is expected to depend on the proton affinity of the measured substance (Hanson et al., 2011). To estimate the validity of this assumption, we compared the mixing ratios measured with the water cluster CI-APi-TOF with the calculated mixing ratios for a period when dimethylamine was actively injected into the CLOUD chamber. A chamber characterization for dimethylamine was already conducted by Simon et al. (2016), where the wall loss lifetime was determined as 432s for conditions where the chamber walls acted as a perfect sink (12% fan speed). Additionally, as discussed in Section 3.7, we use a lifetime of 108s at 100% fan speed (change in a factor of 4 when the fan speed is changed from 12% to 100%). The dilution life time during CLOUD13 is 6000 s and represents the maximum possible life time when wall loss would be negligible. Thus, the wall loss lifetime used in this study gives a lower limit for dimethylamine mixing ratios in the CLOUD chamber. Figure 9a shows the time period when dimethylamine was added. Since it takes a certain time until the stainless steel pipes of the gas dilution system are saturated with dimethylamine there is a short time delay between the switching of a valve that allows dimethylamine to enter the chamber and the rise in the measured dimethylamine mixing ratio. Once the lines are conditioned and the dimethylamine is homogenously mixed into the chamber, the measured and estimated mixing ratios are generally in good agreement with each other when the wall loss life time is used to estimate the mixing ratios. Fluctuations in the measured mixing ratio can be explained by changes in the fan speed. To estimate the consistency of the approach of scaling the calibration factor derived for ammonia to estimate dimethylamine mixing ratios, we use the ratio between the mixing ratio calculated for the Water Cluster CI-APi-TOF and the calculated mixing ratios based on the wall loss lifetime for the CLOUD chamber. For these measurements, we estimated a wall loss rate in the sampling lines of ~1.96 for dimethylamine, where a diffusivity of 0.1 cm^2s^{-1} was used (Freshour et al., 2014; Simon et al., 2016). The mean deviation between the estimated dimethylamine mixing ratio and the calculated mixing ratio is 3.48 indicating that the approach of scaling the calibration factor derived for ammonia introduces uncertainties within a factor of ~3.5. The deviations at the end of the time series shown in Figure 9a are caused by nucleation experiments in which high concentrations of other vapors are used. During these stages a significant uptake of dimethylamine on particles can explain the discrepancy between measured and expected dimethylamine. Figure 9b shows a measurement of the chamber background for dimethylamine carried out during CLOUD13 over a time period of 5 days. The mean instrumental background for the time period shown in Figure 9b is ~0.14 pptv (for a temperature of 278 to 290 K and a relative humidity between ~50 and 60 %). The background values shown here are close to the background values obtained for 80% RH and 278 K (see Table 1). The observed variations are in a range of ~0.1 to 0.3 pptv provided that the measurement is not interrupted, e.g., due to the replenishment of the water source that humidifies the flow for generating the reagent ions (which explains the first drop of the background measurement in Figure 9b). The estimated detection limits shown here are below or at similar detection limits reported in previous publications (You et al., 2014; Simon et al., 2016).

4. Discussion and application to ambient measurements

The present study demonstrates the successful application of a water cluster CI-APi-TOF during controlled chamber experiments for ammonia, dimethylamine and iodic acid measurements. During the experiments involving iodide, neutral clusters containing up to 4 iodine atoms are detected. The technique has unprecedented low detection limits regarding the ammonia measurement as well as a fast time response and time resolution. A next step is its application to atmospheric measurements. The technique should be suitable for such measurements as the amount of clean gas required (ca. 2 slm of argon and some oxygen) is rather small and can easily be supplied with gas bottles (one argon gas bottle, 50 liters at 200 bar should last ~3 days). At CLOUD there is a restriction regarding the maximum sample flow that can be taken from the chamber. During atmospheric measurements much higher flow rates can easily be realized. Therefore, the suggested design of the inlet system using a blower and a core sample inlet should be used (see Section 3.8). Furthermore, the use of an internal calibration standard would be beneficial. We have tried to add a defined mixing ratio of ND_3 to the sample flow. However, besides the expected signal at (ND_3H^+, *m*/*z* 21) further signals corresponding to NH_4^+, NDH_3+, $ND_2H_2^+$ were also visible in the spectra due to deuterium-hydrogen exchange, which makes this method unfavorable. Use of $^{15}NH_3$ for calibration is also unfavorable since the $^{15}NH_4^+$ signal is hard to distinguish from the comparatively high H_3O^+ signal at the same integer mass even with a high resolution mass spectrometer.

Roscioli et al. (2016) demonstrated that the addition of 1H,1H-perfluorooctylamine to the sample flow can be used to passivate an inlet, which leads to greatly reduced sampling line losses and improved time response during ammonia measurements. Recently, Pollack et al. (2019) implemented this passivation technique for ambient measurements on an aircraft. For these measurements, a tunable infrared laser was used (TILDAS-CS, Aerodyne Inc.). We also tested the passivation technique, however, the high mixing ratio of 1H,1H-perfluorooctylamine (~100 ppm to 0.1% injection into the sample flow) that is required led to a consumption of the reagent ions since 1H,1H-perfluorooctylamine has a high proton affinity and is therefore also efficiently ionized by the protonated water clusters. For this reason, the passivation technique for the measurement of ammonia can in our opinion only be used with spectroscopic techniques as it was the case in the studies by Rosciolli et al. (2016) and Pollack et al. (2019).

5. Summary and Conclusion

The set-up and characterization of a water cluster Chemical Ionization-Atmospheric Pressure interface-Time Of Flight mass spectrometer (CI-APi-TOF) is described. The instrument includes a new home-built cross-flow ion source operated at atmospheric pressure. The generated protonated water clusters ($(H_2O)_{n\geq1}H_3O^+$) are used to selectively ionize compounds of high proton affinity at short reaction times. The instrument's response is linear up to a mixing ratio of at least 10 ppbv for ammonia when the derived calibration factor is applied to the normalized counts per second. The water cluster CI-APi-TOF was used at the CLOUD chamber where very low background ammonia mixing ratios (ca. 4 pptv at 278 K) were achieved.

The level of detection (LOD) was estimated as 0.5 pptv for NH_3. To our knowledge, such a low detection limit for ammonia measurements has not been reported so far. We attribute the low LOD mainly to the use of ultraclean argon (5.0 purity) as the main ion source gas for the reagent ion generation. Much higher background NH_3 was observed when using nitrogen instead of argon. Although, the sensitivity towards the measurement of NH_3 depends somewhat on the relative humidity of the sample flow, the observed sensitivity changes were rather low and can be taken into account by a correction factor. We did not explicitly demonstrate the quantitative measurement of diamines (and other amines than dimethylamine) in the present study but the instrument should also be well-suited for such measurements.

During experiments involving iodine, it was observed that the protonated water clusters can also be used to detect various iodine species. A total of 29 different iodine-containing compounds were unambiguously identified, including iodic acid (HIO_3) and neutral clusters containing up to four iodine atoms. The water cluster CI-APi-TOF was cross-calibrated against a nitrate CI-APi-TOF measuring iodic acid during CLOUD. The two instruments showed exactly the same time-dependent trends. As there is no established calibration method for iodic acid, detection limits have been derived under the assumption that HIO_3 is measured with the same efficiency as sulfuric acid, for which the nitrate CI-APi-TOF is calibrated for. The estimated LOD for the water cluster CI-APi-TOF regarding iodic acid was as low as 0.007 pptv.

Future studies will focus on the evaluation of the iodine signals and also on further signal identification in the mass spectra. Due to the instrument characteristics, we plan to apply the method to ambient atmospheric measurements to study the influence of ammonia, amines, diamines, and iodic acid on new particle formation. Airborne measurements in the upper troposphere, where very low ammonia mixing ratios can be expected (Höpfner et al., 2016) should in principle be feasible as well. For such measurement the water cluster CI-APi-TOF technique should be very well-suited due to the very low LODs that can be realized.

Acknowledgements

We would like to thank CERN for the support of CLOUD with financial and technical resources. We thank the PS/SPS team from CERN for providing the CLOUD experiment with a particle beam from the proton synchroton. We also want to thank L.-P. De Menezes for providing us with a mass flow controller used during the calibrations. Next to this, we would like to thank R. Sitals, T. Keber, S. Mathot, H.E. Manninen, A. Onnela, S. K. Weber and R. Kristic for their contributions to the experiment. The discussion with Xucheng He during the creation of the paper is gratefully acknowledged. We thank C. Hüglin for providing us with the PIARRCO and its calibration unit. This work was funded by: the German Federal Ministry of Education and Research "CLOUD-16" (no. 01LK1601A), EC Horizon 2020 MSCA-ITN "CLOUD-MOTION" (no. 764991), and EC Seventh Framework Programme MC-ITN "CLOUD-TRAIN" (no. 316662).

References

Aljawhary, D., Lee, A. K. Y., and Abbatt, J. P. D.: High-resolution chemical ionization mass spectrometry (ToF-CIMS): application to study SOA composition and processing, Atmos. Meas. Tech., 6, 3211–3224, doi:10.5194/amt-6-3211-2013, 2013.

Almeida, J., Schobesberger, S., Kürten, A., Ortega, I. K., Kupiainen-Määttä, O., Praplan, A. P., Adamov, A., Amorim, A., Bianchi, F., Breitenlechner, M., David, A., Dommen, J., Donahue, N. M., Downard, A., Dunne, E., Duplissy, J., Ehrhart, S., Flagan, R. C., Franchin, A., Guida, R., Hakala, J., Hansel, A., Heinritzi, M., Henschel, H., Jokinen, T., Junninen, H., Kajos, M., Kangasluoma, J., Keskinen, H., Kupc, A., Kurtén, T., Kvashin, A. N., Laaksonen, A., Lehtipalo, K., Leiminger, M., Leppä, J., Loukonen, V., Makhmutov, V., Mathot, S., McGrath, M. J., Nieminen, T., Olenius, T., Onnela, A., Petäjä, T., Riccobono, F., Riipinen, I., Rissanen, M., Rondo, L., Ruuskanen, T., Santos, F. D., Sarnela, N., Schallhart, S., Schnitzhofer, R., Seinfeld, J. H., Simon, M., Sipilä, M., Stozhkov, Y., Stratmann, F., Tomé, A., Tröstl, J., Tsagkogeorgas, G., Vaattovaara, P., Viisanen, Y., Virtanen, A., Vrtala, A., Wagner, P. E., Weingartner, E., Wex, H., Williamson, C., Wimmer, D., Ye, P., Yli-Juuti, T., Carslaw, K. S., Kulmala, M., Curtius, J., Baltensperger, U., Worsnop, D. R., Vehkamäki, H., and Kirkby, J.: Molecular understanding of sulphuric acid-amine particle nucleation in the atmosphere, Nature, 502, 359–363, doi:10.1038/nature12663, 2013.

Baron, P. A. and Willeke, K.: Aerosol measurement: Principles, techniques, and applications, 2nd ed., Wiley, New York, xxiii, 1131, 2001.

Bell, C. L., Dhib, M., Hancock, G., Ritchie, G. A. D., van Helden, J. H., and van Leeuwen, N. J.: Cavity enhanced absorption spectroscopy measurements of pressure-induced broadening and shift coefficients in the υ 1+υ 3 combination band of ammonia, Appl. Phys. B, 94, 327–336, doi:10.1007/s00340-008-3238-5, 2009.

Benson, D. R., Markovich, A., Al-Refai, M., and Lee, S.-H.: A Chemical Ionization Mass Spectrometer for ambient measurements of Ammonia, Atmos. Meas. Tech., 3, 1075–1087, doi:10.5194/amt-3-1075-2010, 2010.

Berresheim, H., Elste, T., Plass-Dülmer, C., Eiseleb, F.L., and Tannerb, D.J.: Chemical ionization mass spectrometer for long-term measurements of atmospheric OH and H2SO4, International Journal of Mass Spectrometry, 202, 91–109, doi:10.1016/S1387-3806(00)00233-5, 2000.

Bianchi, F., Dommen, J., Mathot, S., and Baltensperger, U.: On-line determination of ammonia at low pptv mixing ratios in the CLOUD chamber, Atmos. Meas. Tech., 5, 1719–1725, doi:10.5194/amt-5-1719-2012, 2012.

Bianchi, F., Tröstl, J., Junninen, H., Frege, C., Henne, S., Hoyle, C. R., Molteni, U., Herrmann, E., Adamov, A., Bukowiecki, N., Chen, X., Duplissy, J., Gysel, M., Hutterli, M., Kangasluoma, J., Kontkanen, J., Kürten, A., Manninen, H. E., Münch, S., Peräkylä, O., Petäjä, T., Rondo, L., Williamson, C., Weingartner, E., Curtius, J., Worsnop, D. R., Kulmala, M., Dommen, J., and Baltensperger, U.: New particle formation in the free troposphere: A question of chemistry and timing, Science (New York, N.Y.), 352, 1109–1112, doi:10.1126/science.aad5456, 2016.

Bobrutzki, K. von, Braban, C. F., Famulari, D., Jones, S. K., Blackall, T., Smith, T. E. L., Blom, M., Coe, H., Gallagher, M., Ghalaieny, M., McGillen, M. R., Percival, C. J., Whitehead, J. D., Ellis, R., Murphy, J., Mohacsi, A., Pogany, A., Junninen, H., Rantanen, S., Sutton, M. A., and Nemitz, E.: Field inter-comparison of eleven atmospheric ammonia measurement techniques, Atmos. Meas. Tech., 3, 91–112, doi:10.5194/amt-3-91-2010, 2010.

Cubison, M. J. and Jimenez, J. L.: Statistical precision of the intensities retrieved from constrained fitting of overlapping peaks in high-resolution mass spectra, Atmos. Meas. Tech., 8, 2333–2345, doi:10.5194/amt-8-2333-2015, 2015.

Dias, A., Ehrhart, S., Vogel, A., Williamson, C., Almeida, J., Kirkby, J., Mathot, S., Mumford, S., and Onnela, A.: Temperature uniformity in the CERN CLOUD chamber, Atmos. Meas. Tech., 10, 5075-5088, doi: 10.5194/amt-10-5075-2017, 2017.

Dunlop, P. J. and Bignell, C. M.: Prediction of the temperature dependence of binary diffusion coefficients of gaseous systems from thermal diffusion factors and diffusion coefficients at 300 K, International Journal of Thermophysics, 18, 939–945, doi:10.1007/BF02575239, 1997.

Dunne, E. M., Gordon, H., Kürten, A., Almeida, J., Duplissy, J., Williamson, C., Ortega, I. K., Pringle, K. J., Adamov, A., Baltensperger, U., Barmet, P., Benduhn, F., Bianchi, F., Breitenlechner, M., Clarke, A., Curtius, J., Dommen, J., Donahue, N. M., Ehrhart, S., Flagan, R. C., Franchin, A., Guida, R., Hakala, J., Hansel, A., Heinritzi, M., Jokinen, T., Kangasluoma, J., Kirkby, J., Kulmala, M., Kupc, A., Lawler, M. J., Lehtipalo, K., Makhmutov, V., Mann, G., Mathot, S., Merikanto, J., Miettinen, P., Nenes, A., Onnela, A., Rap, A., Reddington, C. L. S., Riccobono, F., Richards, N. A. D., Rissanen, M. P., Rondo, L., Sarnela, N., Schobesberger, S., Sengupta, K., Simon, M., Sipilä, M., Smith, J. N., Stozkhov, Y., Tomé, A., Tröstl, J., Wagner, P. E., Wimmer, D., Winkler, P. M., Worsnop, D. R., and Carslaw, K. S.: Global atmospheric particle formation from CERN CLOUD measurements, Science (New York, N.Y.), 354, 1119–1124, doi:10.1126/science.aaf2649, 2016.

Duplissy, J., Merikanto, J., Franchin, A., Tsagkogeorgas, G., Kangasluoma, J., Wimmer, D., Vuollekoski, H.,Schobesberger, S., Lehtipalo, K., Flagan, R. C., Brus, D., Donahue, N. M., Vehkamäki, H., Almeida, J., Amorim, A., Barmet, P., Bianchi, F., Breitenlechner, M., Dunne, E. M., Guida, R., Henschel, H., Junninen, H., Kirkby, J., Kürten, A., Kupc, A., Määttänen, A., Makhmutov, V., Mathot, S., Nieminen, T., Onnela, A., Praplan, A. P., Riccobono, F., Rondo, L., Steiner, G., Tome, A., Walther, H., Baltensperger, U., Carslaw, K. S., Dommen, J., Hansel, A., Petäjä, T., Sipilä, M., Stratmann, F., Vrtala, A., Wagner, P. E., Worsnop, D. R, Curtius, J., and Kulmala, M.: Effect of ions on sulfuric acid-water binary particle formation: 2. Experimental data and comparison with QC-normalized classical nucleation theory, *J. Geophys. Res. Atmos.*, 121, 1752– 1775, doi: 10.1002/2015JD023539, 2016.

Ehn, M., Thornton, J. A., Kleist, E., Sipilä, M., Junninen, H., Pullinen, I., Springer, M., Rubach, F., Tillmann, R., Lee, B., Lopez-Hilfiker, F., Andres, S., Acir, I.-H., Rissanen, M., Jokinen, T., Schobesberger, S., Kangasluoma, J., Kontkanen, J., Nieminen, T., Kurtén, T., Nielsen, L. B., Jørgensen, S., Kjaergaard, H. G., Canagaratna, M., Maso, M. D., Berndt, T., Petäjä, T., Wahner, A., Kerminen, V.-M., Kulmala, M., Worsnop, D. R., Wildt, J., and Mentel, T. F.: A large source of low-volatility secondary organic aerosol, Nature, 506, 476 EP -, doi:10.1038/nature13032, 2014.

Eisele, F. L. and Tanner, D. J.: Measurement of the gas phase concentration of H2SO4 and methane sulfonic acid and estimates of H2SO4 production and loss in the atmosphere, Journal of Geophysical Research: Atmospheres, 98, 9001–9010, doi:10.1029/93JD00031, 1993.

Eisele, F.L. and Hanson, D.R.: First Measurement of Prenucleation Molecular Clusters, The Journal of Physical Chemistry A, 104 (4), 830-836, doi:10.1021/jp9930651, 2000.

Ellis,R. A., J. G., Pattey, E., van Haarlem, R., O'Brien, J. M., and Herndon, S. C.: Characterizing a Quantum Cascade Tunable Infrared Laser Differential Absorption Spectrometer (QC-TILDAS) for measurements of atmospheric ammonia, Atmos. Meas. Tech., 3, 397–406, https://doi.org/10.5194/amt-3-397-2010, 2010.

Elm, J., Passananti, M., Kurtén, T., and Vehkamäki, H.: Diamines Can Initiate New Particle Formation in the Atmosphere, The Journal of Physical Chemistry A, 121, 6155–6164, doi:10.1021/acs.jpca.7b05658, 2017.

Ge, X., Wexler, S.; Clegg, S.L.: Atmospheric amines- Part I. A review, Atmospheric Environment, 45, 524-546, doi: 10.1016/j.atmosenv.2010.10.012, 2011.

Good, A., Durden, D. A., and Kebarle, P.: Mechanism and Rate Constants of Ion–Molecule Reactions Leading to Formation of H + (H 2 O) n in Moist Oxygen and Air, The Journal of Chemical Physics, 52, 222–229, doi:10.1063/1.1672668, 1970.

Hansel, A., Scholz, W., Mentler, B., Fischer, L., and Berndt, T.: Detection of RO 2 radicals and other products from cyclohexene ozonolysis with NH 4 + and acetate chemical ionization mass spectrometry, Atmospheric Environment, 186, doi:10.1016/j.atmosenv.2018.04.023, 2018.

Hanson, D. R., McMurry, P. H., Jiang, J., Tanner, D., and Huey, L. G.: Ambient pressure proton transfer mass spectrometry: detection of amines and ammonia, Environmental science & technology, 45, 8881–8888, doi:10.1021/es201819a, 2011.

Haruyama, T., Namise, T., Shimoshimizu, N., Uemura, S., Takatsuji, Y., Hino, M., Yamasaki, R., Kamachi, T., and Kohno, M..: Non-catalyzed one-step synthesis of ammonia from atmospheric air and water, Green Chem., 18, 4536-4541, doi: 10.1039/C6GC01560C, 2016.

Heinritzi, M., Simon, M., Steiner, G., Wagner, A. C., Kürten, A., Hansel, A., and Curtius, J.: Characterization of the mass-dependent transmission efficiency of a CIMS, Atmos. Meas. Tech., 9, 1449–1460, doi:10.5194/amt-9-1449-2016, 2016.

Höpfner, M., Volkamer, R., Grabowski, U., Grutter, M., Orphal, J., Stiller, G., Clarmann, T. von, and Wetzel, G.: First detection of ammonia (NH3) in the Asian summer monsoon upper troposphere, Atmos. Chem. Phys., 16, 14357–14369, doi:10.5194/acp-16-14357-2016, 2016.

Jen, C. N., Bachman, R., Zhao, J., McMurry, P. H., and Hanson, D. R.: Diamine-sulfuric acid reactions are a potent source of new particle formation, Geophys. Res. Lett., 43, 867–873, doi:10.1002/2015GL066958, 2016.

Jimenez, J. L., Canagaratna, M. R., Donahue, N. M., Prevot, A. S. H., Zhang, Q., Kroll, J. H., DeCarlo, P. F., Allan, J. D., Coe, H., Ng, N. L., Aiken, A. C., Docherty, K. S., Ulbrich, I. M., Grieshop, A. P., Robinson, A. L., Duplissy, J., Smith, J. D., Wilson, K. R., Lanz, V. A., Hueglin, C., Sun, Y. L., Tian, J., Laaksonen, A., Raatikainen, T., Rautiainen, J., Vaattovaara, P., Ehn, M., Kulmala, M., Tomlinson, J. M., Collins, D. R., Cubison, M. J., Dunlea, J., Huffman, J. A., Onasch, T. B., Alfarra, M. R., Williams, P. I., Bower, K., Kondo, Y., Schneider, J., Drewnick, F., Borrmann, S., Weimer, S., Demerjian, K., Salcedo, D., Cottrell, L., Griffin, R., Takami, A., Miyoshi, T., Hatakeyama, S., Shimono, A., Sun, J. Y., Zhang, Y. M., Dzepina, K., Kimmel, J. R., Sueper, D., Jayne, J. T., Herndon, S. C., Trimborn, A. M., Williams, L. R., Wood, E. C., Middlebrook, A. M., Kolb, C. E., Baltensperger, U., and Worsnop, D. R.: Evolution of Organic Aerosols in the Atmosphere, Science (New York, N.Y.), 326, 1525–1529, doi:10.1126/science.1180353, 2009.

Jokinen, T., Sipilä, M., Junninen, H., Ehn, M., Lönn, G., Hakala, J., Petäjä, T., Mauldin III, R. L., Kulmala, M., and Worsnop, D. R.: Atmospheric sulphuric acid and neutral cluster measurements using CI-APi-TOF, Atmos. Chem. Phys., 12, 4117–4125, doi:10.5194/acp-12-4117-2012, 2012.

Jokinen, T., Sipilä, M., Kontkanen, J., Vakkari, V., Tisler, P., Duplissy, E.-M., Junninen, H., Kangasluoma, J., Manninen, H. E., Petäjä, T., Kulmala, M., Worsnop, D. R., Kirkby, J., Virkkula, A., and Kerminen, V.-M.: Ion-induced sulfuric acid\textendashammonia nucleation drives particle formation in coastal Antarctica, Science Advances, 4, doi:10.1126/sciadv.aat9744, 2018.

Kebarle, P.: Higher-Order Reactions--Ion Clusters and Ion Solvation, in: Ion-Molecule Reactions: Volume 1, Franklin, J. L. (Ed.), Springer US, Boston, MA, 315–362, 1972.

Kirkby, J., Curtius, J., Almeida, J., Dunne, E., Duplissy, J., Ehrhart, S., Franchin, A., Gagné, S., Ickes, L., Kürten, A., Kupc, A., Metzger, A., Riccobono, F., Rondo, L., Schobesberger, S., Tsagkogeorgas, G., Wimmer, D., Amorim, A., Bianchi, F., Breitenlechner, M., David, A., Dommen, J., Downard, A., Ehn, M., Flagan, R. C., Haider, S., Hansel, A., Hauser, D., Jud, W., Junninen, H., Kreissl, F., Kvashin, A., Laaksonen, A., Lehtipalo, K., Lima, J., Lovejoy, E. R., Makhmutov, V., Mathot, S., Mikkilä, J., Minginette, P., Mogo, S., Nieminen, T., Onnela, A., Pereira, P., Petäjä, T., Schnitzhofer, R., Seinfeld, J. H., Sipilä, M., Stozhkov, Y., Stratmann, F., Tomé, A., Vanhanen, J., Viisanen, Y., Vrtala, A., Wagner, P. E., Walther, H., Weingartner, E., Wex, H., Winkler, P. M., Carslaw, K. S., Worsnop, D. R., Baltensperger, U., and Kulmala, M.: Role of sulphuric acid, ammonia and galactic cosmic rays in atmospheric aerosol nucleation, Nature, 476, 429 EP -, doi:10.1038/nature10343, 2011.

Kirkby, J., Duplissy, J., Sengupta, K., Frege, C., Gordon, H., Williamson, C., Heinritzi, M., Simon, M., Yan, C., Almeida, J., Tröstl, J., Nieminen, T., Ortega, I. K., Wagner, R., Adamov, A., Amorim, A., Bernhammer, A.-K., Bianchi, F., Breitenlechner, M., Brilke, S., Chen, X., Craven, J., Dias, A., Ehrhart, S., Flagan, R. C., Franchin, A., Fuchs, C., Guida, R., Hakala, J., Hoyle, C. R., Jokinen, T., Junninen, H., Kangasluoma, J., Kim, J., Krapf, M., Kürten, A., Laaksonen, A., Lehtipalo, K., Makhmutov, V., Mathot, S., Molteni, U., Onnela, A., Peräkylä, O., Piel, F., Petäjä, T., Praplan, A. P., Pringle, K., Rap, A., Richards, N. A. D., Riipinen, I., Rissanen, M. P., Rondo, L., Sarnela, N., Schobesberger, S., Scott, C. E., Seinfeld, J. H., Sipilä, M., Steiner, G., Stozhkov, Y., Stratmann, F., Tomé, A., Virtanen, A., Vogel, A. L., Wagner, A. C., Wagner, P. E., Weingartner, E., Wimmer, D., Winkler, P. M., Ye, P., Zhang, X., Hansel, A., Dommen, J., Donahue, N. M., Worsnop, D. R., Baltensperger, U., Kulmala, M., Carslaw, K. S., and Curtius, J.: Ion-induced nucleation of pure biogenic particles, Nature, 533, 521 EP -, doi:10.1038/nature17953, 2016.

Kupc, A., Amorim, A., Curtius, J., Danielczok, A., Duplissy, J., Ehrhart, S., Walther, H., Ickes, L., Kirkby, J., Kürten, A., Lima, J. M., Mathot, S., Minginette, P., Onnela, A., Rondo, and Rondo, L.: A fibre-optic UV system for H2SO4 production in aerosol chambers causing minimal thermal effects, Journal of Aerosol Science, 42, 532–543, doi:10.1016/j.jaerosci.2011.05.001, 2011.

Kurtén, T., Loukonen, V., Vehkamäki, H., and Kulmala, M.: Amines are likely to enhance neutral and ion-induced sulfuric acid-water nucleation in the atmosphere more effectively than ammonia, Atmos. Chem. Phys. Discuss., 8, 7455–7476, doi:10.5194/acpd-8-7455-2008, 2008.

Kürten, A.: New particle formation from sulfuric acid and ammonia: nucleation and growth model based on thermodynamics derived from CLOUD measurements for a wide range of conditions, Atmos. Chem. Phys.,19, 5033-5050, doi:10.5194/acp-19-5033-2019, 2019.

Kürten, A., Bergen, A., Heinritzi, M., Leiminger, M., Lorenz, V., Piel, F., Simon, M., Sitals, R., Wagner, A. C., and Curtius, J.: Observation of new particle formation and measurement of sulfuric acid, ammonia, amines and highly oxidized organic molecules at a rural site in central Germany, Atmos. Chem. Phys., 16, 12793–12813, doi:10.5194/acp-16-12793-2016, 2016b.

Kürten, A., Bianchi, F., Almeida, J., Kupiainen-Määttä, O., Dunne, E. M., Duplissy, J., Williamson, C., Barmet, P., Breitenlechner, M., Dommen, J., Donahue, N. M., Flagan, R. C., Franchin, A., Gordon, H., Hakala, J., Hansel, A., Heinritzi, M., Ickes, L., Jokinen, T., Kangasluoma, J., Kim, J., Kirkby, J., Kupc, A., Lehtipalo, K., Leiminger, M., Makhmutov, V., Onnela, A., Ortega, I. K., Petäjä, T., Praplan, A. P., Riccobono, F., Rissanen, M. P., Rondo, L., Schnitzhofer, R., Schobesberger, S., Smith, J. N., Steiner, G., Stozhkov, Y., Tomé, A., Tröstl, J., Tsagkogeorgas, G., Wagner, P. E., Wimmer, D., Ye, P., Baltensperger, U., Carslaw, K., Kulmala, M., and Curtius, J.: Experimental particle formation rates spanning tropospheric sulfuric acid and ammonia abundances, ion production rates, and temperatures, J. Geophys. Res. Atmos., 121, 12,377-12,400, doi:10.1002/2015JD023908, 2016a.

Kürten, A., Jokinen, T., Simon, M., Sipilä, M., Sarnela, N., Junninen, H., Adamov, A., Almeida, J., Amorim, A., Bianchi, F., Breitenlechner, M., Dommen, J., Donahue, N. M., Duplissy, J., Ehrhart, S., Flagan, R. C., Franchin, A., Hakala, J., Hansel, A., Heinritzi, M., Hutterli, M., Kangasluoma, J., Kirkby, J., Laaksonen, A., Lehtipalo, K., Leiminger, M., Makhmutov, V., Mathot, S., Onnela, A., Petäjä, T., Praplan, A. P., Riccobono, F., Rissanen, M. P., Rondo, L., Schobesberger, S., Seinfeld, J. H., Steiner, G., Tomé, A., Tröstl, J., Winkler, P. M., Williamson, C., Wimmer, D., Ye, P., Baltensperger, U., Carslaw, K. S., Kulmala, M., Worsnop, D. R., and Curtius, J.: Neutral molecular cluster formation of sulfuric acid-dimethylamine observed in real time under atmospheric conditions, Proceedings of the National Academy of Sciences of the United States of America, 111, 15019–15024, doi:10.1073/pnas.1404853111, 2014.

Kürten, A., Rondo, L., Ehrhart, S., and Curtius, J.: Performance of a corona ion source for measurement of sulfuric acid by chemical ionization mass spectrometry, Atmos. Meas. Tech., 4, 437–443, doi:10.5194/amt-4-437-2011, 2011.

Kürten, A., Rondo, L., Ehrhart, S., and Curtius, J.: Calibration of a Chemical Ionization Mass Spectrometer for the Measurement of Gaseous Sulfuric Acid, The Journal of Physical Chemistry A, 116, 6375–6386, doi:10.1021/jp212123n, 2012.

Lehtipalo, K., Yan, C., Dada, L., Bianchi, F., Xiao, M., Wagner, R., Stolzenburg, D., Ahonen, L. R., Amorim, A., Baccarini, A., Bauer, P. S., Baumgartner, B., Bergen, A., Bernhammer, A.-K., Breitenlechner, M., Brilke, S., Buchholz, A., Mazon, S. B., Chen, D., Chen, X., Dias, A., Dommen, J., Draper, D. C., Duplissy, J., Ehn, M., Finkenzeller, H., Fischer, L., Frege, C., Fuchs, C., Garmash, O., Gordon, H., Hakala, J., He, X., Heikkinen, L., Heinritzi, M., Helm, J. C., Hofbauer, V., Hoyle, C. R., Jokinen, T., Kangasluoma, J., Kerminen, V.-M., Kim, C., Kirkby, J., Kontkanen, J., Kürten, A., Lawler, M. J., Mai, H., Mathot, S., Mauldin, R. L., Molteni, U., Nichman, L., Nie, W., Nieminen, T., Ojdanic, A., Onnela, A., Passananti, M., Petäjä, T., Piel, F., Pospisilova, V., Quéléver, L. L. J., Rissanen, M. P., Rose, C., Sarnela, N., Schallhart, S., Schuchmann, S., Sengupta, K., Simon, M., Sipilä, M., Tauber, C., Tomé, A., Tröstl, J., Väisänen, O., Vogel, A. L., Volkamer, R., Wagner, A. C., Wang, M., Weitz, L., Wimmer, D., Ye, P., Ylisirniö, A., Zha, Q., Carslaw, K. S., Curtius, J., Donahue, N. M., Flagan, R. C., Hansel, A., Riipinen, I., Virtanen, A., Winkler, P. M., Baltensperger, U., Kulmala, M., and Worsnop, D. R.: Multicomponent new particle formation from sulfuric acid, ammonia, and biogenic vapors, Science Advances, 4, doi:10.1126/sciadv.aau5363, 2018.

Leifer, I., Melton, C., Tratt, D. M., Buckland, K. N., Clarisse, L., Coheur, P., Frash, J., Gupta, M., Johnson, P. D., Leen, J. B., van Damme, M., Whitburn, S., and Yurganov, L.: Remote sensing and in situ measurements of methane and ammonia emissions from a megacity dairy complex: Chino, CA, Environmental pollution (Barking, Essex 1987), 221, 37–51, doi:10.1016/j.envpol.2016.09.083, 2017.

Martin, N. A., Ferracci, V., Cassidy, N., and Hoffnagle, J. A.: The application of a cavity ring-down spectrometer to measurements of ambient ammonia using traceable primary standard gas mixtures, Appl. Phys. B, 122, 219, doi:10.1007/s00340-016-6486-9, 2016.

Murphy, D. M. and Koop, T.: Review of the vapour pressures of ice and supercooled water for atmospheric applications, Quarterly Journal of the Royal Meteorological Society, 131, 1539–1565, doi:10.1256/qj.04.94, 2005.

Norman, M., Hansel, A., and Wisthaler, A.: O2+ as reagent ion in the PTR-MS instrument: Detection of gas-phase ammonia, International Journal of Mass Spectrometry, 265, 382–387, doi:10.1016/j.ijms.2007.06.010, 2007.

Norman, M., Spierig, C., Wolff, V., Trebs, I., Flechard, C., Wisthaler, A., Schnitzhofer, R., Hansel, A., and Neftel, A.: Intercomparison of ammonia measurement techniques at an intensively managed grassland site (Oensingen, Switzerland), Atmospheric Chemistry and Physics Discussions, v.8, 19791-19818 (2008), 2009.

Nowak, J. B., Huey, L. G., Eisele, F. L., Tanner, D. J., Mauldin, R. L., Cantrell, C., Kosciuch, E., and Davis, D., Chemical ionization mass spectrometry technique for the detection of dimethylsulfoxide and ammonia, J. Geophys. Res., 107(D18), 4363, doi:10.1029/2001JD001058, 2002.

Nowak, J. B., Huey, L. G., Russel, A.G., Tian D., Neuman, J.A., Orsini, D., Sjostedt, S.J., Sullivan, A.P., Tanner, D.J., Weber, R.J., Nenes, A.,Edgerton, E., and Fehsenfeld, F.C., Analysis of urban gas phase ammonia measurements from the 2002 Atlanta Aerosol Nucleation and Real-Time Characterization Experiment (ANARChE), J. Geophys. Res., 111, D17308, doi:10.1029/2006JD007113, 2006.

Nowak, J., Neuman, J., Bahreini, R., A. Brock, C., M. Middlebrook, A., G. Wollny, A., Holloway, J., Peischl, J., B. Ryerson, T., and Fehsenfeld, F.: Airborne observations of ammonia and ammonium nitrate formation over Houston, Texas, J. Geophys. Res., 115, doi:10.1029/2010JD014195, 2010.

Nowak, J., Neuman, J., Kozai, K., G. Huey, L., Tanner, D., Holloway, J., B. Ryerson, T., Frost, G., McKeen, S., and Fehsenfeld, F.: A chemical ionization mass spectrometry technique for airborne measurements of ammonia, J. Geophys. Res., 112, D10S02, doi:10.1029/2006JD007589, 2007.

Pollack, I. B., Lindaas, J., Roscioli, J. R., Agnese, M., Permar, W., Hu, L., and Fischer, E. V.: Evaluation of ambient ammonia measurements from a research aircraft using a closed-path QC-TILDAS spectrometer operated with active continuous passivation, Atmos. Meas. Tech. Discuss., https://doi.org/10.5194/amt-2019-11, in review, 2019.

Pozzer, A., Tsimpidi, A. P., Karydis, V. A., Meij, A. de, and Lelieveld, J.: Impact of agricultural emission reductions on fine-particulate matter and public health, Atmos. Chem. Phys., 17, 12813–12826, doi:10.5194/acp-17-12813-2017, 2017.

Roscioli, J. R., Zahniser, M. S., Nelson, D. D., Herndon, S. C., and Kolb, C. E.: New Approaches to Measuring Sticky Molecules: Improvement of Instrumental Response Times Using Active Passivation, The journal of physical chemistry. A, 120, 1347–1357, doi:10.1021/acs.jpca.5b04395, 2016.

Simon, M., Heinritzi, M., Herzog, S., Leiminger, M., Bianchi, F., Praplan, A., Dommen, J., Curtius, J., and Kürten, A.: Detection of dimethylamine in the low pptv range using nitrate chemical ionization atmospheric pressure interface time-of-flight (CI-APi-TOF) mass spectrometry, Atmos. Meas. Tech., 9, 2135–2145, doi:10.5194/amt-9-2135-2016, 2016.

Sipilä, M., Sarnela, N., Jokinen, T., Henschel, H., Junninen, H., Kontkanen, J., Richters, S., Kangasluoma, J., Franchin, A., Peräkylä, O., Rissanen, M. P., Ehn, M., Vehkamäki, H., Kurten, T., Berndt, T., Petäjä, T., Worsnop, D., Ceburnis, D., Kerminen, V.-M., Kulmala, M., and O'Dowd, C.: Molecular-scale evidence of aerosol particle formation via sequential addition of HIO3, Nature, 537, 532 EP -, doi:10.1038/nature19314, 2016.

Sipilä, M., Sarnela, N., Jokinen, T., Junninen, H., Hakala, J., Rissanen, M. P., Praplan, A., Simon, M., Kürten, A., Bianchi, F., Dommen, J., Curtius, J., Petäjä, T., and Worsnop, D. R.: Bisulfate – cluster based atmospheric pressure chemical ionization mass spectrometer for high-sensitivity (< 100 ppqV) detection of atmospheric dimethyl amine: proof-of-concept and first ambient data from boreal forest, Atmos. Meas. Tech., 8, 4001–4011, doi:10.5194/amt-8-4001-2015, 2015.

Skrotzki, J.: High-accuracy multiphase humidity measurements using TDLAS: application to the investigation of ice growth in simulated cirrus clouds, Ruperto-Carola University of Heidelberg, Heidelberg, 2012.

Stark, H., Yatavelli, R. L.N., Thompson, S. L., Kimmel, J. R., Cubison, M. J., Chhabra, P. S., Canagaratna, M. R., Jayne, J. T., Worsnop, D.R. and Jimenez, J. L.: Methods to extract molecular and bulk chemical information from series of complex mass spectra with limited mass resolution, International Journal of Mass Spectrometry, 389, 26–38, doi:10.1016/j.ijms.2015.08.011, 2015.

Sunner, J., Nicol, G., and Kebarle, P.: Factors determining relative sensitivity of analytes in positive mode atmospheric pressure ionization mass spectrometry, Analytical Chemistry, 60, 1300–1307, doi:10.1021/ac00164a012, 1988.

Tang, M. J., Shiraiwa, M., Pöschl, U., Cox, R. A., and Kalberer, M.: Compilation and evaluation of gas phase diffusion coefficients of reactive trace gases in the atmosphere: Volume 2. Diffusivities of organic compounds, pressure-normalised mean free paths, and average Knudsen numbers for gas uptake calculations, Atmos. Chem. Phys., 15, 5585-5598, https://doi.org/10.5194/acp-15-5585-2015, 2015.

Timonen, H., Cubison, M., Aurela, M., Brus, D., Lihavainen, H., Hillamo, R., Canagaratna, M., Nekat, B., Weller, R., Worsnop, D., and Saarikoski, S.: Applications and limitations of constrained high-resolution peak fitting on low resolving power mass spectra from the ToF-ACSM, Atmos. Meas. Tech., 9, 3263–3281, doi:10.5194/amt-9-3263-2016, 2016.

Vaittinen, O., Metsälä, M., Persijn, S., Vainio, M., and Halonen, L.: Adsorption of ammonia on treated stainless steel and polymer surfaces, Appl. Phys. B, 115, doi:10.1007/s00340-013-5590-3, 2014.

Verriele, M., Plaisance, H., Depelchin, L., Benchabane, S., Locoge, N., and Meunier, G.: Determination of 14 amines in air samples using midget impingers sampling followed by analysis with ion chromatography in tandem with mass spectrometry, Journal of environmental monitoring JEM, 14, 402–408, doi:10.1039/c2em10636a, 2012.

W.J. Massman: A review of the molecular diffusivities of H2O, CO2, CH4, CO, O3, SO2, NH3, N2O, NO, and NO2 in air, O2 and N2 near STP, Atmospheric Environment, 32, 1111–1127, doi:10.1016/S1352-2310(97)00391-9, 1998.

Wang, S., Nan, J., Shi, C., Fu, Q., Gao, S., Wang, D., Cui, H., Saiz-Lopez, A., and Zhou, B.: Atmospheric ammonia and its impacts on regional air quality over the megacity of Shanghai, China, Scientific reports, 5, 15842, doi:10.1038/srep15842, 2015.

Weissler, G. L.: Positive and Negative Point-to-Plane Corona in Pure and Impure Hydrogen, Nitrogen, and Argon, Phys. Rev., 63, 96–107, doi:10.1103/PhysRev.63.96, 1943.

Wilkinson, G. N. and Rogers, C. E.: Symbolic Description of Factorial Models for Analysis of Variance, Journal of the Royal Statistical Society. Series C (Applied Statistics), 22, 392–399, doi:10.2307/2346786, 1973.

Yan, C., Dada, L., Rose, C., Jokinen, T., Nie, W., Schobesberger, S., Junninen, H., Lehtipalo, K., Sarnela, N., Makkonen, U., Garmash, O., Wang, Y., Zha, Q., Paasonen, P., Bianchi, F., Sipilä, M., Ehn, M., Petäjä, T., Kerminen, V.-M., Worsnop, D. R., and Kulmala, M.: The role of H2SO4-NH3 anion clusters in ion-induced aerosol nucleation mechanisms in the boreal forest, Atmos. Chem. Phys., 18, 13231–13243, doi:10.5194/acp-18-13231-2018, 2018.

Yao, L., Wang, M.-Y., Wang, X.-K., Liu, Y.-J., Chen, H.-F., Zheng, J., Nie, W., Ding, A.-J., Geng, F.-H., Wang, D.-F., Chen, J.-M., Worsnop, D. R., and Wang, L.: Detection of atmospheric gaseous amines and amides by a high-resolution time-of-flight chemical ionization mass spectrometer with protonated ethanol reagent ions, Atmos. Chem. Phys., 16, 14527–14543, doi:10.5194/acp-16-14527-2016, 2016.

Yokelson, R. J.: Evaluation of adsorption effects on measurements of ammonia, acetic acid, and methanol, J. Geophys. Res., 108, 75, doi:10.1029/2003JD003549, 2003.

You, Y., Kanawade, V. P., Gouw, J. A. de, Guenther, A. B., Madronich, S., Sierra-Hernández, M. R., Lawler, M., Smith, J. N., Takahama, S., Ruggeri, G., Koss, A., Olson, K., Baumann, K., Weber, R. J., Nenes, A., Guo, H., Edgerton, E. S., Porcelli, L., Brune, W. H., Goldstein, A. H., and Lee, S.-H.: Atmospheric amines and ammonia measured with a chemical ionization mass spectrometer (CIMS), Atmos. Chem. Phys., 14, 12181–12194, doi:10.5194/acp-14-12181-2014, 2014.

Yu, F., Nadykto, A. B., Herb, J., Luo, G., Nazarenko, K. M., and Uvarova, L. A.: H2SO4–H2O–NH3 ternary ion-mediated nucleation (TIMN): kinetic-based model and comparison with CLOUD measurements, Atmos. Chem. Phys., 18, 17451–17474, doi:10.5194/acp-18-17451-2018, 2018.

Zhao, J. and Zhang, R.: Proton transfer reaction rate constants between hydronium ion (H3O+) and volatile organic compounds, Atmospheric Environment, 38, 2177–2185, doi:10.1016/j.atmosenv.2004.01.019, 2004.

Table 1. Estimated limits of detection (LOD) for some compounds with high proton affinity, and for iodic acid, measured with the water cluster CI-APi-TOF. The LOD is derived by background measurements at the CLOUD chamber, where LOD = 3•σ (You et al., 2014). σ is defined as the standard deviation of the background signal. The detection limits are based on a measurement at 278 K and 80% RH (1 minute averaging time). The measured instrumental background mixing ratios (mean values) during this time period are also indicated.

Detected compound	**LOD (pptv)**	**Instrumental background (pptv)**	**Measured *m/z* values (Th)**
NH_3 (ammonia)	0.5 ± 0.05	3.73 ± 0.35	18.0338 (NH_4^+); 36.0444 ($(H_2O)NH_4^+$)
$(CH_3)_2NH$ (dimethylamine)*	0.047*	0.058*	46.0651 ($(CH_3)_2NH_2^+$)
HIO_3 (iodic acid)**	0.007**	< LOD**	176.9043 ($(HIO_3)H^+$); 194.9149 ($(HIO_3)H_3O^+$)

*Amine mixing ratios are estimated using the same calibration factor derived for ammonia. This can cause uncertainties. The applicability of this assumption is discussed in Section 3.9.

**Iodic acid mixing ratios are derived from an inter-comparison with a nitrate CI-APi-TOF, which evaluates HIO_3 based on a calibration factor derived for sulfuric acid. This assumption can lead to uncertainties but is necessary because no direct calibration method exists for such low gas phase HIO_3 concentrations.

Table 2. Iodine-containing compounds (atomic composition), together with their *m*/*z* values, identified in the water cluster CI-APi-TOF spectra during the CLOUD13 campaign.

Detected compound	***m*/*z* value (Th)**
I^+	126.9039
IO^+	142.8988
HIO^+	143.9067
IO_2^+	158.8938
$H_2IO_2^+$	160.9094
$H_3IO_2^+$	161.9172
$H_4IO_2^+$	162.9251
HIO_3^+	175.8965
$H_2IO_3^+$	176.9043
$H_3IO_3^+$	177.9121
$H_4IO_3^+$	178.9200
$H_4IO_4^+$	194.9149
$H_6IO_5^+$	212.9254
I_2^+	253.8084
$HI_2O_5^+$	334.7908
$H_3I_2O_5^+$	336.8064
$H_3I_2O_6^+$	352.8014
$H_5I_2O_6^+$	354.8170
$H_5I_2O_7^+$	370.8119
$H_2I_3O_7^+$	494.6929
$HI_3O_8^+$	509.6800
$H_2I_3O_8^+$	510.6878
$H_4I_3O_8^+$	512.7035
$H_4I_3O_9^+$	528.6984
$HI_4O_8^+$	636.5845
$HI_4O_9^+$	652.5794
$H_3I_4O_9^+$	654.5950
$H_3I_4O_{10}^+$	670.5900
$H_3I_4O_{11}^+$	686.5849

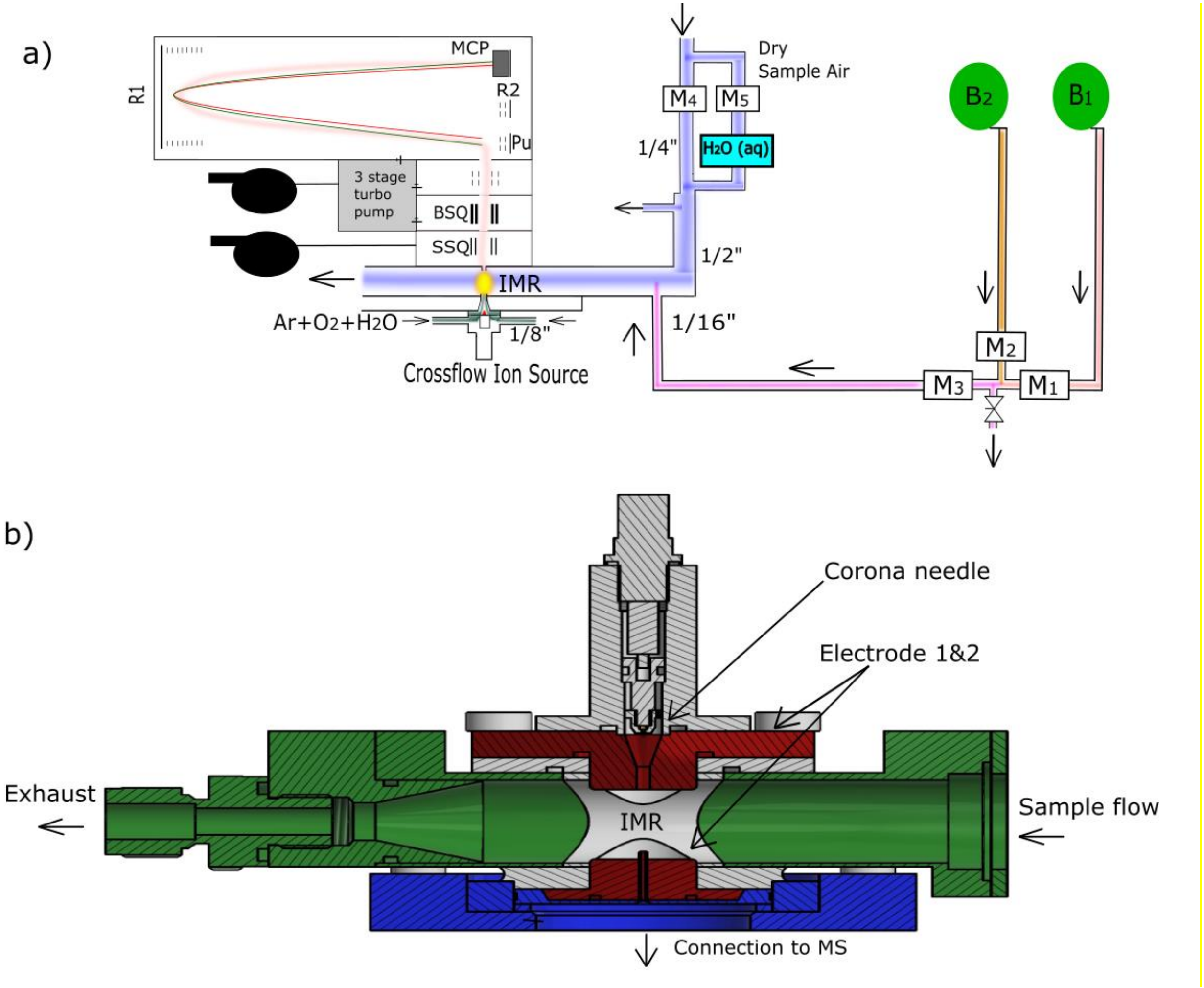

Figure 1: The experimental setup of the water cluster CI-APi-TOF during ammonia calibration is shown in panel a). The blue color indicates the sample flow. It consists of a mixture of 80% nitrogen and 20% oxygen. A portion of the sample flow can be humidified with a water bubbler (H_2O aq) to achieve different relative humidities. B_1 represents the ammonia gas bottle, while B_2 represents a gas bottle containing pure nitrogen. There are five mass flow controllers (MFCs; labeled as $M_{1\text{-}5}$) allowing two dilution steps. Three MFCs (M_1, M_2, M_3) control the amount of ammonia that is added through a 1/16'' capillary into the center of the sample flow, where the second dilution stage occurs. The reagent ions (i.e., protonated water clusters) are produced when the ion source gas (argon, oxygen, water vapor) passes a corona needle at a positive high voltage (detailed in panel b). The calibration setup is disconnected during the measurements at the CLOUD chamber to reduce backgrounds (leakage from the 1/16'' capillary). Details of the ion source used during CLOUD13 are shown in panel b. The primary ions are guided towards the sample flow using a counter electrode (Electrode 1). Additionally, a funnel is used to accelerate the primary ions towards the sample flow. A second electrode (Electrode 2) is installed directly in front of the pinhole of the mass spectrometer. The ions enter the mass spectrometer through a capillary on the top of Electrode 2.

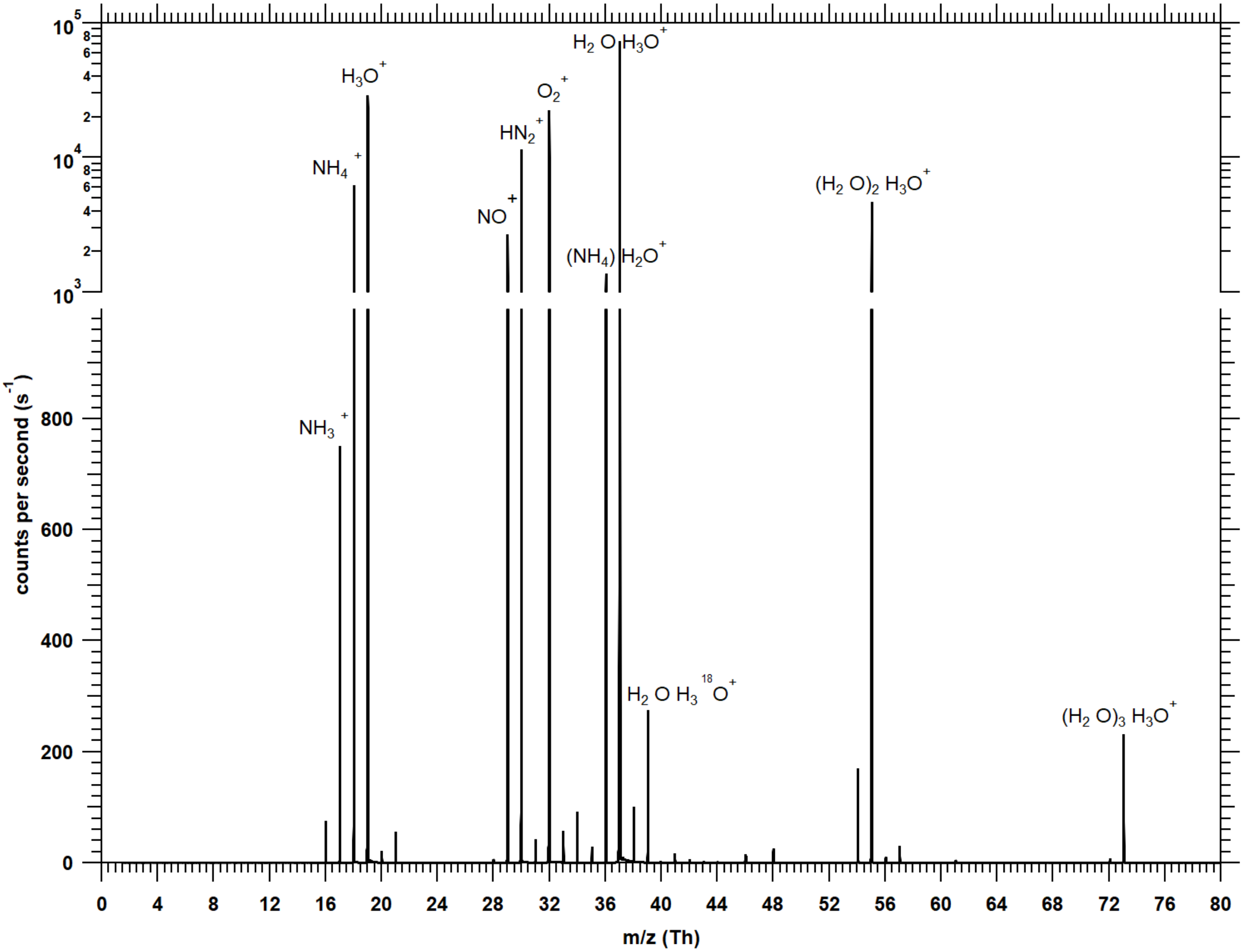

Figure 2: Typical mass spectrum recorded with the water cluster CI-APi-TOF when about 10 ppbv of ammonia are added during a calibration. Signals below 1000 counts per second are shown on a linear scale, while the dominant signals (> 1000 cps) are shown on a logarithmic scale. To calculate the ammonia mixing ratio, the product ion signals (NH_4^+ and $(H_2O)NH_4^+$) are normalized against the most prominent reagent ion signals (H_3O^+, $(H_2O)H_3O^+$, $(H_2O)_2H_3O^+$, $(H_2O)_3H_3O^+$). Larger water clusters are probably also present in the ion-molecule reaction zone but a significant fraction of water evaporates upon crossing the pinhole at the atmospheric pressure interface of the instrument. Background peaks from N_2H^+, NO^+ and O_2^+ are always present but are neglected in the data evaluation. Due to the short reaction time (< 1 ms) in the ion-molecule reaction zone, the count rates of the reagent ions dominate the spectrum even at high ammonia mixing ratios near 1 ppbv.

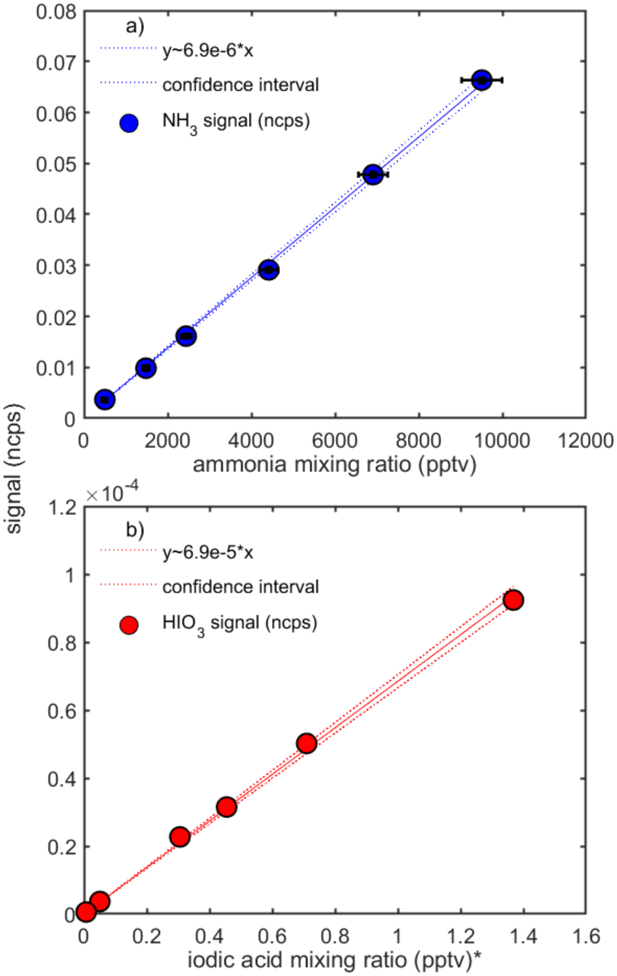

Figure 3: Calibration curves for ammonia (a) and iodic acid (b) at 40% relative humidity. The *y*-axes show the normalized counts per second (ncps) measured with the water cluster CI-APi-TOF. The ammonia mixing ratios are determined from the calibration set-up and the iodic acid mixing ratios are taken from simultaneous measurements with a nitrate CI-APi-TOF at the CLOUD chamber. The systematic uncertainty of the iodic acid mixing ratios is estimated as +100%/-50% (Sipilä et al., 2016). The inverse slopes from the linear fits yield the calibration factors (see equation (1) and (2)).

*Note that the iodic acid mixing ratio is derived by applying a calibration factor for sulfuric acid to the nitrate CI-APi-TOF data.

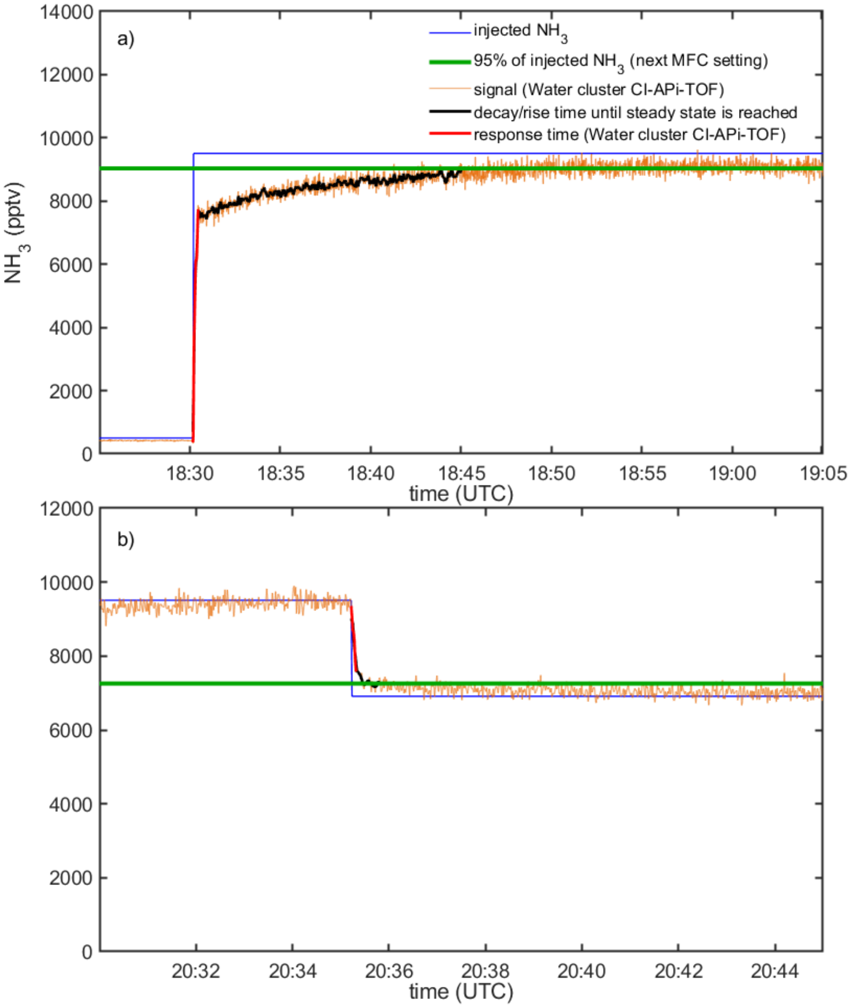

Figure 4: Response time of the water cluster CI-APi-TOF during calibrations at 60% RH. The injected ammonia mixing ratio from MFC settings is shown by the blue line. The signal of the water cluster CI-APi-TOF is shown by the orange line (here the data are shown with a 1 second time resolution i.e. no time-averaging is applied). The green line represents 95% of the mixing ratio being applied with the next MFC setting. The black line shows the response time until a steady state (panel a) or 95% of the final measured concentration is reached (panel b). The response time is the sum of the response time of the water-cluster CI-APi-TOF (red line) and the (slower) response time for the lines to reach a steady state where the walls are conditioned.

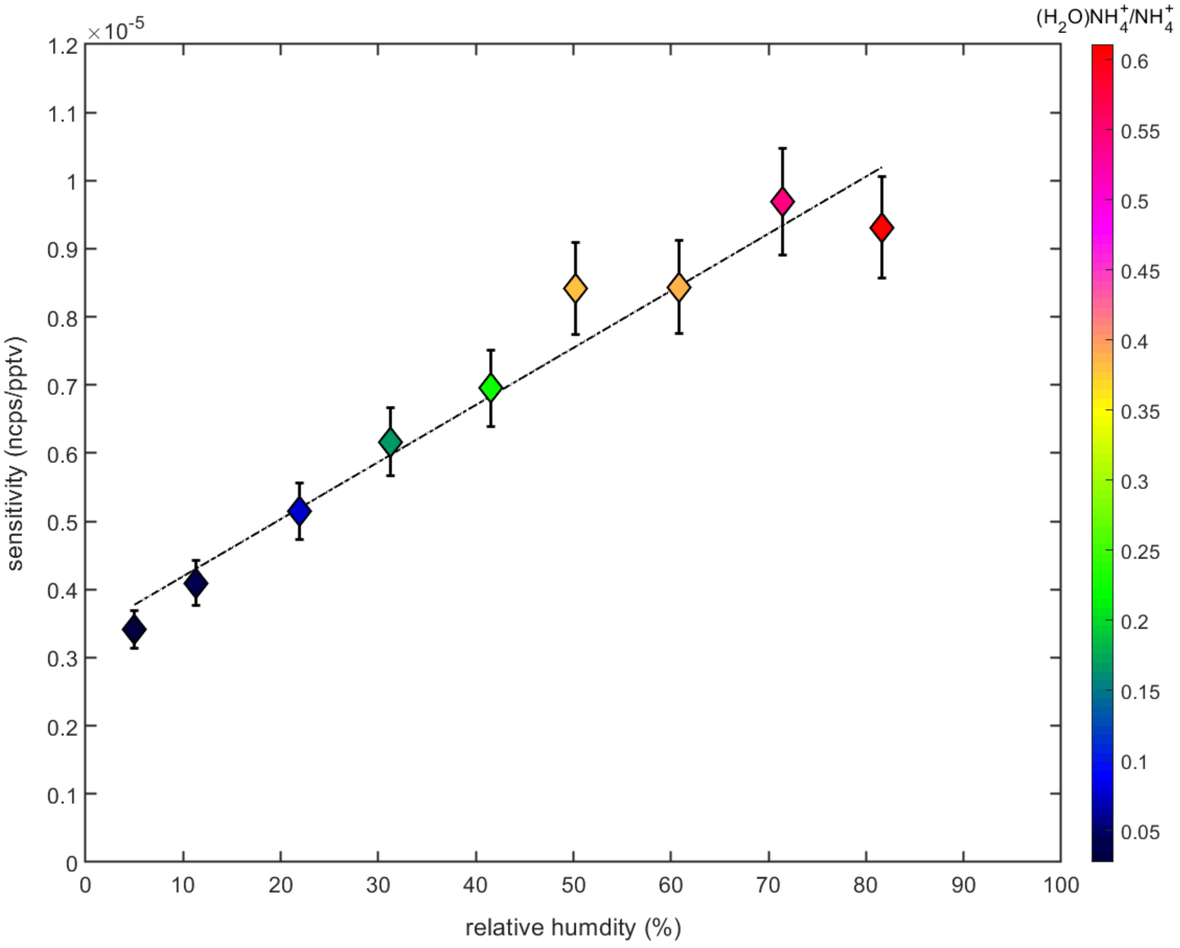

Figure 5: Dependency of the ammonia sensitivity as a function of the relative humidity (in %). A linear increase with relative humidity is observed, which tracks an increase of the ratio of the $(H_2O)NH_4^+$ and NH_4^+ ion signals (indicated by the color-code).

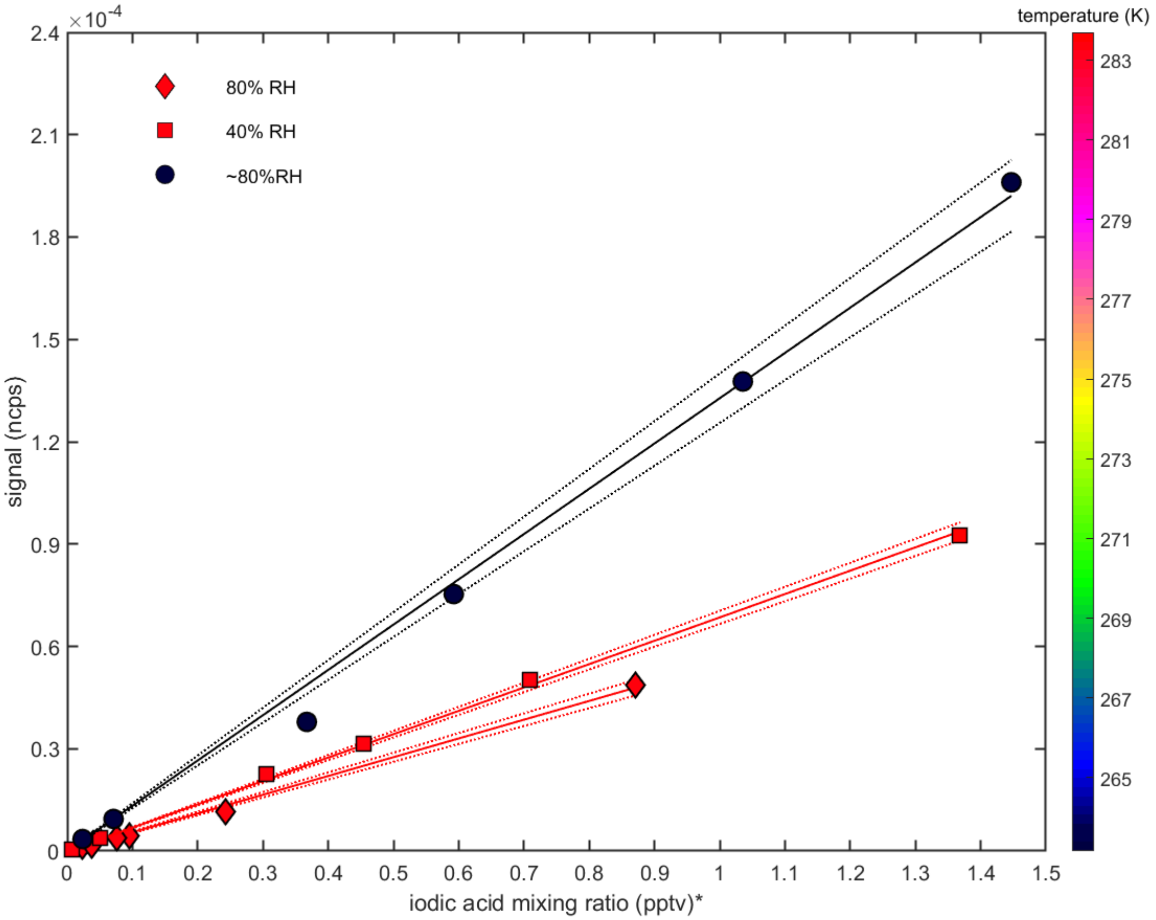

Figure 6: Calibration curves for iodic acid at different relative humidities and temperatures in the CLOUD chamber. The normalized counts per second (*y*-axis) are shown against the iodic acid mixing ratio measured with a nitrate CI-APi-TOF (*x*-axis). The sensitivity increases at lower temperatures, while no strong dependency on relative humidity is found at 283 K.

* Note that the iodic acid mixing ratio is derived by applying a calibration factor for sulfuric acid to the nitrate CI-APi-TOF data.

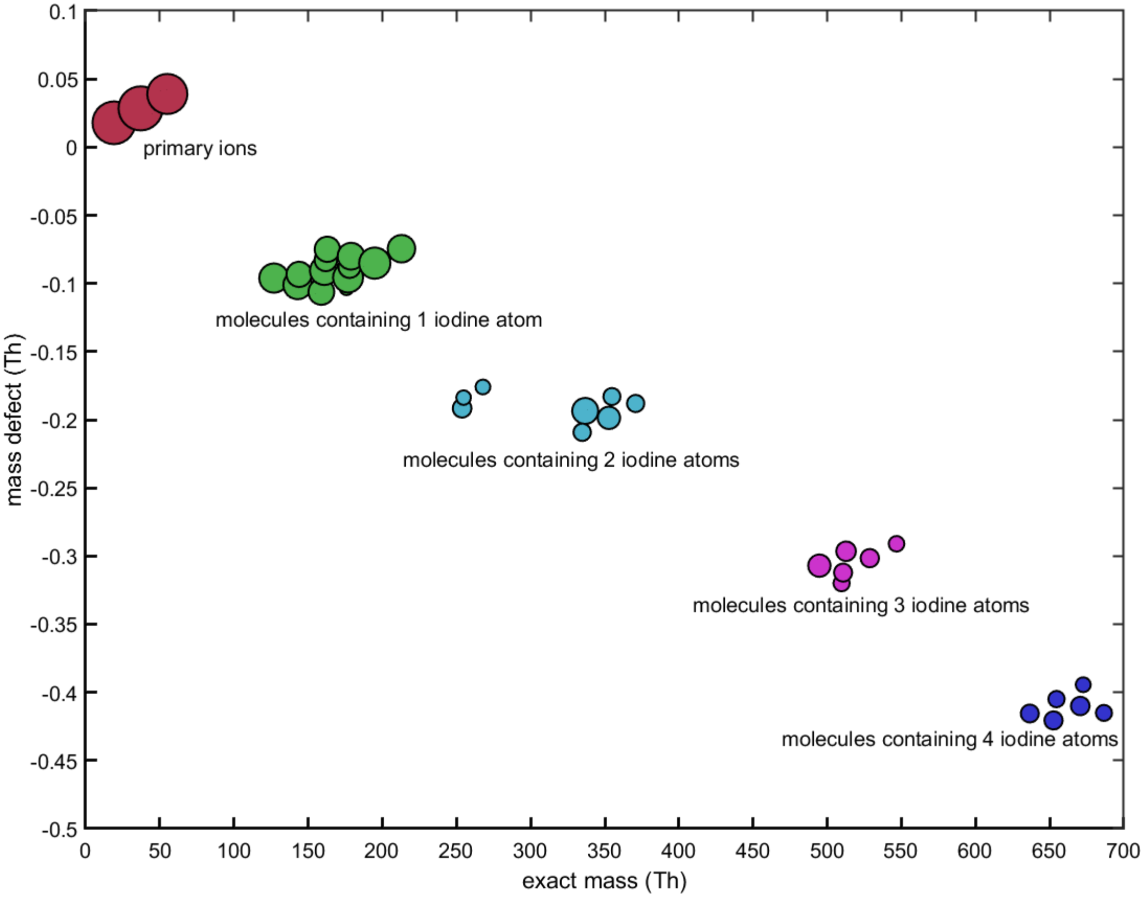

Figure 7: Mass defect plot for the iodine compounds, as well as the most prominent reagent ions, during a CLOUD experiment on new particle formation from iodine. The estimated iodic acid mixing ratio is ~0.98 pptv. The *y*-axis shows the mass defects of the compounds (see Table 2 and text for details), while the *x*-axis shows the absolute masses. The size of the symbols is proportional to the measured signal intensities on a logarithmic scale (from $1.24 \cdot 10^{-6}$ to 14.04 ions/s).

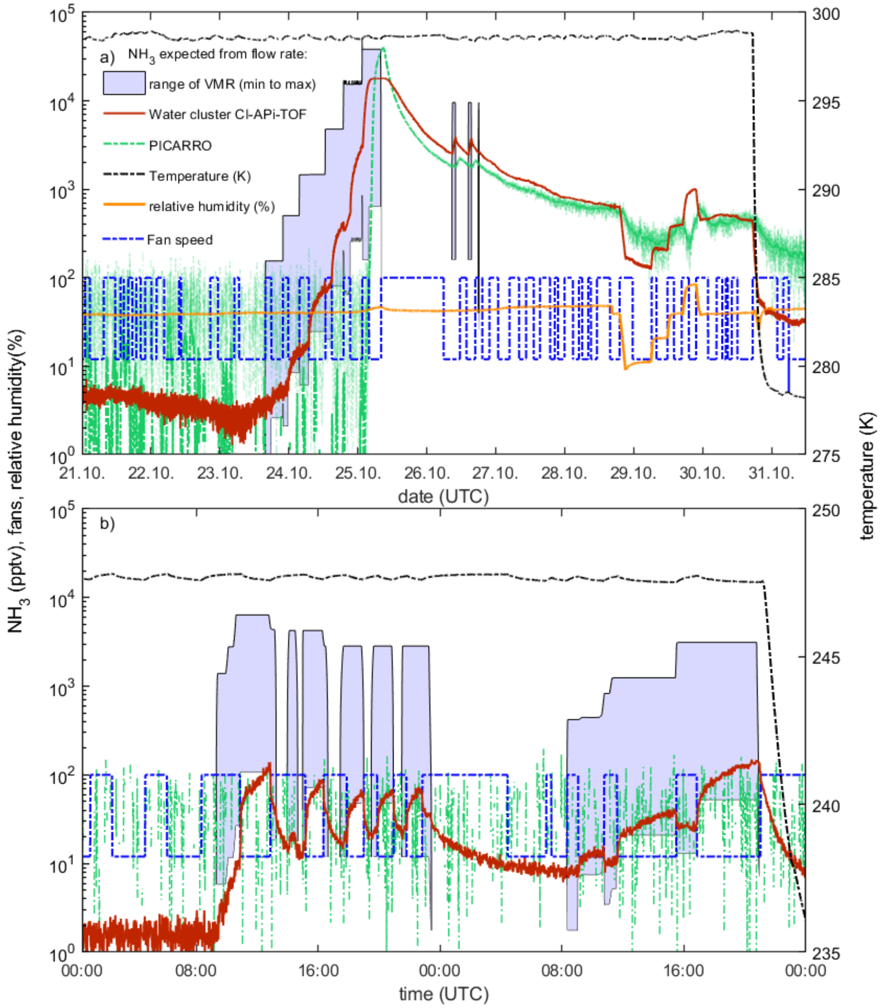

Figure 8: Inter-comparison between calculated (shaded blue area) and measured ammonia mixing ratios (PICARRO: solid green line; water cluster CI-APi-TOF: solid red line) at CLOUD. The PICARRO background (~200 pptv) has been subtracted, while no background was subtracted from the water cluster CI-APi-TOF. The temperature inside the chamber is indicated by the dashed black line. The speed (% of maximum, 397 revolutions per minute) of the two fans that mix the air inside the chamber is shown by the dashed blue line. The calculated ammonia mixing ratios (based on the calculated injection of ammonia into the chamber from the MFC settings) have a wide range due to uncertainties of the ammonia loss rate in the chamber. We display the maximum calculated range assuming, for the lower limit, that the chamber walls act as a perfect sink (wall loss dominated, 25s and 100 s lifetime for fan speeds 100% and 12%, respectively) and, for the upper limit, no net uptake of NH_3 on the walls and a loss rate determined by dilution (6000 s lifetime). For higher fan speeds, the lifetime decreases due to increased turbulence and, in turn, increased wall loss rate. Relative humidity is indicated by the orange line. The water cluster CI-APi-TOF reacts rapidly to changing conditions, such as the ammonia flow into the chamber, relative humidity, temperature or fan speed. At low concentrations, the ammonia lifetime is determined by the wall loss rate (panel b and initial stages of panel a). However, at high ammonia concentrations, the walls of the CLOUD chamber progressively become conditioned and a source of ammonia, with

corresponding increases in the ammonia lifetime and the time to reach new equilibria at lower ammonia flow rates (later stages of panel a).

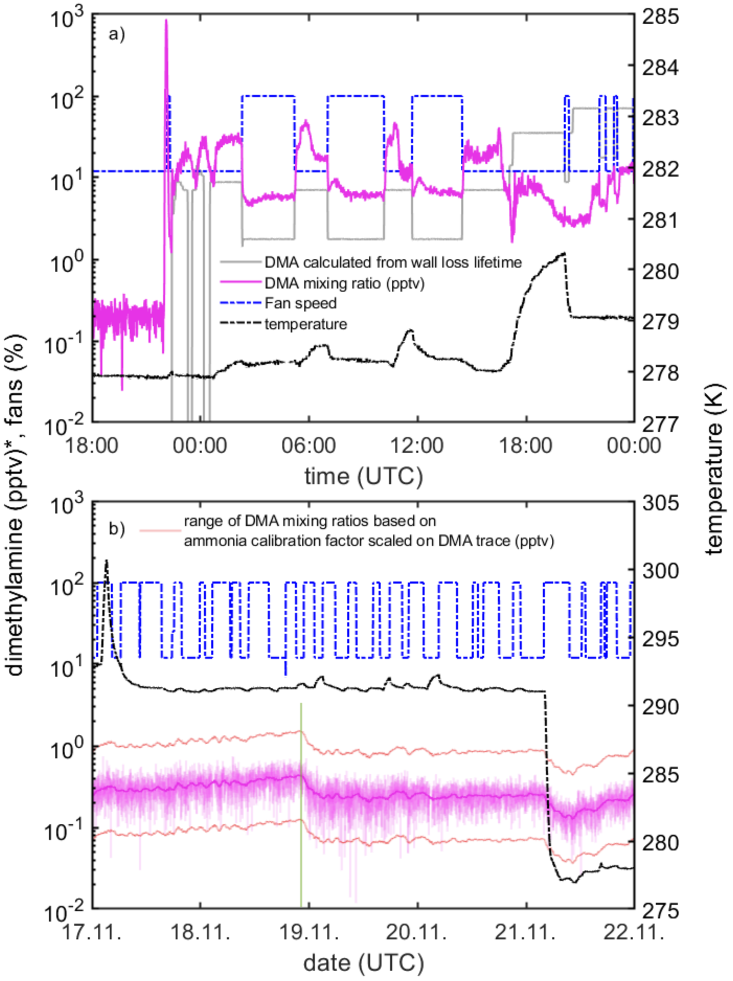

Figure 9: Dimethylamine mixing ratios (magenta line) during the CLOUD13 experiment. The dashed black line shows the temperature inside the CLOUD chamber. The dashed blue line shows the fan speed. Panel a) shows the dimethylamine signal during active injection into the chamber. The grey line indicates the dimethylamine mixing ratio in the chamber calculated from the MFC settings and the wall loss lifetime. The upper limit for the uncertainty in the dimethylamine mixing ratio is a factor of ~3.5 (see text for details). Panel b) shows a measurement of background dimethylamine in the chamber over a period of 5 days, when there was zero dimethylamine flow. We consider this to be due to instrumental background and not to an actual dimethylamine background in the chamber. The thin red lines show the possible range of dimethylamine based on the scaled calibration factor (factor 3.48, 95% CL). The thick magenta line indicates a moving average of the dimethylamine background measurement. The water source has been replenished during the period shown (green line). The mean instrumental background of dimethylamine over this period is ~0.14 pptv.

*Note that the dimethylamine mixing ratio is determined with the calibration factor for ammonia.